



**Michigan
Technological
University**

Michigan Technological University
Digital Commons @ Michigan Tech

Dissertations, Master's Theses and Master's Reports

2023

ALTERNATIVE METHOD FOR LOW FREQUENCY IMPACT SOUND MEASUREMENT FOR BUILDING FIELD TESTS

Sunit Girdhar

Michigan Technological University, sgirdhar@mtu.edu

Copyright 2023 Sunit Girdhar

Recommended Citation

Girdhar, Sunit, "ALTERNATIVE METHOD FOR LOW FREQUENCY IMPACT SOUND MEASUREMENT FOR BUILDING FIELD TESTS", Open Access Dissertation, Michigan Technological University, 2023.
<https://doi.org/10.37099/mtu.dc.etr/1566>

Follow this and additional works at: <https://digitalcommons.mtu.edu/etr>



Part of the [Acoustics, Dynamics, and Controls Commons](#)

ALTERNATIVE METHOD FOR LOW FREQUENCY IMPACT SOUND
MEASUREMENT FOR BUILDING FIELD TESTS

By

Sunit Girdhar

A DISSERTATION

Submitted in partial fulfillment of the requirements for the degree of

DOCTOR OF PHILOSOPHY

In Mechanical Engineering-Engineering Mechanics

MICHIGAN TECHNOLOGICAL UNIVERSITY

2023

© 2023 Sunit Girdhar

This dissertation has been approved in partial fulfillment of the requirements for the Degree of DOCTOR OF PHILOSOPHY in Mechanical Engineering-Engineering Mechanics.

Department of Mechanical Engineering – Engineering Mechanics

Dissertation Co-Advisor: *Andrew R. Barnard*

Dissertation Co-Advisor: *Jason R. Blough*

Committee Member: *Vijaya V. N. Sriram Malladi*

Committee Member: *Stephen M. Morse*

Committee Member: *David M. Labyak*

Department Chair: *Jason R. Blough*

Table of Contents

List of Figures	vi
List of Tables.....	xii
Acknowledgements	xiii
List of Abbreviations	xiv
Abstract.....	xv
1 Introduction and Objective.....	1
1.1 Objectives.....	2
2 Literature Review	3
2.1 History of impact noise testing methods.....	3
2.2 The existing impact noise test standard	4
2.3 Problems highlighted with the current method	8
2.4 Progress made by other researchers.....	11
2.4.1 Exploring the standard input force	11
2.4.2 Radiated sound measurements	18
2.5 Reciprocity method.....	24
3 Development and Methodology	27
3.1 Input force measurement methods.....	27
3.1.1 Force measurement instrumentation details.....	27
3.1.1.1 Tapping machine	28
3.1.1.2 ISO Impact ball	29
3.1.1.3 Modal hammer	31
3.1.2 Details of the floors tested.....	31
3.1.3 Data acquisition parameters	32
3.2 Simulation model details.....	32
3.2.1 Details of the simulation model.....	33
3.2.2 Sound Power based on simulated intensity.....	35
3.2.3 Reciprocity method simulations	36
3.2.3.1 Q source placed near the ceiling	38
3.2.3.2 Q source placed near the room corner.....	38
3.3 Evaluating reciprocal measurements in buildings.....	38
3.3.1 Test R1: Heavy concrete.....	39
3.3.2 Test R2: Hollow core concrete.....	39
3.3.3 Test R3: Wooden joist-framed assembly.....	40
3.3.4 Test R4: Wooden joist-framed assembly.....	41
3.4 Overall proposed method testing.....	42
3.4.1 Test O1: Heavy concrete.....	43
3.4.2 Test O2: Wooden joist-framed assembly.....	44

3.4.3	Test O3: Wooden joist-framed assembly with carpet finish.....	45
4	Results.....	47
4.1	Input force measurement results.....	47
4.1.1	Time domain comparison.....	47
4.1.2	Frequency domain comparison.....	50
4.1.3	Impulse comparison.....	54
4.2	Exploring measurement ideas using the simulation model.....	56
4.2.1	Sound Power based on simulated sound intensity.....	56
4.2.2	Reciprocity method simulation.....	57
4.2.3	Comparing the intensity and reciprocity simulation results.....	58
4.3	Evaluating reciprocal measurements for real structures	58
4.3.1	Test R1: Heavy Concrete Assembly.....	59
4.3.2	Test R2: Hollow Core Concrete	60
4.3.3	Test R3: Wood Joist-framed Assembly	62
4.3.4	Test R4: Wooden Joist-framed Assembly	63
4.4	Proposed reciprocity-based measurement method	65
4.4.1	Developing measurement guidelines for the Q source placed near the ceiling	67
4.4.2	Developing measurement guidelines for the Q source placed near a room corner	70
4.4.3	Comparing the simulated FRF from the ceiling and the corner placement	75
4.4.4	Proposed measurement guidelines based on the simulation model..	76
4.5	Evaluating the impact performance using the proposed test method	77
4.5.1	Test results based on the proposed method.....	77
4.5.1.1	Test O1: Heavy concrete.....	78
4.5.1.2	Test O2: Wooden joist-framed assembly	80
4.5.1.3	Test O3: Wooden joist-framed assembly with carpet finish	83
4.5.2	Comparison between the existing and proposed single number performance ratings	87
4.5.2.1	Calculation of LIRR rating	88
4.5.2.2	Calculation of standard ASTM ISR and LIR ratings	89
4.5.2.3	Comparing the standard and the proposed method ratings	90
5	Discussion	92
6	Conclusions and Future Scope	94
7	Reference List.....	96
A	APPENDIX – Additional details from various sections of the document.....	103
A.1	Hammer-head impedance correction for the instrumented tapping hammer	103

A.2	Impact-to-impact variation with continuous drops from the instrumented tapping hammer	103
A.3	Non-destructive accelerometer mounting on carpet.....	105
A.4	Floor impedance instrumentation details	106
A.5	Validation of the simulation model	107
A.6	Details of additional measurement methods simulated	108
A.6.1	Monte Carlo analysis	108
A.6.2	ISO Corner method.....	109
A.6.3	Diagonal measurement method	111
A.6.4	Sound Power based on room intensity.....	112
A.7	PCB Array microphone validation	113
A.8	Floor Impedance comparison	113
A.9	Additional plots for reciprocity testing.....	117
A.9.1	Supporting plots for Test R2	118
A.9.2	Additional SoRe and ReSo combinations for Test R3	119
A.9.3	Supporting plots for Test R3	121
A.9.4	Supporting plots for Test R4	122
A.10	Additional plots for reciprocity simulation models.....	124
A.11	Additional plots for the Proposed method tests.....	127
A.11.1	Supporting plots for Test O1	127
A.11.2	Supporting plots for Test O2.....	128
A.11.3	Supporting plots for Test O3.....	129
A.11.4	Ceiling RPF comparison for all assemblies	131
B	Copyright documentation.....	132
B.1	Copyright permission for Figure 2-4	132
B.2	Copyright permission for Figure 2-5	132

List of Figures

Figure 2-1 An example of a standard tapping machine used for ASTM and ISO tests	5
Figure 2-2 The four tapping machine positions for a homogeneous floor as defined in the ASTM standards	6
Figure 2-3 An example procedure to calculate ASTM single number rating.....	7
Figure 2-4 Test setup to measure the human foot impedance.....	15
Figure 2-5 A schematic showing the operation of the bang machine	17
Figure 2-6 Direct measurements and reciprocal measurements for a car assembly	26
Figure 3-1 Four of the five hammers were removed for simplicity from a standard tapping machine (left) and a force transducer was added.....	28
Figure 3-2 The force injected by the tapping machine into the floor (<i>F_{floor}</i>) is corrected	29
Figure 3-3 The impact ball force plate	30
Figure 3-4 A PCB 086D20 modal hammer was used as a reference source	31
Figure 3-5 Seven floors were tested for the input force measurement with the tapping machine, an impact ball, and the modal hammer	32
Figure 3-6 The simulation model showing the 10 ft × 13 ft × 9 ft room.....	33
Figure 3-7 The top view of the rectangular shape (left), Coupled Space (CS) assembly with two coupled spaces (center) and a Bay Window (BW) shaped assembly (right).....	35
Figure 3-8 The simulation models used to study reciprocity.....	37
Figure 3-9 Field test R1 for reciprocity.	39
Figure 3-10 Field test R2 for reciprocity	40
Figure 3-11 Field test R3 for reciprocity	41
Figure 3-12 Field test R4 for reciprocity	42
Figure 3-13 Field test O1 for the final proposed method	44
Figure 3-14 Field test O2 for the final proposed method.	45
Figure 3-15 Field test O3 for the final proposed method.	46
Figure 4-1 The time domain input force levels with the instrumented tapping machine..	48
Figure 4-2 The time domain peaks from the ISO impact ball	49
Figure 4-3 The time domain impact data for the tapping machine, the modal hammer, and the impact ball are compared.....	50
Figure 4-4 The input force spectra due to tapping machine impacts	51

Figure 4-5 Tapping machine input force spectra for the floor LC2 (top) and the coherence for the three floor accelerometers	52
Figure 4-6 The frequency spectra values for the impact ball below 100 Hz were approximately the same.....	53
Figure 4-7 The frequency spectra of the three input methods	54
Figure 4-8 The time domain force impulse for the impact ball	55
Figure 4-9 The free field Lw (solid black) compared with the forward propagating Lw (solid blue) and the raw intensity-based Lw (dashed red).....	56
Figure 4-10 The difference between the free field Lw , the raw intensity Lw , and the forward propagating Lw	57
Figure 4-11 Reciprocity comparison in the simulation model.....	58
Figure 4-12 The solid blue line represents the hammer P/F FRF and the dashed red line represents the A/Q FRF using the Q source speaker	60
Figure 4-13 The hammer and the impact ball P/F FRFs compare within 1 dB with the reciprocal A/Q FRF	61
Figure 4-14 Test R2: Measurement coherence with all the force input methods (left) and the Q source (right)	62
Figure 4-15 The direct FRFs obtained with the modal hammer, the impact ball, and the tapping machine, compared with the reciprocal FRF	63
Figure 4-16 The direct P/F FRFs obtained using the modal hammer (solid blue), impact ball (dotted red), and the tapping machine (dash dot magenta) are compared with the reciprocal A/Q FRF.....	64
Figure 4-17 The normalized RMS error as random Q source locations were selected near the ceiling for the CS shaped concrete floor.	65
Figure 4-18 Floor measurement strategy using the cross configuration (left) and the diagonal configuration (right).....	66
Figure 4-19 Two room diagonal selections (solid cyan) and the associated measurement points (black cross marks) are shown for the CS shaped assembly.....	67
Figure 4-20 The A/Q FRF when the Q source was placed close to the ceiling with the room impedance conditions (solid blue) and the free field conditions (solid red)	68
Figure 4-21 The diagonally averaged FRF (blue) compared with the baseline A/Q FRF (red) for the rectangular concrete (left) and the wood-joint (right) assembly	69
Figure 4-22 The baseline FRF (solid red) compared with the diagonal FRF over the entire floor (solid blue) and only the main floor space ignoring the coupled spaces (dashed blue).....	70
Figure 4-23 The diagonal FRF compared with the baseline when the Q source is placed near the corner for the rectangular concrete and wood-joint assembly	71

Figure 4-24 The diagonal and the baseline FRFs (solid red) compared for the CS shaped wood-joint floor by including the coupled spaces (solid blue) or excluding the coupled spaces (dashed blue)	72
Figure 4-25 The standard deviation observed if any point combination is picked for different radii around the diagonal locations.....	73
Figure 4-26 Four diagonal FRFs for all four corners in the CS shaped room assembly ..	74
Figure 4-27 The standard deviation (right axis) between all corner combinations for the Q source placement showed less than 1 dB deviation for the CS floor (left) and less than 0.5 dB variation for the BW floor (right) in the 40 – 100 Hz OTO bands	75
Figure 4-28 <i>A/Q</i> FRFs obtained using ceiling Q source and corner Q source placement for CS shaped concrete and wood-joint assemblies	75
Figure 4-29 Test O1: The corner Q source RPF (red) compared with the ceiling Q source RPF (blue)	79
Figure 4-30 Test O1: The direct FRFs measured using a modal hammer and the reciprocal RPFs measured using the Q source	80
Figure 4-31 Test O2: The upstairs dining space (red) and the downstairs room (blue)....	81
Figure 4-32 Test O2: The corner Q source RPF (red) compared with the ceiling Q source RPF (blue)	82
Figure 4-33 Test O2: The direct FRFs measured using a modal hammer and the reciprocal RPFs measured using the Q source	83
Figure 4-34 Test O3: The upstairs room (red) and the downstairs room (blue).....	84
Figure 4-35 Test O3: The direct FRFs and reciprocal RPFs compared	85
Figure 4-36 Test O3: The narrowband spectra comparison for the direct FRFs and the reciprocal RPFs.....	85
Figure 4-37 Test O3: The metal Velcro mount for the accelerometer was removed and re-applied at the same location without changing the Q source location.....	86
Figure 4-38 Test O3: The corner direct <i>P/F</i> FRF (red) compared with the ceiling FRF (blue).....	87
Figure 4-39 Corner RPFs compared for all floors based on the proposed measurement method.....	88
Figure 4-40 The average ASTM scanning SPL for all three test assemblies	89
Figure 4-41 <i>P/F</i> RPF calculated using the measured SPL with the tapping machine and measured force.....	91
Figure A-1 FRF measured between force transducer location (<i>Fmid</i>) and impact tip location (<i>Ffloor</i>).....	103

Figure A-2 The time domain impact data from the single instrumented tapping hammer	104
Figure A-3 The frequency spectra from a single impact test (solid blue) compared to the frequency spectra from a continuous impact test (solid red).....	105
Figure A-4 The red curve was the FRF obtained by supergluing an accelerometer on carpet (destructive testing) and the blue curve was obtained using the accelerometer mounted on a 26 × 32 × 3 mm steel piece with hook side of Velcro on the carpet (non-destructive testing).....	105
Figure A-5 Three accelerometers (green squares) were mounted equidistant from each other (1.22 m, 4 ft) and the impact location (red circle)	106
Figure A-6 The simulation room impedance boundary condition of 10414 kg/(m.s ²) led to approximately 0.5 second reverberation time in the room.....	107
Figure A-7 The mean and standard deviation values for the ASTM Monte Carlo analysis	109
Figure A-8 (Left) The blue and red curves respectively show the mean and standard deviation for all microphone nodes near the floor and ceiling corners.....	110
Figure A-9 Solid lines represent all different equidistant microphone combinations and the dashed red line represents the room averaged SPL.....	111
Figure A-10 The free field sound power (blue) compared with the room intensity-based sound power (red)	112
Figure A-11 Narrowband (left) and OTO band (right) comparison between the free field sound power (blue) and the intensity-based sound power with floor AML conditions	112
Figure A-12 The measured SPL autopower from six array microphones (solid blue) and free field mic (solid red).....	113
Figure A-13 Heavy floors showed approximately 30 – 40 dB higher impedance than the lightweight structures.....	114
Figure A-14 Impedance calculated using the impact ball (dotted lines with square markers) compares well with the tapping machine (solid lines with asterisk markers).....	115
Figure A-15 The impedance calculated using the modal hammer (considered as a 'control' source for this study) is compared with the tapping machine.....	116
Figure A-16 Floor impedance with the impact ball	117
Figure A-17 The floor vibration due to the Q source (blue lines) compared to the background floor vibration levels.....	118
Figure A-18 The radiated SPL due to the tapping machine impacts (blue curve) compared with the background SPL data.....	118

Figure A-19 The modal hammer and the impact ball FRF compare within 2 dB with the reciprocal measurements	119
Figure A-20 The direct FRFs with the modal hammer, impact ball, and the tapping machine for combination 3 (test R3) compare within 2 dB of the reciprocal FRF	120
Figure A-21 The direct FRFs with the modal hammer, impact ball, and the tapping machine compare within 3 dB of the reciprocal FRF	120
Figure A-22 The radiated SPL due to impact ball drops (blue lines) are compared with the background levels.....	121
Figure A-23 The A/Q FRFs obtained using a white noise and a sine sweep signal played through the Q source.....	122
Figure A-24 The measured floor acceleration due to the Q source input (blue lines) compared with the background floor acceleration.....	122
Figure A-25 The radiated SPL due to modal hammer impacts (blue lines) compared to the background noise	123
Figure A-26 The measurement coherence for the Q source for test R4	124
Figure A-27 The baseline A/Q FRF (solid red) compared with the diagonal FRF of the main floor (dashed blue) and the entire floor (solid blue).....	124
Figure A-28 The baseline A/Q FRF (solid red) compared with the diagonal FRF of the main floor (dashed blue) and the entire floor (solid blue).....	125
Figure A-29 The baseline A/Q FRF (solid red) compared with the diagonal FRF of the main floor (dashed blue) and the entire floor (solid blue).....	125
Figure A-30 The baseline A/Q FRF (solid red) compared with the diagonal FRF of the main floor (dashed blue) and the entire floor (solid blue).....	126
Figure A-31 The ceiling Q source correction needed based on the distance from the ceiling.....	127
Figure A-32 Test O1: Q source placed near the ceiling (left) and near the corners (right)	127
Figure A-33 Test O1: The cross (solid) and diagonal (dashed) averaged RPFs for two corners	128
Figure A-34 Test O2: Q source placed near the ceiling (left) and near the corners (right)	128
Figure A-35 Test O2: The cross (solid) and diagonal (dashed) averaged RPFs for two corners	129
Figure A-36 Test O3: Microphone placed near the ceiling (left) and near the corners (right).....	129
Figure A-37 Test O3: The cross (solid) and the diagonal (dashed) averaged FRFs for the two corners	130

Figure A-38 Ceiling RPFs compared for all three floors based on the proposed measurement method 131

List of Tables

Table 3-1 Floor assembly details (where available) for all floors under test.....	31
Table 3-2 Material properties used in the simulation model	34
Table 3-3 Mesh size and frequency bandwidth for the simulation model.....	34
Table 4-1 Proposed LIRR ratings for the corner and the ceiling Q source placement.....	88
Table 4-2 ASTM ISR and LIR ratings obtained for the three test floors	90
Table 4-3 Proposed LIRR ratings compared with standard ASTM ratings.....	91
Table A-1 First ten simulated and calculated acoustical natural frequencies.....	107
Table A-2 First ten simulated and calculated structural natural frequencies.....	108

Acknowledgements

It's impossible to thank everyone who has positively touched my life and inspired me to get to this point in my career, but I will try.

This work was primarily funded by the Paul S. Veneklasen Research Foundation (PSVRF). Part of this work was also funded by the INCE Student Scholarship and the Martin Hirschorn IAC Best Student Project Award. Thank you to PSVRF and INCE for the grants and awards. Also, thanks to ASA and NCAC for numerous travel awards that helped me present my work at multiple conferences. Thanks to Carey Widder from GrassWorx LLC for donating the tapping machine and to Siemens and GM for donating the Q source speaker. Both were used for almost all the work presented here. It would have been literally impossible to do the work that I did without all this support.

I have had a wonderful advisor – Dr. Andrew Barnard – whom I can never thank enough. I don't know how you put up with me, Dr. B, but I truly appreciate it. The insights and learnings I have received from him over the past few years have been truly wonderful. I would also like to thank the rest of my committee – Dr. Jason Blough, Dr. Sriram Malladi, and Dr. Stephen Morse. Thank you for your guidance through this process, and an early apology for having to read through this long dissertation. Oops!

I wouldn't be here without the support of my friends and most importantly, my partner – Moira Tracey. She of all people knows that it takes a lot of patience to deal with me so thank you for being the most patient and kind person I have ever met. You are a remarkable human being and you make me want to be a better person every day. Thank you for supporting me, especially on days when my imposter syndrome would make it impossible for me to get anything done. I am extremely lucky to have found you.

Thanks to my family who constantly supports me even from the other side of the world. Most of my motivation to do anything comes from me trying to make you all proud. Thanks to my dad for being an excellent role model growing up, and still asking me if I need money every time we talk. I appreciate that!

I would also like to thank my friends (technically, colleagues) at the Michigan Tech DSL lab and Penn State – Cora, Gita, Carter, Kourtney, and several more. I have had a lot of interesting conversations with all of you and I always learn something new from you all. Keep shining!

List of Abbreviations

AML – Automatically Matched Layer

FFT – Fast Fourier Transform

FRF – Frequency Response Function

HIR – High frequency Impact Rating

IIC – Impact Insulation Class

ISO – International Standards Organization

ISR – Impact Sound Rating

LIR – Low frequency Impact Rating

MAC – Modal Assurance Criteria

OTO – One Third Octave

RPF – Ratio of Powers Function

SLM – Sound Level Meter

SNR – Signal to Noise Ratio

SPL – Sound Pressure Level

Abstract

What do high heels, dog nails, and dragging furniture have in common? They are all frequent sources of noise pollution and annoyance in multi-story buildings. Building codes exist to control and mitigate such noise, but these codes are outdated and fail to protect the residents against noise annoyance. Footstep noise is still the number one cause of complaints among the residents. The impact performance of floor-ceiling assemblies is characterized using a single-number rating called the Impact Sound Rating (ISR). A standard tapping machine is used in pre-defined locations on the floor and the radiated Sound Pressure Level (SPL) is measured in the receiving room downstairs to calculate the ISR rating. This measurement method has a lot of variabilities that cause problems for the residents or the acoustical consultants. The force from the tapping machine depends on the floor compliance but it is not measured for the test. An FRF-like measurement is required to account for this force difference and compare the performance of different assemblies. Additionally, a non-diffuse sound field exists in rooms at low frequencies that cause high variation in the test results based on the microphone positions. In this work, a new measurement method is proposed that provides an FRF-like (without consideration of phase) performance using a ratio of autopower spectra (RPF) and shows an improved reproducibility in the low-frequency non-diffuse sound field region. A 1 – 1.5 dB measurement variability is expected as compared to 4 – 10 dB variability observed with the existing method. The guidelines to conduct the proposed test are detailed in this work.

1 Introduction and Objective

Humans spend approximately 90% of their time indoors [1] and it is imperative to make these indoor spaces comfortable. With a growing population, the need for multistory residential houses has increased, especially in big cities. New York City, for example, has a population density of more than 27,000 people per square mile [2]. In places so dense, acoustical comfort inside residential spaces is a priority, especially with the increased use of lightweight and sustainable building materials, such as wood. The acoustical annoyance often leads to a loss of productivity [3, 4], sleep problems [5, 6], complaints to the building owners, or even class-action lawsuits [7].

To address this issue, President Nixon signed the Noise Control Act in the US in 1972, directing the Environmental Protection Agency (EPA) to conduct a large-scale noise study to understand the effects of cars, trains, and airport noise on communities [8]. EPA developed guidelines for indoor and outdoor Sound Pressure Level (SPL) and comfort and defined the maximum 24-hour sound exposure level to prevent hearing loss [9, 10]. This propelled the noise requirements to be written in the building codes [11], specifically addressing airborne and impact noise transmission between individual dwellings.

Impact noise in buildings is generally caused due to footsteps on floor assemblies that radiate noise in the dwelling below. This can lead to annoyance. Research has shown that footsteps are the most common source of impact noise in buildings [12-14], and other sources such as children running, jumping, moving furniture, etc. have also been identified to cause annoyance among the residents [15-17]. Building codes use ASTM standards [18-20] to evaluate the impact noise performance of floor-ceiling assemblies. A standard tapping machine is used to generate the impacts on the floor and the radiated SPL is measured in the downstairs room.

Researchers have broadly highlighted two categories of problems with the current standard:

- The test method does not rank-order the floor-ceiling assemblies the same way as the subjective response to footsteps [7, 13, 14, 21-31]
- The SPL-based test method has high measurement uncertainty due to a non-diffuse sound field in low frequencies [32-38]

Such problems have caused harm to the acoustics industry and the end-users alike. The end-users are unhappy with the inability of the building codes to create a quiet and healthy environment. This may lead to annoyance, long-term health issues due to lack of rest, and may affect their day-to-day life at school or at work. On the other hand, the acoustical industry is unhappy because even after following the standard test method and the building codes, customers still frequently complain about the performance of the assemblies. Acoustical consultants are often asked to testify in court whether a certain assembly is following the building codes or not. The acousticians may sometimes resort to non-standard testing to resolve customer complaints. Every acoustician does this

differently based on their personal experience, which in turn negates the usefulness of a standard method. The goal thus becomes to improve the standard measurement method and tackle the two problems bulleted above. An improved test method can lead to satisfaction of the end-users and the acousticians, both.

1.1 Objectives

The first objective is to **scale the output radiated sound with input force levels** so that a Frequency Response Function (FRF) – like measurement could be made. The impact input force depends on the combined impedance of the impactor and the structure. The impedance of a tapping machine hammer (steel) is much different than the footsteps, which changes the force levels and spectra. However, there is no provision to measure the input force from the tapping machine in the standards. This causes a disconnect between the objective test data obtained using a tapping machine, and the subjective response of the residents due to footsteps, which leads to poor rank-ordering of assemblies. It is important to measure the input force and scale the output to get an FRF-like performance measurement of floor-ceiling assemblies.

The second objective of this work is to **improve the reproducibility of the measurement process**. Currently, the standards require the user to measure SPL in the receiving rooms, which is dependent on the room modes in non-diffuse fields. This causes uncertainty issues and increases the non-reproducibility of measurement. The problem is more pronounced in lower frequencies. By proposing a way to control the effect of room modes on the measurement data, this uncertainty can be mitigated. Users can compare one-floor ceiling assembly to another without the effects of the room's non-diffuse field. This would be primarily helpful for the recently introduced ASTM LIR (Low frequency Impact Rating) standard [39], which measures data from 50 Hz – 80 Hz One Third Octave (OTO) bands and is highly susceptible to the non-diffuse field-based uncertainty.

2 Literature Review

In this chapter, we will discuss the history of how the current impact noise testing methods were developed, detail the current test standard, highlight some of the research showing problems with the current standard, and discuss some previous work done to address such concerns.

2.1 History of impact noise testing methods

An impactor was developed in 1932 by Reiher [22, 40] as a more repeatable way to mimic footstep impacts. The impactor was made using a beechwood hammer weighing 280 g, free-falling from a height of 30 mm to create an impact. The weight and height were decided based on a ‘trial and error’ experiment so that the sound radiated from a particular floor was similar to the footstep noise of an adult walking with leather-heeled shoes. Much of Reiher’s work focused on the subjective evaluation of footstep impacts on the residents.

Drastic changes were made to this impactor in the next few years. Bausch [22, 41] summarizes that it was difficult to make error-free and background noise-free measurements of good-performing floors with the wood impactor using the technology at the time. Changes were made to Reiher’s design to create an easily measurable, semi-continuous noise source. The wood impactor was switched to a hard, metal impactor, and five impactors were used instead of one. This shifted the focus from subjective evaluation of the residents to objective measurements of the assembly. The first standard tapping machine was adopted in Germany in 1938 [22].

When the research efforts continued after World War II, round-robin studies were conducted all over Europe and the first draft standard was introduced within ISO (International Organization for Standardization) in 1948 [42]. The tapping machine was used as an input source and the radiated SPL was measured in the room below from 100 to 3150 Hz OTO bands. The draft drew instant criticism for the inability of the tapping machine to represent real footsteps, which led to a disconnect with the subjective response of the residents. Gösele [22, 43, 44] tested two floors that showed similar subjective acceptability based on footstep noise, but one of the floors tested 16 dB louder than the other using the draft ISO standard. After much deliberation within ISO, the draft was formally accepted in 1960, largely unchanged.

Importance was also given to communicating the test results with architects and builders in an effective manner [45]. Single numbers were introduced to easily communicate the performance in the entire frequency bandwidth using just one number. Early work used a simple average of all SPL values measured. However, it was quickly proved that a poor performing assembly in a certain frequency range cannot be compensated by improving its performance in a different frequency range. A ‘grading curve’ was introduced in Germany in the 1950s, and later introduced within ISO. Brandt [45] introduced the term ‘Impact Insulation Index’, based on a similar German name, as a single number calculated by comparing the measured test data with the grading curve. A positive

number represents performs better ‘than required’. The grading curve was based on an assembly found to be ‘satisfactory’ in practice [22, 46, 47].

Within the US, while efforts were made to measure impact noise as early as 1927 [42], there were no requirements set for the builders at least until 1964 [45]. In the early 1960s, ASTM was tasked by the Federal Housing Association (FHA) to create a noise testing standard for America. The first proposal introduced within ASTM was based on the ISO standard using the tapping machine and it drew instant criticism, mostly along the same lines as the early draft within ISO. After intense discussions between two strongly opposed factions within ASTM, the standard was adopted in the US in 1968, with the hopes that future research will help improve the standard when comparing tapping machine results to subjective reaction [42]. Even after more than five decades, the tapping machine is still the only input source used in the ASTM standards [18-20], detailed in the next section.

2.2 The existing impact noise test standard

The building codes in the US refer to Impact Sound Rating (ISR) to evaluate the field performance of floor-ceiling assemblies. Impact Insulation Class (IIC) rating is used to quantify the impact noise performance of an assembly in the lab. These single-number ratings are calculated and measured using ASTM standards [18-20] developed by the ASTM E33 committee on Building and Environmental Acoustics.

The standard tapping machine uses five hammers, each weighing 500 ± 6 g, spaced apart by 100 ± 3 mm. An example of a standard tapping machine is shown in Fig. 2-1. Each hammer drops on the floor from a free fall from a height of 40 ± 3 mm. The hammers are shaped as a cylinder with a diameter of 30 ± 0.2 mm and the impact surface is spherical with a radius of 500 ± 100 mm. The hammer fall frequency is 2 Hz and they are spaced apart such that the overall frequency of a tapping machine is 10 Hz.

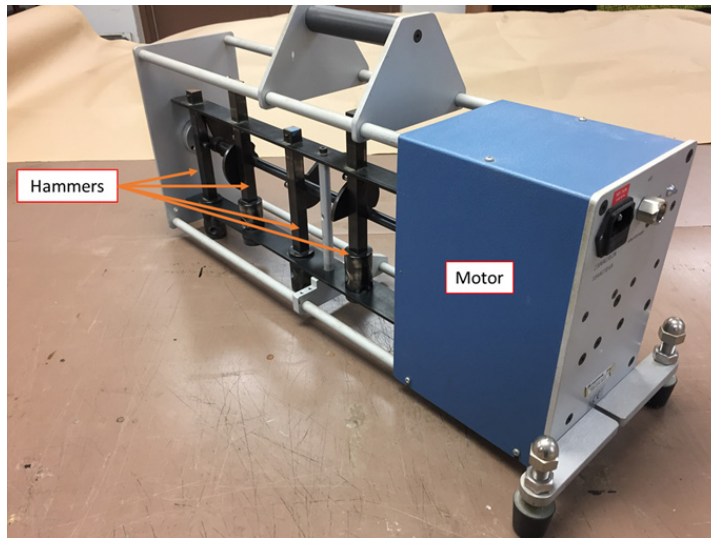


Figure 2-1 An example of a standard tapping machine used for ASTM and ISO tests showing the motor and the five hammers that free fall on the floor at a frequency of 10 Hz

The ASTM standard provides guidelines on tapping machine placement and orientation, shown in Fig. 2-2. Positions 1 and 2 must be in the approximate center of the test span, and should be perpendicular to each other. Position 3 is parallel to the first position and displaced by 0.6 m. Position 4 is at a 45° angle from position 1 (or position 2), and displaced by 0.6 m. These requirements should be followed if the floor construction is unknown or homogeneous. The former is usually the case for field tests, especially in the later phase of construction. Please refer to ASTM standards [19, 20] for tapping machine placement information if the floor is non-homogeneous and/or the joist information is available.

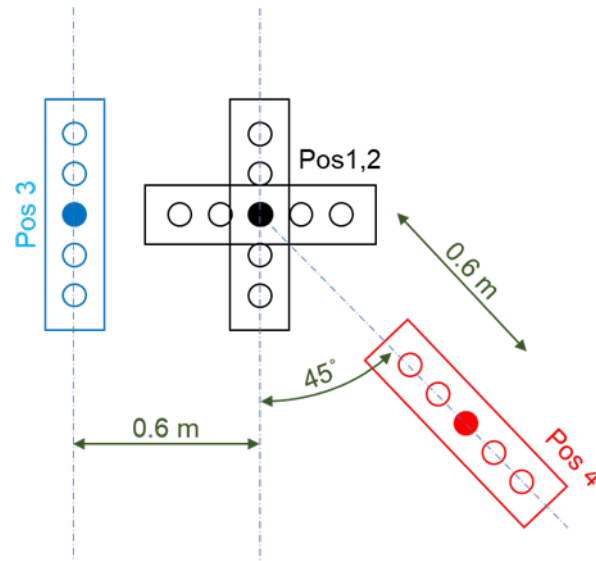


Figure 2-2 The four tapping machine positions for a homogeneous floor as defined in the ASTM standards [19, 20] are located at the approximate center of the test area or the room. The highlighted circle is the middle hammer, which is often used to locate all four positions and orientations

The radiated sound from the tapping machine impacts is measured in the receiving room below using either of the two methods: fixed microphone method, and moving microphone method. For the fixed microphone method, at least four room locations are measured and each location should be at least 1 m from all room boundaries and each other. The microphones should not be placed at obviously symmetrical locations and should not be on the same horizontal or vertical plane. However, the most common measurement method is the moving microphone method, where the microphone can be moved either mechanically, or manually. The microphone should be at least 1 m from all room surfaces and the scan path should not be parallel to any room boundaries. The sweep time should be between 30 to 60 s. The measured SPL from either measurement method is averaged to get the overall SPL of the room. This is done from 100 – 3150 Hz OTO bands, with a provision to measure and process data from 50 – 80 Hz OTO separately [39]. More details can be found in the ASTM standards [19, 20].

The average SPL in the receiving room is compared to a reference curve (defined in the standards) to get single number ratings such as the Impact Sound Rating (ISR) for field tests [18], presented in Fig. 2-3. The reference curve is represented using the solid blue line and the measurement curve is represented using the solid pink line. The reference curve is incrementally moved closer to the measurement data in steps of 1 dB until:

- The positive deficiencies in any OTO band are not greater than 8 dB
- The sum of all positive deficiencies is less than or equal to 32 dB

The positive deficiencies here refer only to the OTO bands where the measured data are higher than the reference curve, highlighted with green arrows in the example in Fig. 2-3.

For this example, the dashed red curve represents the modified reference data where the bulleted conditions are met. The ISR rating is given by the level of the reference curve at 500 Hz subtracted by 110. In this case, the ISR rating is 55.

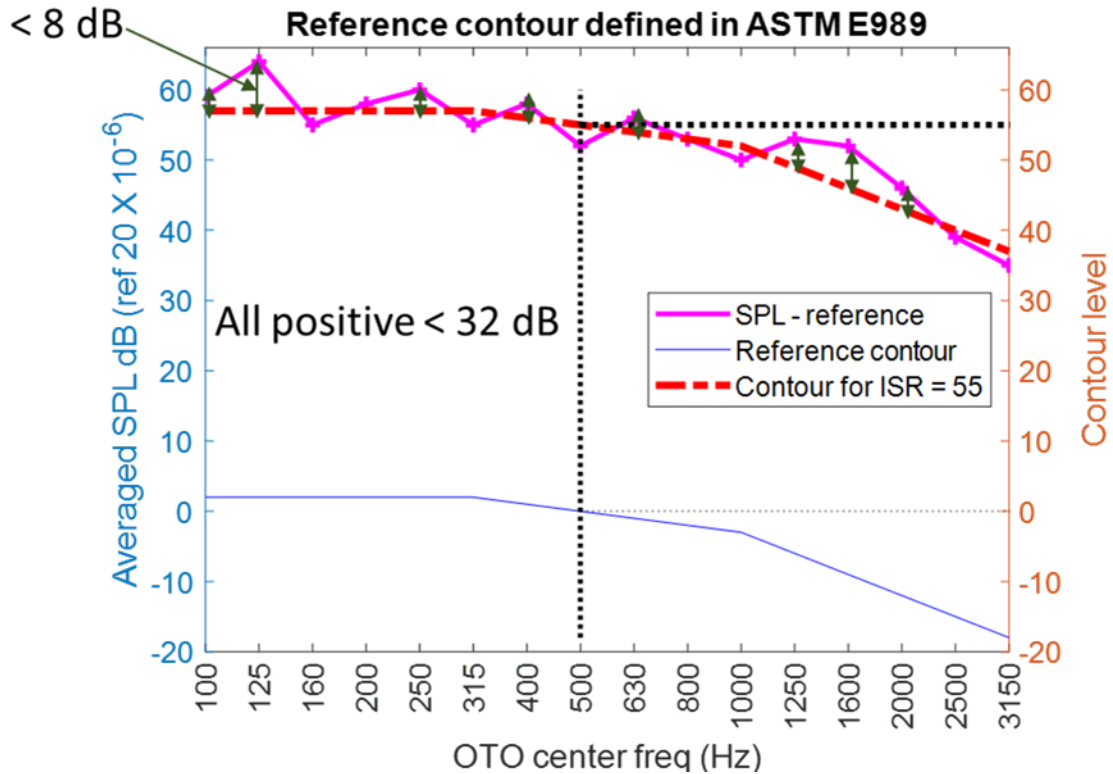


Figure 2-3 An example procedure to calculate ASTM single number rating from measured SPL values [18]. The measured data (solid pink) are compared with the adjusted reference curve (dashed red) and positive deficiencies (green arrows) are evaluated to get a single number rating.

Most of the field tests are conducted when the residential units are unoccupied. However, the room absorption changes once the residents move in and the measured SPL in the receiving room would be different. To account for this, the measured SPL data can be normalized to a standard reverberation time of 0.5 s, which is shown to be the standard reverberation time of furnished, livable spaces [45]. The new dataset is called the Reverberation Time Normalized Impact Sound Pressure Level (RTNISPL) and the single number rating obtained is called Normalized Impact Sound Rating (NISR).

The noise requirements are built into the building codes where these single number ratings are used to certify assemblies as pass or fail. For impact insulation, assemblies must have a minimum NISR of 45 for field testing. The assemblies that do not meet this rating must be reworked and tested again until the required rating is achieved. Over the years, acousticians have created their own set of NISR ratings to classify assemblies as acceptable (just meeting the building codes), preferred, or luxury. Different ranges of ratings are assigned to different categories and depend on the acoustician's experience.

In practice, the impact performance of an assembly predicted using this standard measurement method shows a disconnect with the subjective response due to footstep noise. In the next section, we will highlight some of these issues.

2.3 Problems highlighted with the current method

The primary problem with the standard is that if an assembly is predicted to do better than another based on this test, the residents may not always agree with it. ASTM lab tests [19] are frequently used to rank order and compare different structures. Design decisions for buildings are made based on these lab tests and it is a problem if these numbers don't match up with the subjective response of the residents due to footstep impacts.

Mariner et al [22] tested 75 floor assemblies in the same test lab using a standard tapping machine and two female walkers with hard heel shoes. The footstep data were used to calculate loudness (in sones) and the single number rating was calculated using the tapping machine impact data. The ratings for two floors with a similar footstep loudness level differed by approximately 11.5 points. On the other hand, one of the floors was ranked twice as loud as another floor, but they had the same single number rating. With such a large spread, the authors concluded that the tapping machine failed to rank-order the floors based on their performance due to real footsteps.

Olynyk et al [21] tested twenty-two wood-joint and seven concrete structures. All tests were performed in actual buildings. The standard tapping machine and the footsteps from multiple female walkers with hard-heeled shoes were used as the input source. The measured data were recorded to conduct a listening test, where the listeners increased the level of a masking noise until the footstep noise, or the tapping machine noise was not audible. This level was used as a criterion to evaluate different assemblies. Two floors where the single number rating differed by 20 points had a very similar subjective reaction. Two other floors from the same test had a very similar single number rating but their subjective rating differed by approximately 15 dB. The authors showed a similar behavior in a previous, smaller study [30].

Lietzén et al [24] tested nine floor coverings with the same base structure (hollow concrete core slab) in a lab. All the floor coverings were the same size and installed at the same location following the same procedure. Standard measurements using a tapping machine were made (according to the equivalent ISO standard), and walking tests were performed with three male walkers with socks, soft-heeled shoes, and hard-heeled shoes. Loudness was calculated from walking noise and single number ISO rating was calculated from the tapping machine data. The rank order of nine assemblies with the tapping machine was completely different than the footstep data. In addition, a 0.33 correlation was found between the tapping machine and the footsteps with socks. The correlation improves to 0.77 when compared to walking noise with hard-heeled shoes.

LoVerde et al [29] showed that two floors with a similar subjective reaction had a 23 point difference in their single number ratings. Another pair of floors showed a very

similar single number rating, but their subjective response differed by 6 points on a 10 point scale. The data were based on 14 different assemblies tested as part of this study and the subjective scale was created internally by the authors based on the number of complaints from the owners, operators, building managers, etc. The highest value on the scale (10 points) corresponds to 20% or more complaints, and the lowest value (1 point) corresponds to no complaints.

Often, the disconnect between objective ratings and subjective reaction to footsteps is tied back to the inability of the tapping machine to generate footstep-type inputs. Watters [14] added a force transducer to a standard tapping machine and set up a high-speed camera to capture the impact. The author also instrumented a woman's high heel shoe to measure the footstep force. Based on the high-speed camera, the author concluded that the shoe heel impacts the structure at an oblique angle (compared to normal for the tapper), and at approximately half the velocity as compared to the tapping machine. The footstep impacts on a hard or a soft surface, have a downward slope in the spectra with an increase in frequency. But the tapping machine on a hard floor shows an increase in force spectra with an increase in frequency. For softer floors, the impact levels in low frequencies are much lower for the tapping machine as compared to footsteps.

Warnock [48] observed a similar behavior for concrete floors. The author measured radiated SPL in the receiving room at one location while using a tapping machine upstairs, along with a human walker. The test was conducted on 75 different assemblies including concrete and wood-joint constructions. The frequency data slope for the tapping machine and the human walker on the bare concrete floor was opposite. The peak SPL levels increased with frequency for the tapping machine while the opposite was observed for the human walker. For example, at 1000 Hz, the radiated SPL due to tapping machine impacts was approximately 30 dB higher than that from a human walker.

Shi et al [23] built a force plate with three force transducers to measure the input force from a tapping machine, along with a human walking, running, and jumping. A gangway bridge was built near the force plate to let the person get into the normal walking/ running rhythm before stepping on the force plate. Using sixteen people for this study, the authors concluded that footsteps have a much stronger low-frequency component than a tapping machine.

Amiryarahmadi et al [26] used calculations to show that footsteps have approximately 10 – 20 dB higher energy as compared to the tapping machine. The authors created a simple assembly with known dynamic properties and measured the response of the structure with the tapping machine and footsteps. The authors used least the mean squared algorithm to calculate the input force for both cases with the assumption that the structure is linear.

The ASTM standard addresses this disconnect between tapping machine impacts and footsteps by specifying that the tapping machine does not represent a real footstep source. ASTM states that the purpose of this standard is to compare the data obtained from one test engineer to another and not to represent footstep impact noise. However, the tapping

machine is still the only accepted source within ASTM to study footstep impact noise for building codes.

While the standard intends to compare the work of one test engineer to another, the reproducibility variability is very high. The standards rely on measuring ‘averaged’ radiated SPL in the receiving room downstairs measured either using the scanning microphone, or multiple discrete point microphone method. However, the existence of a non-diffuse field, especially at low frequencies, makes it difficult to decide measurement locations in the room.

Barnard et al [34] instrumented a floor-ceiling assembly with accelerometers and placed six microphones in the receiving room below. A modal hammer was used to generate the impacts and the input force was measured. During the test, all microphones recorded a peak in the 100 Hz OTO band, which is also the lowest OTO band studied for the building codes. In this particular case, the high levels in 100 Hz OTO data were controlling the single number rating calculated for the floor. The accelerometers mounted directly on the assembly did not show any peak in this frequency band. Later calculations revealed that a room mode exists at the frequency where microphones recorded a peak. The single number rating for the assembly in this case was directly affected by the room it was being tested in.

Hopkins et al [33] set up a dense microphone grid in the source room and the receiver room for an airborne insulation test (Average SPL measured in the receiving room based on the speaker placed in the source room). The authors showed that the standard deviation for different microphone locations was approximately 4 – 5 dB due to the non-diffuse field. In the diffuse field (high frequencies), the observed standard deviation was approximately 2 – 3 dB.

Oliva et al [32], as part of their work for the Finnish Institute of Occupational Health, used a Finite Element Model (FEM) to show that in a standard room, the variation between different microphone locations can be as high as 16 dB at 25 Hz, and 4 – 10 dB from 40 to 160 Hz OTO bands. The authors concluded that the low number of room modes in low frequencies is responsible for such a variation.

The non-diffuse region generally depends on the size and characteristics of the room. Schroeder’s formula [49] is generally used to define the cut-off frequency below which, the field is considered non-diffuse. This frequency is defined as

$$f_{co} = 2000 \sqrt{\frac{T_{60}}{V}}, \quad (2-1)$$

where, f_{co} is the Schroeder’s cut-off frequency (Hz), V is the volume of the enclosed space (m^3), and T_{60} is the time (seconds) it takes for the overall sound energy in the room to decay by 60 dB, also known as the reverberation time. Barnard et al [34] used this equation to calculate the Schroeder’s frequency for most of the ASTM accredited labs in North America. Most labs did not have a diffuse field below 170 – 250 Hz. As a

reminder, the lowest frequency for the ASTM ISR rating is 100 Hz. This shows that at least some part of the frequency bandwidth of interest lies in the non-diffuse field for most accredited labs.

Measurements in the non-diffuse sound field rely heavily on the measurement locations. The measured SPL can be different for different locations. This variability will lead to uncertainty in single number ratings. Some labs overcome this by establishing standard test procedure that includes microphone measurement position definitions. However, lab-to-lab variability still exists. The same assembly tested in different labs by different test engineers may lead to completely different results, even if the operators followed the same standard. The problem is more pronounced for field tests, where the room sizes can be very different and a pre-defined microphone location strategy won't work. This reproducibility problem leads to high variability in the test data. Reducing this non-reproducibility is one of the goals of this research.

Over the years, researchers have suggested multiple ideas to address the issues with the current standards. In the following section, we will discuss some of the prominent works.

2.4 Progress made by other researchers

For this work, we focused on past research done on understanding the input force and the output sound radiation. These two are discussed individually in the following sub-sections.

2.4.1 Exploring the standard input force

To understand the input force from the tapping machine, several numerical models were created. Rabold et al [50] summarized most of the work done before 2010. One of the very first prediction model was developed by Cremer [51] who calculated the time-based impact force levels based on the weight of the hammer and the impact velocity. The time domain levels were then converted to the frequency domain. For the formulation, the author assumed that the duration of the impact is much shorter than the time between impacts and that the impacted surface is heavy and rigid.

Vér [52] used the known properties of a floor to calculate the contact stiffness. This, along with the mass of the impactor, was used to calculate the duration of the impact. A perfect half-sinusoidal wave was assumed for the impact and the impactor was assumed to have the same rebound velocity as the impact velocity in the opposite direction. The latter assumption restricts the applicability of this formulation to only heavy and rigid floors. The dynamic properties of the structure were also used to calculate the average floor mobility and radiated sound power. The predictions of this formula were not compared with experimental values.

Scholl et al [53] considered a mass-spring-mass system where the mass of the impactor and the local mass of the floor were used. The spring component came from the contact stiffness, defined based on the shear modulus of the material, Poisson's ratio, contact area, and a form factor. The author defined different form factors based on the

distribution of impact over the contact surface. The force-time curve was assumed to be a half-sine wave during contact and zero afterward. The inclusion of the contact stiffness in the prediction model made it possible to consider other impact sources too, not just the standard tapping machine.

Brunskog et al [54, 55] used a similar lumped parameter modeling approach and included damping in the system. The floor is considered to be a resilient layer with stiffness and damping and only the mass of the impactor is considered. This model assumes that the stiffness and damping comes only from the resilient layer on a rigid floor. The authors postulated that for lightweight floors, the resilient part was due to local deformation and the resistive part was due to energy dissipation. The impact force was calculated using equilibrium conditions during the contact of the hammer with the floor. The force was calculated in the frequency domain and then converted to the time domain, where the values were forced to be zero after the duration of the impact. This new time signal was taken back to the frequency domain to get the force spectra on the floor. The resilient layer assumption broadened the applicability of this prediction model to include floors with a finish flooring layer. However, the predicted force levels on lightweight structures showed poor correlation with measurements.

Rabold et al [50] increased the model complexity further and included the effects of the previous impacts. The floor velocity from previous impacts was used as an initial boundary condition for the next impact. This is done by using the local and global admittance of the floor. The authors were able to tie all the impacts of the tapping machine together leading to an extremely complex model. The new model showed only a slight improvement in correlation with experimental data as compared to the older models. Qian et al [56] showed in their work that the added complexity of the model is not worth the slight improvement in correlation with test data.

Researchers have also created models to predict the sound radiated from the tapping machine impacts. Guigou-Carter et al [57] glued wood floorboards to a resilient layer on a heavy concrete structure. The authors tested all individual elements to get their dynamic properties. The resonance frequencies of the wood floorboards were calculated based on mechanical impedance measurements in free-free boundary conditions. Once the analytical model was built, the velocity at the top and bottom of the slab was calculated in the wavenumber domain. This velocity was used to predict the radiated sound power, assuming that the structure is infinite and the location of the tapping machine does not affect the radiated sound power. The analytical model showed a poor correlation with the experimental data and the authors conclude that the glue used in the system is changing the dynamic properties significantly and affecting the correlation.

Kimura et al [58] developed an analytical model for composite floors. The authors assumed that the floor is a single homogeneous layer with known properties and incrementally added different composite layers to build the complete dynamic model. The total impedance of the slab was calculated based on infinite plate assumptions, and the dynamic properties were assumed to be frequency independent. The vibration field in the slab was assumed to be diffuse, along with the sound field in the receiving room. The

effective area for sound radiation was calculated as one-fourth of the wavelength from the edges with fixed boundary conditions. The overall prediction model failed to correlate well with assemblies with an air cavity, but showed a good correlation with simple structures. The authors conclude that the air cavity acts as an elastic body and may affect the sound radiation in the mid and high-frequency regions.

Brunskog et al [59] consider this cavity in their model. The authors used the periodicity of a lightweight structure to postulate sound power radiated in the wavenumber domain using Poisson's sum rule. The radiated sound field in the receiving room was assumed to be diffuse and the floor was assumed to be linear. The top and bottom layers were assumed to be infinite and rigidly connected to each other in the transverse direction and were free to rotate on framing beams. The input force from the tapping machine was calculated based on previous work by the authors [54, 55]. The predicted sound energy was underpredicted by approximately 3 – 5 dB when compared to literature values but the peaks and dips were in similar frequency bands.

Lindblad [60] created a model to study the effect of adding a resilient layer to a floor structure. The improvement was postulated using the point impedance of an infinite slab with the assumption that all five tapping machine hammers impact the floor at a single location. The author calculated the rebound conditions and the time of impact to calculate the input force. The formulation showed poor correlation with experimental values and the author concluded that this is because of floor non-linearities.

Wittstock [61] assumed the input frequency of the modal hammer to be 2 Hz, instead of 10 Hz which has generally been used by other authors in the past. The author showed this to be true based on experiments on a timber joist floor and a concrete floor using the standard tapping machine. For a heavy floor like concrete, the bending wavelengths are larger so the 10 Hz excitation is almost 40 dB higher than the 2 Hz excitation. However, for a lightweight, chipboard structure, the 2 Hz excitation was only approximately 10 dB lower than the 10 Hz excitation. The author argues that for a real tapping machine, the friction in the mechanism may cause this difference to be lower and the 2Hz excitation may become dominant. The sound power calculated with a single hammer at 2 Hz was multiplied by five to get the overall radiated sound power. The predicted values were not compared to experimental data.

Qian et al [62] calculated the input force from the tapping machine based on the response of a CLT (Cross Laminated Timber) floor with known dynamic properties (from the literature). A CLT model was created and the acceleration response from the tapping machine impacts was compared with an FE model. The damping was taken directly from the experiments and the literature dynamic properties were tweaked until a good correlation was observed. The author does not give more information about this adjustment. The authors show good MAC (Modal Assurance Criteria) values for the first three modes. In a follow-up work [56], the authors used a roving modal hammer test on the CLT structure to directly get the dynamic properties. With the new properties, the correlation between experimental and analytical tapping machine data slightly improved

but significant frequency shifts were observed above 100 Hz. The authors cite a lack of reliable material properties information in higher frequencies for this poor correlation.

Caniato et al [63] performed an in-depth review of all the prediction models, at least until 2017, and summarized that for lightweight structures, no method exists that can truly come up with predicted values that give accurate results when compared to experimental data. The authors mentioned that the variability in raw material, assembly process, etc., is so high that no prediction model can predict this behavior. The sentiment is shared by much of the industry. Brunskog et al [64] also concluded that analytical models exist that can handle periodicity in structures and point inputs, but complicated structures will fail with the same models.

The lack of prediction models means that the relationship between the output sound radiated based on the input force is still unknown. The industry continues to use the standard tapping machine as a way to predict and rank-order floor-ceiling structures based on footfall noise, even though the two sources are completely different. Studies also show that the floor-ceiling assemblies are non-linear [13, 21-23, 60, 64]. Lindblad [60] tested a thick concrete structure with a resilient layer for different hammer drop heights – 40 mm, 12.6 mm, and 4 mm. Based on the linear theory, the curves were predicted to be approximately 5 dB apart. However, this behavior was not observed and the curves seemed to depend on the resilient layer itself. The cork carpet performed the best with a 40 mm drop height while a felt carpet layer performed best with a 4 mm drop height. The author concluded that the floors were non-linear.

Watters [14] measured the impact force from a standard tapping machine while consecutively decreasing force levels and observed non-linearities. Mariner [65] used five different input force levels on the same floor and observed a non-linear behavior. Olsson et al [66] tested the floor using a shaker with a stepped-sine signal with different amplitude signals, along with a modal hammer and a modified tapping machine equipped with a force transducer. When comparing the FRFs between the output radiated SPL and the input force from these input sources, non-linearities were evident. Almost 3 dB differences in amplitudes were observed along with a shift in the natural frequencies. The authors concluded that the floors were non-linear and recommended using an input source similar to human footsteps as a standard input. This is consistent with the initial push in the industry to modify the tapping machine to match it better with real footsteps.

Lindblad [60] proposed using a 200 g hammer falling from a height of 20 mm to better represent footsteps. The author also proposed to change the dynamics of the impactor. A heavy mass (simulating the leg) is connected to a lighter mass (representing a heel of a shoe), but the author stops short of better defining how these two parts should be connected.

Schultz [67] also proposed to reduce the mass of the hammer weights and replace the impactor tip with something more representative of a human shoe. The author suggested spring loading the impactor to reduce the impact force levels, and using only a single hammer operating at 2 Hz, which is more representative of human footsteps. The author

also commented that the impedance of human footsteps is extremely complex, especially below 150 Hz, and it is difficult to create an impactor that will have the same impedance as human footsteps below 150 Hz. Nordstedt [68] created a tapping machine based on Schultz's [67] proposal. Only one input hammer was used, weighing 200 g, and a spring was attached to the hammer. A semi-resilient layer was used on the floor to simulate a human shoe-like impactor tip. This modified machine was used on a concrete floor and a wood-joint floor and a subjective analysis was conducted to compare the results with a standard tapping machine. The author did not find any improvement in the subjective evaluation or the single number ratings with this modification.

Scholl [69] used an electrodynamic shaker to measure the impedance of a human foot. The moving shaft of the shaker was attached to a person's shoe using a 45mm thick Aluminum plate, a force transducer, and an accelerometer. The test setup is shown in Fig. 2-4 and the impedance was measured in standing and sitting positions. The spectra for both cases were very similar and the author concluded that the impedance of the foot was controlled by the lower part of the leg. Assuming a footstep impact as a single degree of freedom event, the author calculated the mass and stiffness properties from the impedance measurement. To simulate the behavior of footsteps better, the author recommended using a thin piece of metal to the existing tapping machine to capture the overall footstep noise characterization. The author did not manufacture such a machine.

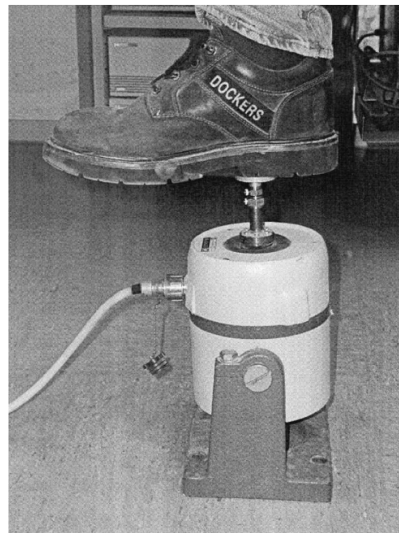


Figure 2-4 Test setup to measure the human foot impedance with shoes on, reprinted with the permission of the journal, see Appendix B.1

Most of the modifications proposed for the tapping machine have been to correlate its input force better with the footstep impacts. Efforts have also been made to conduct in-situ measurements of the force from the tapping machine. Such efforts are limited due to the complexity involved in this type of measurement, as noted by an author in 2018 [70].

Watters [14] added a piezoelectric transducer at the bottom of the tapping hammer to compare the measured force with the footstep impact force. The author observed that the tapping hammer rebounds after each impact which is considered to be an expected behavior for the machines built at the time (1965). This rebound was observed for a concrete floor and a wood frame floor.

Lietzén et al [70] modified one of the five hammers in the tapping machine to add a force transducer and an accelerometer. The authors used these to observe the difference in the measured input force levels with a cushion vinyl floor on a CLT structure. The peak input force level was reduced from 1700 N to 500 N, and the duration of the impact increased from 0.8 sec to 1.5 sec. No details of the modifications for the tapping machine are present. However, later work by the author [71] provide a schematic and some photos of the modified machine. A custom impact tip was built to accommodate the force transducer while still meeting the curvature requirement on the impact tip. Twenty-four mock-up constructions were tested and the differences between different assemblies were evident above 500 Hz. Below 100 Hz, the impact force on all the floors was within 3 dB, regardless of the type of construction. The authors also had to manually set the force level to zero between impacts so that the force transducer does not read the impact force from other hammers in the tapping machine and cause unwanted noise in the signal.

Shi et al [23] created a force plate with three transducers to measure the in-situ input force from a tapping machine. Dodd et al [72] converted a tapping machine hammer into a modal hammer by creating a hinge so that the hammer could be held but could also fall freely on the floor. The impact force was calculated using an ultrasonic proximity sensor. Olsson et al [66] performed a modal analysis on a tapping machine hammer and showed that it could be considered a rigid body below 1500 Hz. They added an accelerometer at the top of the hammer and calculated the input force based on the mass and the measured acceleration.

Research has also led to the development of alternate input sources, although none so far have been incorporated within the ASTM standards. The most prevalent alternate source is a rubber impact ball that is dropped from a height of 1 m (Fig. 2-5 right), and its predecessor, the bang machine (Fig. 2-5 left). These impactors are a result of extensive research done in Japan and Korea where children running and jumping are considered the most annoying noise sources for residents [17]. These heavy-soft impacts do not correlate well with a light-hard impactor such as a tapping machine [16] and there was a need to build a new heavy-soft impactor.

In 1978, the Japanese JIS A 1418 standard was modified to add a new impactor where an automobile tire was attached to an arm on a motor [73]. This machine is more commonly known as the ‘bang machine’, possibly because of the loud ‘bang’ created during the impact on a floor assembly. The soft tire would remain in contact with the floor for longer and would provide high excitation levels in low frequencies, as compared to the tapping machine. A schematic for such a machine is shown in Fig. 2-5 on the left. This schematic was reproduced with permission from the journal, as documented in Appendix B.2.

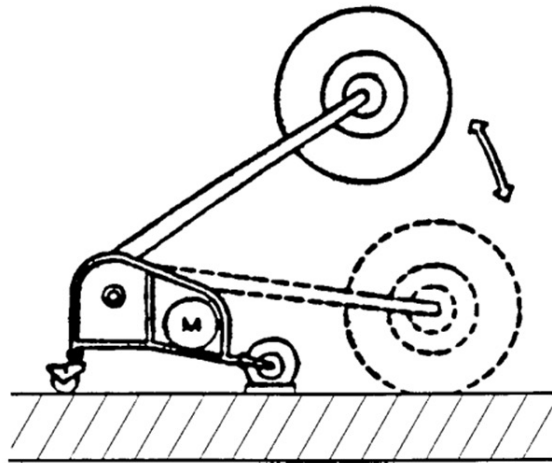


Figure 2-5 A schematic showing the operation of the bang machine , reproduced with the permission of the journal (see Appendix B.2) – left, and the rubber impact ball – right.

There were complaints of floor damage due to the bang machine, especially on lighter floors [16, 17, 73] and a new and improved heavy-soft impact source was needed. This new source was reverse engineered based on the desirable peak input blocked force level and the duration of the impact. This new rubber ball is commonly known as an impact ball, shown in Fig. 2-5 (right). The rubber ball showed approximately 6 – 7 dB lesser force exposure levels in low-frequencies than the bang machine but had a very similar performance in the mid and high-frequency range [16]. The force measurement method has not been discussed in this work. Another study showed that the mean force level with the rubber ball is approximately 1500 N, as compared to the bang machine of approximately 3890 N [74].

In a study by Tachibana et al [16], the authors compared the radiated SPL from impacts from a standard tapping machine, bang machine, new impact ball, child jumping, and child running. These were compared for different floor coverings. The child jumping and the impact ball showed a very good correlation for most of the floors. The bang machine, however, showed 3 – 7 dB higher force levels and the tapping machine showed approximately 15 – 25 dB lower force levels in low frequencies as compared to child jumping. After 125 Hz, the tapping machine had approximately 7 – 10 dB higher force levels for most of the floors when compared to a child jumping.

Jeon et al [17] compared the noise spectra from an impact ball, bang machine, tapping machine, high heel walking, barefoot walking, child running, and child jumping. The tests were conducted in a box-frame type structure with reinforced concrete slab floors, a representative construction of buildings in Korea. Their work showed that the impact ball showed the best correlation with child running and jumping inputs. The authors also conducted a subjective evaluation of over 35 apartments with representative impact sources (jumping, walking, etc.) and standard impact sources (tapping machine, impact ball, and bang machine). The listeners were asked to mark the impact source that sounds

the closest to representative impact sources. This analysis showed that the bang machine and the impact ball ‘sounds’ the most similar to children running and jumping. For this work, the impacts were made only in the center of the floor and the SPL was measured only at a single location in the receiving room using a binaural head.

In a separate work by the same authors [15], the authors measured the impedance of a human foot (while sitting in a hammock), bang machine, impact ball, and a tapping machine. The first natural frequency for the human foot was observed at around 4 Hz, the impact ball and bang machine were at around 20 Hz, and the tapping machine was at approximately 40 Hz. The force measured due to different impact sources was also compared and the authors concluded that the impact force spectra for footsteps most closely match the impact ball.

Späh et al [75] measured the radiated SPL in receiving room at general occupant locations using a dummy head for human walking and dragging furniture. The authors also tested the impact ball, standard tapping machine, and a modified tapping machine with a 12.5 mm elastic pad below the hammers to reduce the high-frequency impact energy. The authors observed the slope of regression for the impact ball to be very close to 1 and the slope was 0.23 for the standard tapping machine.

Olsson et al [76] measured the input force from the impact ball on a timber and a concrete floor and observed that the frequency spectra for the force were within 1 dB of each other from 150 – 170 Hz for both floors. This is advantageous, especially because currently, there is no stipulation within the standards to measure the impact force. Warnock [25] tested approximately 190 floors with the impact ball, tapping machine, and a human walker and concluded that the impact ball correlated the best with footsteps for these floors. This impact ball is now standardized within the ISO standards [77] and can be used in conjunction with the standard tapping machine to evaluate floors where low-frequency noise is a concern. The standard restricts SPL measurements with the impact ball below 630 Hz OTO band, instead of 3150 Hz OTO band used for the tapping machine. Within the US, ASTM has not added the impact ball within the standards but acousticians occasionally use it to study the low-frequency performance of floors.

In the next sub-section, we will discuss some of the prominent work done to better understand and improve the existing sound measurement methods, particularly looking at the low frequencies.

2.4.2 Radiated sound measurements

One of the early efforts to improve the correlation of the tapping machine measurements with subjective response was to change the reference curve used to calculate single number ratings. Olynyk et al [30] recommended using a flat reference curve for the entire bandwidth and showed an improvement in rank ordering 25 concrete floors with different floor coverings. Gerretsen [13] proposed using a flat curve with upward bent edges at the low-frequency and high-frequency ends, shaping it like a saucer. This proposal was based on testing 49 structures with male footsteps and a standard tapping machine. Bodlund [12] re-iterated using a flat reference curve. The author conducted 160 tests on 22

structures and obtained the subjective response of 398 residents. Several different reference curves were studied and the author used linear regression to show that the flat reference curve had the best correlation. Scholl et al [78] proposed using A-weighting to get single number performance, simply for the reason that it will make it easier for the laymen to relate the performance of the floor with other sources, such as traffic noise.

Efforts were also made to modify how the measurements were made in the receiving room. Schultz [67] proposed measuring peak SPL in the receiving room instead of room-averaged levels, based on an idea proposed by Hamme [67, 79]. The author argued that the tapping machine produces a transient event and it should be treated as such. The author predicts that the peak level measurements will not be affected by room diffusivity and allow error-free measurements in low frequencies. It will also eradicate the need to normalize the measured data with a standard reverberation time of 0.5 seconds. Nordstedt [68] evaluated the recommended measurement method for a concrete and a wood-frame assembly and did not find any significant improvement in the correlation between the subjective reaction and single-number ratings.

The focus of research has also been to evaluate whether low-frequency OTO bands are important to truly understand impact noise performance of floor structures. Low-frequency noise is a difficult problem to tackle because the performance is difficult to change without drastic modifications to the structure, for example adding mass using a thick, suspended ceiling [63]. Most of the floor coverings and resilient layers do not show any significant improvement in performance below 350 – 400 Hz [67, 80]. A study showed that complaints from a carpeted area (IIC 80) were just as many as complaints from a non-carpeted area (IIC 55) from the residents in a building [7]. Low frequency noise is also difficult to mask due to background noise, so it is generally reported annoying [7].

Researchers have long postulated that the 100 Hz lower limit for impact noise standards may be insufficient and lead to a poor correlation of single number ratings with the subjective reaction of the residents. Research in Sweden explains that until 1994, buildings taller than two stories were not allowed due to fire risk, and therefore, the lower limit of 100 Hz was ‘adequate’ at the time. With the advent of better building construction materials, higher buildings were allowed and frequencies below 100 Hz became important. In fact, the Swedish impact noise standards reduced their low-frequency limit to 50 Hz, and then recently further down to 20 Hz based on a study by Öqvist et al [81].

Warnock [48] showed that most of the energy due to footsteps lies in frequency bands below 100 Hz, which are not a part of the standards. This is based on a test with a human walker on 75 structures with various configurations – concrete floors with floating floors, carpet, carpet and underpad, and wood frame floors.

Ljunggren et al [31] evaluated ten building structures with different configurations subjectively and based on the standards. The standard data were processed using multiple lower cut-off frequency bands and were correlated with the subjective data. 26%

correlation was observed when data at 100 Hz and above were considered. This correlation improved to 32% by including frequencies down to 50 Hz and to 75% correlation with data down to 20 Hz OTO band. The authors recommend making measurements down to the 20 Hz for the current standards.

Öqvist et al [81] also recommend that the measurements should be made down to 20 Hz for lightweight structures and 40 Hz for heavyweight structures if the walker is wearing socks. The author argues that the existing standards were written based on hard-heel impacts but wearing socks or soft-sole shoes is more common inside residential spaces and the standards should reflect that. A concrete and a wood structure with the same ISO impact rating differed by 12 points on the subjective annoyance scale with a walker wearing socks. The metric that best correlates with this subjective evaluation is when the frequencies down to 20 Hz are included.

Nordby [27] presented the SPL spectra from the tapping machine impacts in a hotel building and showed that a considerable part of the impact energy lies below 100 Hz. The author recommends making measurements as low as 20 Hz. Blazier et al [7] instrumented a tapping machine with a force transducer and showed that a significant part of the impact lies below 100 Hz which should be included to improve correlation with subjective response.

Bodlund [12] tested two assemblies that showed the same impact noise rating but had different subjective ratings. The author observed that there were differences in performance between the two assemblies below 100 Hz. The assembly that was subjectively better had a lower low-frequency content than the other assembly but the ASTM standards failed to quantify this because of the low-frequency measurement limit. This seems to be the consensus in the acoustics industry [14, 23-25, 29, 42, 48, 67, 78, 82].

Based on this research, ISO adopted a spectrum adaptation term in 1996 and allowed measurements down to the 50 Hz OTO band [77, 83]. The COST Action TU0901 study [84] (now ISO technical specification 19488 [85]) recommends using this spectrum adaptation term for an improved correlation between impact ratings and walking noise. Scholl et al [78] state that the adaptation term was introduced to transform the original ISO single-number rating to A-weighted SPL due to people walking on the floor. Currently, the ISO impact rating can be provided with or without a spectrum adaptation term.

Research also shows that floors fundamentally perform differently in different frequency regions. LoVerde et al [29] postulated that the impact noise from floor-ceiling assemblies is generated, experienced, and mitigated independently in the low-frequency and high-frequency domains. Any change to the structure affects the low-frequency and high-frequency response independently. This observation was made after reviewing over 1900 assemblies tested over a span of 15 years by the authors. The authors also measured the airborne transmission performance of these assemblies and showed that the correlation between the low-frequency and high-frequency components was 0.89, however, such a

correlation for impact noise transmission was 0.13. This showed that the performance of the floors is different in low and high-frequency regions. The authors showed that this phenomenon also relates to the subjective complaints from such assemblies. Previous work by Watters [14] correlates with this conclusion where the author explains that the response of a structure in different frequency ranges is dependent on different processes. The low-frequency response is dependent on the change in momentum on impact, while the high-frequency response depends on the product of the local compliance and the mass of the structure.

LoVerde et al [29] suggest using a Low-frequency Impact Rating (LIR) and a High-frequency Impact Rating (HIR) instead of a single-number rating as defined within ASTM. A draft standard was introduced within ASTM based on this work and after much deliberation, both ratings were recently standardized [39, 86]. The ratings can be reported alongside the ASTM single number ratings to give a better indication of the impact performance of an assembly.

Measurement of sound in low frequencies is challenging. Even though sound prediction models exist, a literature review [64] divides most of the existing models into two categories: Statistical methods such as Statistical Energy Analysis (SEA), or, deterministic modeling methods. The statistical methods work well for higher frequencies, but fail to work at low frequencies where the field is non-diffuse [32-34]. Deterministic modeling approaches require considerable knowledge of the material properties, which are not easily available. Even with this level of detail, such models are prone to be very susceptible to real-world assembly uncertainties.

Research interest has increased in low-frequency noise measurement in recent years. Pedersen et al [38] detail the Swedish and the Danish standard method for measuring low-frequency noise. For the Swedish method, the sound is measured from 31.5 – 200 Hz OTO bands at three locations: two locations represent normal ear locations for the residents, and the third location was found by scanning all the room corners and edges to find the loudest point, which was then C-weighted. The three datasets were averaged to get the overall sound level in the room. The Danish method was a modified version of the Swedish method where the first two microphone locations have a minimum distance requirement from the room boundaries. For the third location, a corner was chosen arbitrarily and explicitly stated in the report. The measurements were made from 5 – 160 Hz OTO bands.

Pedersen et al [38] used a computer simulation model to understand the sound field in a room below 200 Hz. The authors observed that for modal frequencies of the room, all the corners had maximum SPL and for non-modal frequencies, some of the corners had maximum SPL compared to any other point in the room. The authors postulated that if multiple corners around the room are measured, the test engineer can get the maximum SPL anywhere in the room. The proposed corner method, the Swedish method, and the Danish method were compared in three small rooms (16 m³, 22 m³, and 33 m³). The target levels in these three rooms was defined as the SPL in more than 10% of the room, which the authors defined as L₁₀. Note that this is different from the generally accepted

L₁₀ definition in acoustics – the SPL exceeded 10% of the time. In their work, the authors found that the Danish method underpredicted the L₁₀ target and showed a larger variability as compared to the Swedish method. The Swedish method provided results within 1 – 2 dB of the set target but failed in one case where a corner was affected by flanking. Since the Swedish method only considers the loudest corner or the edge points, it is highly susceptible to flanking noise. The authors' corner method overestimated the target values by 3 – 5 dB and they proposed that the corner measurements should be averaged with the measurements in the middle of the room to improve this comparison.

This corner method was later standardized within ISO 16283-2 [77] for rooms with a volume below 25 m³ for the 50 – 80 Hz OTO bands. At least four room corners should be measured – two near the floor and two near the ceiling. The measurements are made within 0.3 – 0.4 m of the three walls that make a corner. The maximum SPL measured in any corner for any OTO band under study is used as the 'corner' SPL. The room-averaged SPL is measured just as before (see Section 2.2) and is averaged with the corner measurements using a 2:1 ratio, respectively. The corrected spectrum is used to calculate the single number rating for the assembly under test. The corner method is not a part of the ASTM standards.

Hopkins et al [33] mention that the 2:1 ratio used in the ISO standard comes only from empirical models. The authors performed an airborne field test with masonry and timber construction using a microphone grid. The reference levels were obtained as an average of the microphone grid measurements. The authors showed that the corner method resulted in a lower single number rating as compared to before. This is primarily driven by the higher SPL recorded in the corners that are now a part of the final spectrum. The authors also observed that the corners opposite to the assembly under test had higher levels as compared to the corners closest to the assembly and they recommend measuring only two corners in the field and skipping the corners close to the assembly under test. The authors showed that for 37 lightweight structures tested with a dense grid, the old room averaged method underpredicts the room average by approximately 5 dB below 250 Hz, while the corner adjusted method produces data within 1 dB of the microphone grid average from 50 – 80 Hz. The authors also recommend making measurements in octave bands instead of one-third octave bands. They argue that by using octave bands, the number of modes in each band is higher, and the uncertainty in measurements may be improved.

Simmons [36] studied the corner measurement method, along with the standard measurement methods [77]. The room average was calculated after making measurements in a dense microphone grid, which was used to calculate the uncertainty of all measurement methods. The author observed a higher standard deviation for the scanning methods as compared to the discrete point method. This is the opposite observation as compared to another study [87] that showed that the scanning method had lesser uncertainty than the discrete method. Simmons mentioned that the scans were made close to the middle of the room, which may be the reason why the scanned results underrepresent the room average. The author also showed that the corner method reduces the variability below 100 Hz but did not compare the SPL from the corner method to

room averaged SPL. This test was conducted for an airborne transmission test, but the results could be applied to impact tests too.

Uosukainen [88] recommends using the ‘Waterhouse Correction’ to account for higher energy density close to the room edges. The author argues that measurements can be made in the middle of the room and Waterhouse correction can be applied using the knowledge of modal density and the final single number rating can be adjusted based on the correction. Getting the modal density can be challenging because it either requires a simulation model for each room to be tested, or it requires manual mode picking based on several narrowband measurements in the room. This correction is also limited to rooms with simple, parallelepiped shapes.

Schoenwald et al [37] found that for a room (volume < 25 m³), the Waterhouse correction failed to predict the sound energy in the room. This was done for a mock-up room built inside a reverberation chamber for airborne sound transmission tests. The target levels were calculated using measurements in a dense microphone grid, and the authors made measurements using all the standard methods, the corner method, and along the diagonal of a room. The standard scanning method underpredicted the room average by approximately 3 – 4 dB in the mid-frequency range. The corner method overpredicted the room average SPL by 1 – 2 dB, and when used above 100 Hz, showed a lot of variation between different corner locations as the wavelength decreased in comparison to the distance from the corners. The authors also observed that for an empty room, all corner SPL values were within 1 – 1.5 dB of each other, but the variation increased to 1 – 6 dB for a furnished room. Additionally, since the corner adjustment is made only for the 50 – 80 Hz OTO bands, a 6 dB discontinuity in the data was observed between the 80 Hz and 100 Hz OTO bands which is not a physical indication of the assembly performance. The measurements along the diagonal overpredicted the average SPL by approximately 1 – 2 dB in low to mid-frequencies and had a slightly higher uncertainty than the scanning of the corner methods.

Garg et al [89] recommended using a hybrid measurement approach to measure the sound energy in receiving rooms to reduce uncertainty. The authors recommend using the existing method from 200 – 5000 Hz OTO bands but measuring sound intensity in lower frequencies (50 – 160 Hz OTO bands). It is unclear how to combine the two datasets to get a single number rating.

The author has previously [35, 90, 91] recommended using a reference panel with known sound power in the test chamber and measuring the radiated SPL. The relationship between the two can provide a set of ‘calibration factors’ that can account for the effect of room modes. While testing the real structure in the same test chamber, the same calibration factors can be used to calculate assembly sound power from the measured SPL values. The authors validated this method for a small-scale assembly in a small room where the Schroeder’s cut-off frequency was approximately 300 Hz. A full-scale floor-ceiling assembly was not evaluated. Additionally, this method was recommended for lab tests and would be nearly impossible to implement for field tests.

To summarize the previous sections, the tapping machine does not produce impacts similar to human footsteps, and it fails to rank order the floors subjectively with footsteps. We have also seen that it is important to measure the low-frequency content during an impact test for a floor-ceiling assembly to better characterize it subjectively, however, no definitive approach to do so currently exists, especially within ASTM. There is a need to define a measurement method that improves the uncertainty of the current measurement method, especially with the introduction of LIR in ASTM, where the sound field is measured in frequencies down to 50 Hz. There is also a need to better characterize the input from a tapping machine, which can be done by making FRF-like measurements.

Blazier et al [7] in 1994 supported developing a transfer function type method to relate the radiated sound with the input force. Olsson et al [66, 76] also recommended creating an FRF-type measurement method to characterize floor-ceiling assemblies. These suggestions are based on the concept of dividing the impact noise problem into a Source-Path-Receiver domain, where the Source is the input mechanism, the receiver is the microphone or the residents, and the path is everything in between. An FRF-like measurement is a way to relate the receiver response due to source input.

The automotive industry faces a similar challenge where the engineers try to ascertain the response at the driver's ear location due to engine noise. In this case, the source is the engine, the receiver is the driver, and the path is the chassis of the car. Similar to footstep noise in buildings, automotive engineers are trying to get an FRF between receiver (driver's ear) and source (engine) locations. The reciprocity method is widely used in the automotive industry to estimate this FRF and the next sub-section provides more details on this method.

2.5 Reciprocity method

In 1860, Hermann Von Helmholtz studied the acoustic behavior of open-ended pipes and asserted that the acoustic fields exhibit reciprocal behavior. Helmholtz later formalized the reciprocal behavior for simple sources (monopoles) and field point pressures, limiting the application to only acoustic fluid mediums. Lord Rayleigh furthered this development and showed that the principle can be extended to harmonic vibrations in dissipative sources if the system is linear. This theory was formally presented to the Mathematical Society of London in 1873 [92]. In the early days, the application of the reciprocity principle was very limited. Early researchers did not trust the theory enough because it seemed too vague and seemed to be applicable to just about any system. It wasn't until 1959 when a Russian scientist L M Lyamshev published a formal proof of the reciprocity theory for vibrational interaction between elastic shells and compressible fluids that paved the way for modern applications of the principle [92].

Rayleigh and Helmholtz also implied that the local impedance boundary conditions should not invalidate the validity of the theory, another avenue where researchers found the theory to be too vague to be of any practical use. Later, Skudrzyk [92, 93] confirmed this postulation in 1954. Even though Rayleigh and Helmholtz limited their earlier theory to only local impedance boundary conditions, Skudrzyk found that all the components in

the entire system could be considered as a ‘total system’ as long as it behaves linearly. This opened the avenue of applications for the reciprocity theory.

The theory was first incorporated within the aerospace industry, where Lyamshev’s work from 1959 was essentially repeated. Lyamshev proved that if there is a localized force on a structure that is causing a response, a speaker could be used instead of the force to understand the same relationship between the force and speaker locations. An omnidirectional source was used at the receiver location and the induced vibration at the force location was measured. These tests were later successfully conducted for an airplane structure in 1985 [94] and a ship structure in 1973 [95]. The reciprocal tests are found to be far simpler, less expensive, and less time-consuming compared to the direct tests. Fahy in 1992 [92] proposed that similar measurements could be made for land vehicles such as automobiles, something that is widely done now.

For cars, the reciprocity principle has been successfully used for identifying the noise contributions of different engine components, exhaust components, etc. for a pass by test [96], but the most used application for the reciprocity method is Transfer Path Analysis (TPA) [97-101]. Consider the example in Fig. 2-6 for a car chassis to explore the SPL response at the driver’s ear location due to engine noise and vibration. The direct measurement procedure is shown on the left. The FRFs between the engine mount location and the driver’s ear location (P/F) can be obtained by mounting a vibration generating source at the engine location and measuring the SPL at the driver’s ear location. Mounting this vibrating source can be difficult since it is very important to align the input force direction with the engine. This is a major source of error in the direct measurements.

For the reciprocal measurements (Fig. 2-6 right), a monopole source is placed at the driver’s ear location and the acceleration response is measured at the engine mount location to get the FRF (A/\dot{Q}). The reciprocity principle states that

$$\frac{P}{F} = \frac{A}{\dot{Q}}, \quad (2-2)$$

where, P is the sound pressure at the driver’s ear location (Pa), F is the engine mount input force (N), A is the acceleration at the engine mount location (m/s^2), and \dot{Q} is the acoustic volume acceleration of the speaker (m^3/s^2). The volume acceleration of a speaker is given as a multiplication of the effective speaker radiation area and the surface acceleration [102].

Measuring the acceleration response at the engine mount location is generally easier, less expensive, less time-consuming, and more accurate than placing a vibration generating source at the engine mount location. This makes reciprocity measurements a useful tool for the automotive industry. Approximately 3 dB differences are generally observed between the direct and reciprocal FRFs and are considered acceptable [97].

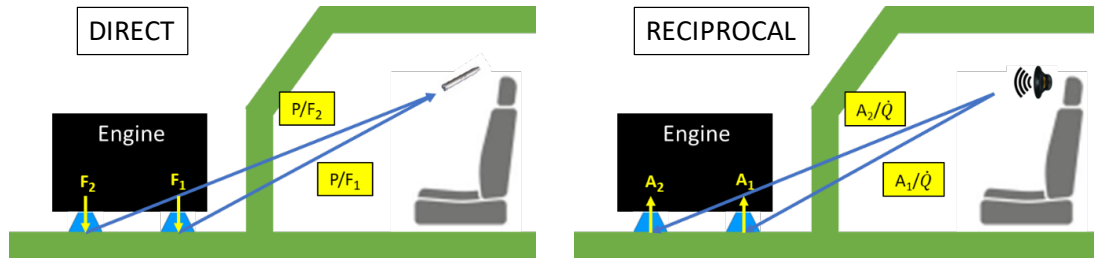


Figure 2-6 Direct measurements and reciprocal measurements for a car assembly are shown on the left and right. Both tests can be used to evaluate the FRF between the engine mount location and the driver's ear location

The automotive industry use case is very similar to the floor-ceiling assemblies where the source (an input force generating mechanism, such as a tapping machine or the impact ball) needs to be related to the receiver (residents, or the measurement microphones) by quantifying the path (floor-ceiling assemblies). In this research, we will evaluate the use of reciprocal measurements as a means to better evaluate and rank-order the impact performance of floor-ceiling assemblies.

The next Chapter discusses the development and methodology of the experimental and simulation work undertaken for this research.

3 Development and Methodology

The first objective of this work addresses the need in the literature for FRF-like measurements to compare the performance of different floor-ceiling assemblies. Two methods are discussed - the direct P/F measurement, or the reciprocal A/\dot{Q} measurement. The current test method does not require for the input force to be measured with the tapping machine and P/F FRF is not measured. The first step of this research was to measure the input force from the tapping machine on different floor structures. The ISO impact ball is also evaluated and the input force is measured. If the peak force variation for different floor types is high, it reinforces that FRF-like measurements are needed to study the impact performance of floor-ceiling assemblies.

A simulation model was used to achieve the second objective defined for this work – improving measurement reproducibility in low-frequencies. Several methods are evaluated, including the reciprocal method to get A/\dot{Q} FRFs. The reciprocal measurements are also compared to the direct measurements by testing field assemblies.

The low-frequency non-diffuse field variability that exists for the direct measurements (due to different microphone locations) will still exist for the reciprocal measurements (for different acoustical source locations). The simulation model was used to develop acoustical source placement guidelines and acceleration measurement guidelines on the floor. These guidelines were evaluated for some real structures and the data were compared with the standard ASTM test method.

This Chapter details the force measurement methodology, the simulation model and the measurement ideas simulated, explains the simulations performed to develop the reciprocal measurement guidelines, and provides details of the test structures evaluated for their impact performance using the proposed method.

3.1 Input force measurement methods

A standard tapping machine, a standard ISO impact ball, and a modal hammer were used for this study. These sources were used to impact seven floor-ceiling structures and the input force was measured. This section provides instrumentation details for force measurement, details of the floor-ceiling assemblies tested, and the data acquisition parameters. Floor impedance was also measured and the details are included in Appendix A.4.

3.1.1 Force measurement instrumentation details

The standard tapping machine and the impact ball do not have a way to measure the input force directly. Therefore, modifications were made to both sources to measure the force during a test. This section provides details of these modifications and provides information about the modal hammer used for this work.

3.1.1.1 Tapping machine

Four of the five hammers on the tapping machine were removed for simplicity, and the fifth hammer was re-designed to add a PCB 208C03 force transducer between the hammer shaft and the hammer head impactor, as shown in Fig. 3-1. The hammer head impactor was left unchanged to meet all the standard requirements and the hammer shaft was re-manufactured to accommodate the transducer. The total weight of the hammer was 503g which meets the standard requirements ($500 \pm 6g$).



Figure 3-1 Four of the five hammers were removed for simplicity from a standard tapping machine (left) and a force transducer was added between the hammer head and the shaft of the fifth hammer to measure the input force (right)

The force transducer is not at the same location as the impact tip, so the force measured with the transducer is not the same as the force injected into the structure. Figure 3-2 shows that the force injected (F_{floor}) is different from the measured force at the transducer location (F_{mid}) and is dependent on the dynamics of the hammer body. An FRF relationship between the two was obtained by suspending the modal hammer in free-free boundary conditions (Fig. 3-2 right) and using a modal hammer to impact the hammer tip (F_{tip}). This FRF was used to scale the input force measured during the tests using

$$F_{floor} = F_{mid} \times \left(\frac{F_{tip}}{F_{mid}} \right)_{free-free BC}, \quad (3-1)$$

This correction was performed in the frequency domain. The term ‘ F ’ in this document is defined as the force spectrum, which is the square root of the power spectrum of the force channel (G_{ff}). A time domain ratio was also calculated based on the peak force level difference between the force transducer and the modal hammer signals. This ratio was used to correct the measured time domain spectra for all the tests on the floors. The assumption here is that the FRF between the force transducer location and the impact tip

location is the same in the free-free test and for impacts on the floor-ceiling assemblies. The correction FRF is shown in Appendix A.1

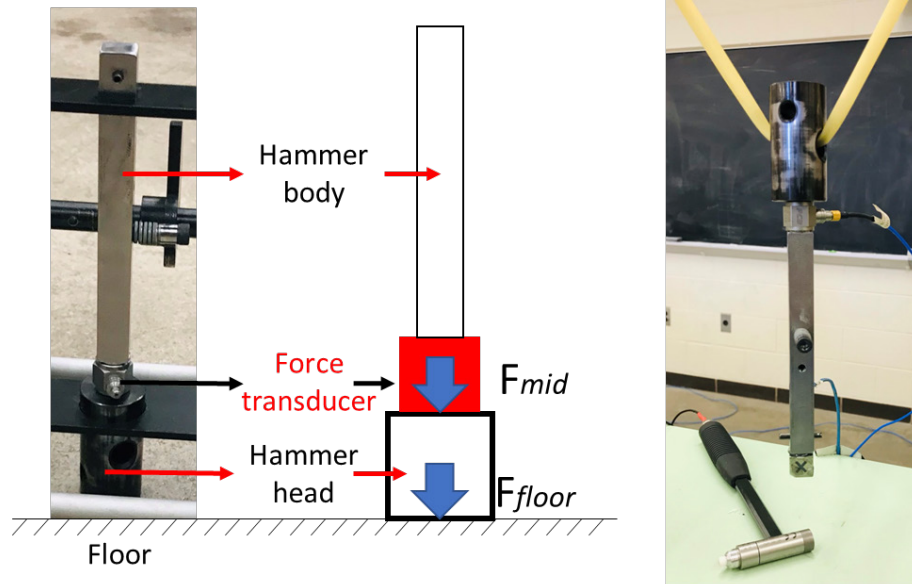


Figure 3-2 The force injected by the tapping machine into the floor (F_{floor}) is corrected using an FRF between the transducer location and impact tip in free-free boundary conditions. The correction is needed due to the mounting location of the transducer

Only a single impact from the tapping machine was used for each average, instead of the 2 Hz frequency for one hammer. This was achieved by letting the hammer fall freely during the acquisition period, and then manually turning off the tapping machine to avoid any further impacts until the next average. This was done to minimize the impact-to-impact variation [103, 104] that was observed when the hammer was allowed to drop freely at a frequency of 2 Hz. More details of this variation are presented in Appendix A.2

3.1.1.2 ISO Impact ball

The baseline input force exposure levels are defined in the ISO standard [77] but it is unclear how these measurements should be made. For this work, a force plate was created using a 12.7 mm (0.5 in) thick, 127 mm (5 in) diameter 6061 Aluminum plate with three PCB 208A03 force transducers, shown in Fig. 3-3. The impact ball was dropped from a height of 1 m on this force plate. The size of the impact ball as compared to the force plate is shown in Fig. 3-3 (c). Figure 3-3 (b) shows the three force transducers at the back of the plate. The accelerometer in the middle of the plate was not used for this work.

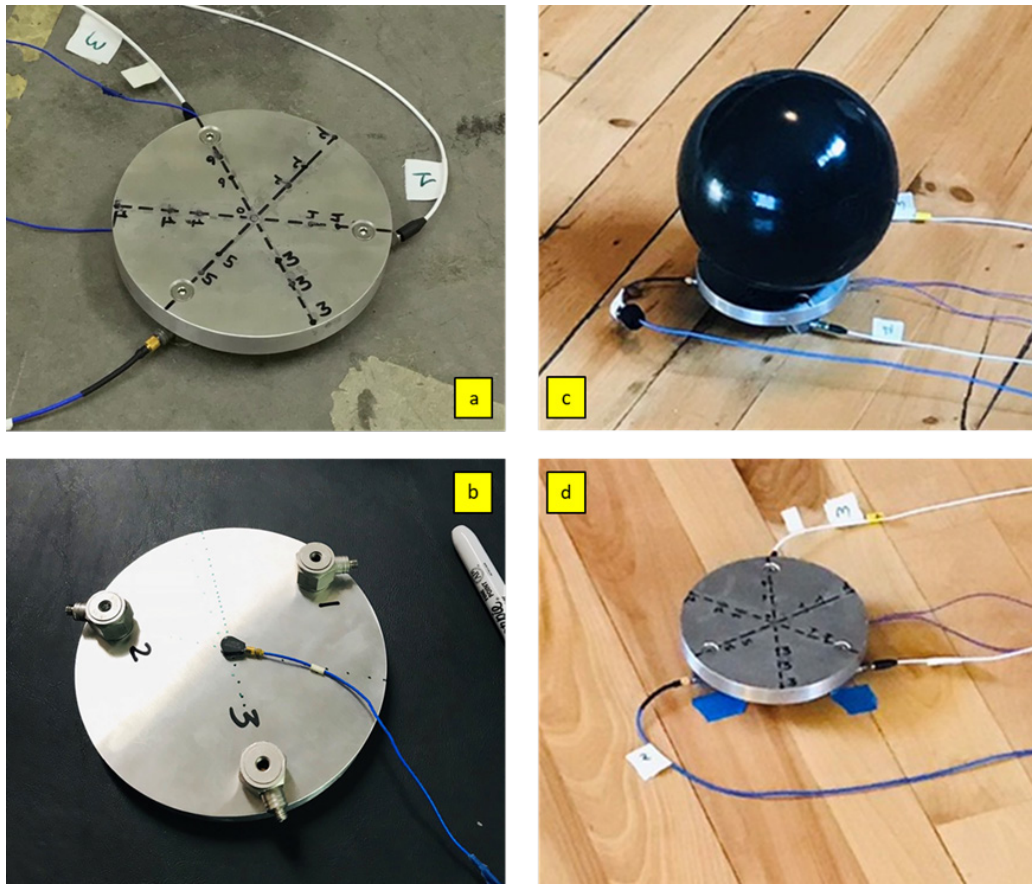


Figure 3-3 The impact ball force plate is shown in assembled condition for one of the floors (a); the three force transducers used to measure the input force and an accelerometer (not used for this work) (b); The size of the impact ball in relation to the force plate (c); and the force plate assembled on another floor under test (d)

The force plate was assembled on the floors using hot glue for all the floors with a hard surface finish. For floors with a carpet finish, a $26 \times 32 \times 3$ mm steel plate with a hook side Velcro was rubbed into the carpet and the force transducers were glued on this steel plate. A separate lab test showed that this mounting method does not significantly affect the dynamic response below 250 Hz for a mounted accelerometer with a force input on the floor (see Appendix A.3). It was assumed that the same would be true for force transducers.

The input force was measured with the three force transducers and added in the time domain to get the overall force which was converted to the frequency domain using Fast Fourier Transform (FFT) process. A simulation model, analytical calculations, and an experimental modal analysis were used to verify that the modes of the force plate will not affect the measurement data below 2000 Hz.

3.1.1.3 Modal hammer

A PCB 3lb modal hammer (PCB 086D20 [105]) was used with the PCB 08461 brown, soft plastic polyurethane impact tip. The modal hammer is outfitted with a force transducer so that the input force can be measured. The hammer was considered as a reference source for all the test floors and Fig. 3-4 shows the modal hammer and the force transducer.

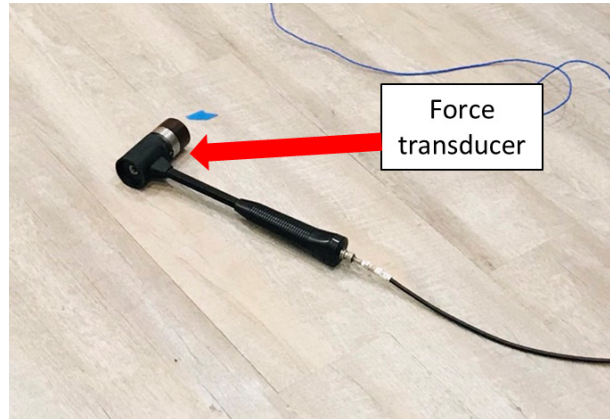


Figure 3-4 A PCB 086D20 modal hammer was used as a reference source for this work to directly measure the input force using the onboard force transducer

3.1.2 Details of the floors tested

To sample a variety of floor-ceiling assemblies encountered in the field, a combination of heavy and lightweight floors was studied. Two heavyweight reinforced concrete floors (referred to as HC1 and HC2), three lightweight joist-framed floors with hardwood finish (referred to as LH1, LH2, and LH3), and two lightweight joist-framed floors with carpet finish (referred to as LC1 and LC2) were studied for this work. Most of the structures were residential assemblies and in some cases, are old enough that either the component drawings weren't available, or the owner/resident was unaware of all the construction details. Table 3-1 provides the details of floor constructions, where available, and Fig. 3-5 shows a snapshot of all seven floors under test.

Table 3-1 Floor assembly details (where available) for all floors under test

Floor Code	Floor Name	Assembly details (where available)
HC1	Heavyweight concrete	Reinforced 8-in concrete slab on grade
HC2	Heavyweight concrete	Reinforced 6-in concrete on a 1/2" metal sheet
LH1	Lightweight hardwood	2×10 joist, 16" O.C. 3/4" sub-floor ship lap, rest unknown
LH2	Lightweight hardwood	TJI truss, 16" O.C. 3/4" solid hardwood subfloor, rest unknown
LH3	Lightweight hardwood	2×8 joist, 16" O.C., rest unknown
LC1	Lightweight carpet	Carpet tile finish, rest unknown

Floor Code	Floor Name	Assembly details (where available)
LC2	Lightweight carpet	High-pile carpet finish, rest unknown



Figure 3-5 Seven floors were tested for the input force measurement with the tapping machine, an impact ball, and the modal hammer: Two heavyweight concrete (HC) floors (left), three lightweight joist-framed floors with hardwood finish (LH) (center), and two lightweight joist-framed floors with carpet finish (LC) (right)

Due to equipment limitations and the test floor unavailability (in that order), floors LC2 and LH2 were not tested with the impact ball. These floors were only tested with the tapping machine and the modal hammer. For all the floors, the input source was placed approximately in the middle of the floor structure and care was taken to move the input location away from heavy sources on the floor (such as a couch, bed, etc.).

3.1.3 Data acquisition parameters

Siemens TestLab software was used for all the force input data measurements for this work. The frequency resolution was 0.5 sec for a total measurement time of 2 sec. The bandwidth was set to 4096 Hz and seven averages were recorded for each floor with each input source. All measurements were triggered based on the input force channel (the reference channel). A force window was used for the tapping machine reference channel, and uniform windows were used for all other cases.

3.2 Simulation model details

A simulation model was created in Simcenter 3D to evaluate different sound measurement strategies. All the simulations were frequency-based and the time dependence of the sound field was ignored. The outputs were calculated based on steady-

state input parameters. This section details the simulation model creation and validation and explains the changes made to the model to simulate specific measurement methods.

3.2.1 Details of the simulation model

A 3.048 m × 3.9624 m × 2.7432 m (10 ft × 13 ft × 9 ft) room was created in Simcenter 3D with standard temperature and pressure conditions of air. The room dimensions are generally what is observed in residential spaces for field tests, but the model was not designed to mimic any specific room. The dimensions were selected to avoid integer multiples and modal overlap. Based on the model, the first simulated room mode exists in the 40 Hz OTO band, and the first OTO band with at least ten room modes is 100 Hz, which is often used as a thumb rule to define a diffuse field. Schroeder's formula from Eq. 2-1 can be used to show that the simulated room is non-diffuse below 245 – 250 Hz. The target of this research is lower frequencies, especially below 100 Hz, and the simulated room was non-diffuse in that range.

Two assemblies were simulated: a 6" concrete assembly (Fig. 3-6 left) and a 1-1/2" wood floor with a 2 × 10 wood joist (19" O.C.) and a 5/8" gypsum ceiling (Fig. 3-6 right). A two-way strong coupling is modeled between the floor vibration and the room sound field. The floor assembly is modeled with fixed boundary conditions and the room floor and the walls are treated with an impedance boundary condition of 10414 kg/(m.s²) to achieve an approximate reverberation time of 0.5 sec (Fig. A-6 in Appendix A.5), similar to the ASTM standards [20].

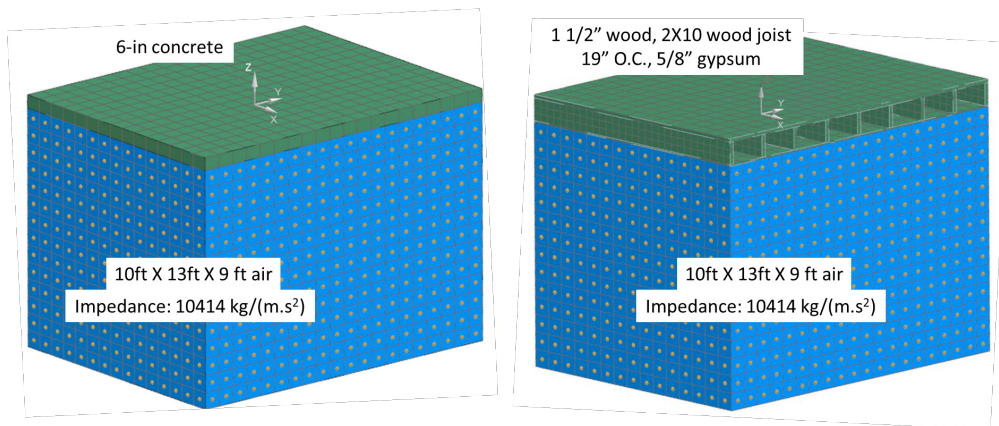


Figure 3-6 The simulation model showing the 10 ft × 13 ft × 9 ft room with 6" concrete assembly (left) and the wood-joist assembly with 1-1/2" floor, 2 × 10 joist 19"O.C., and 5/8" gypsum ceiling. The floor and the walls were modeled with an impedance boundary condition to achieve 0.5 sec reverberation time

The material properties used in the simulation model for concrete [106], wood [107], and gypsum are shown in Table 3-2. The material properties of a field assembly may differ from the values used in the model but these values would allow comparison between different measurement strategies.

Table 3-2 Material properties used in the simulation model

	Mass Density (kg/m³)	Young's Modulus (GPa)	Poisson's Ratio (N/A)
Concrete	2320	27.5	0.2
Wood	640	10.3	0.2
Gypsum	673	0.381	0.2

Five methods were evaluated – ASTM discrete point test method, ISO corner method, diagonal measurement method, intensity method, and reciprocity method. The mesh size used for each measurement method along with the simulated frequency bandwidth are shown in Table 3-3. The mesh size was increased for the reciprocal method to decrease computation time and the frequency bandwidth was reduced to follow the six elements per wavelength recommendation [108, 109]. The frequency resolution used for each method was 1 Hz. All methods were evaluated with the concrete assembly (Fig. 3-6 left) and the reciprocal method was also evaluated with the wood-joint assembly (Fig. 3-6 right).

Table 3-3 Mesh size and frequency bandwidth for the simulation model

	Floor mesh size (mm)	Room mesh size (mm)	Frequency bandwidth (Hz)
ASTM Discrete	56.67	76.67	10 to 561
ISO Corner	56.67	76.67	10 to 561
Diagonal	56.67	76.67	10 to 561
Intensity	56.67	76.67	10 to 561
Reciprocity	200	200	10 to 250

All measurement methods were simulated using a rectangular assembly shape (Fig. 3-7 left) and the reciprocal method was also evaluated with a floor with coupled spaces. A rectangular floor with a 1.83 m × 1 m (6 ft × 3.25 ft) coupled space and a 2.13 m × 0.61 m (7 ft × 2 ft) coupled space (CS shape assembly) as shown in Fig. 3-7 (center). These coupled spaces can be visualized as a kitchen, a dining corner, a closet, etc. A rectangular room with a non-rectangular side primarily used for a bay window (BW assembly) is shown in Fig. 3-7 (right) where a 2 ft addition is shown using 45° edges. The concrete assembly was simulated with all three shapes for the reciprocal method and the wood-joint assembly was only simulated with the rectangular and CS shape for ease of modeling.



Figure 3-7 The top view of the rectangular shape (left), Coupled Space (CS) assembly with two coupled spaces (center) and a Bay Window (BW) shaped assembly (right) used in the simulation model. For ease of modeling, only concrete assembly was created with the BW shape.

The acoustical simulation was validated by comparing the simulated room's natural frequencies with the literature [110]. The first ten acoustical frequencies showed less than 0.1% deviation. The structural simulation was validated similarly by comparing the simply supported natural frequencies with the literature [110] based on a thin plate assumption. The first ten natural frequencies differed by less than 7%. The higher deviation with the structural modes may be due to the thin plate assumption used for literature calculations. More details on the model validation are presented in Appendix A.5 but overall, the simulation model performs as expected from the literature.

The ASTM discrete microphone method, ISO corner method, and diagonal measurement method are discussed in Appendix A.6. The details of the sound intensity and reciprocity methods are provided in the following sub-sections.

3.2.2 Sound Power based on simulated intensity

Sound power is a source quantity (in this case, the floor-ceiling assembly) and it does not depend on the path (the room). This makes sound power an ideal candidate for comparing the performance of different floor-ceiling assemblies. The sound power is given by the multiple of the free-field intensity with the area of the measurement plane. In a room, the reflected sound field may affect the measured intensity negatively. This effect can be minimized by separating the forward and backward propagating sound waves [111].

If the outgoing and incoming waves on a measurement plane can be successfully separated, the intensity calculated using only the outgoing sound waves would be similar to the free field sound intensity. In the simulation model, the SPL and particle velocity

were simulated at a measurement plane 25 mm from the ceiling on 1312 measurement nodes due to a 1N input force in the middle of the floor. The SPL can be defined as

$$p(\vec{r}) = Ae^{jk\vec{r}} + Be^{-jk\vec{r}}, \quad (3-2)$$

where, $p(\vec{r})$ is the total SPL at distance \vec{r} from the radiating surface, $Ae^{jk\vec{r}}$ is the outward propagating sound wave, and $Be^{-jk\vec{r}}$ is the backward propagating sound waves. Separating the coefficients A and B using the simulated SPL would help separate the outward and backward propagating sound wave. Euler's equation [49] relates the SPL and particle velocity using

$$U = \frac{-1}{j\omega\rho} \frac{\partial p}{\partial r}, \quad (3-3)$$

where, U is the particle velocity (m/s), ω is the radial frequency (rad/sec), and ρ is the density of air (kg/m^3). Two equations ($p(\vec{r})$ and U) can be used to solve for two unknowns (coefficients A and B) and outgoing and incoming sound waves can be separated.

The data processing steps are detailed below:

1. Perform a spatial Fourier transform of the SPL on the measurement surface (details in [112])
2. Multiply with a k-filter to prevent noise [113]
3. Use the SPL and particle velocity equations to calculate coefficients A and B
4. Calculate the outward propagating SPL ($Ae^{jk\vec{r}}$) and perform an inverse spatial Fourier transform
5. Multiply the outward propagating SPL with particle velocity to calculate the sound intensity. Multiply with the area of the measurement surface to calculate sound power

This process was simulated for different simulation models with a reverberation time of 0.25, 0.5, 0.75, 1, 1.25, and 1.5 seconds. The outward propagating sound power was compared with the free field sound power for all cases.

3.2.3 Reciprocity method simulations

Two different models shown in Fig. 3-8 were simulated to understand the reciprocal relationship. A 1N input force was applied in the middle of the room and radiated SPL at all microphone locations was simulated (Fig. 3-8 left). At a given microphone node near the corner, the P/F FRF was calculated. At the same microphone node, a monopole source was placed in a separate simulation model (Fig. 3-8 right). The floor acceleration was simulated and the A/\dot{Q} FRF was calculated from the acceleration at the previous force location.

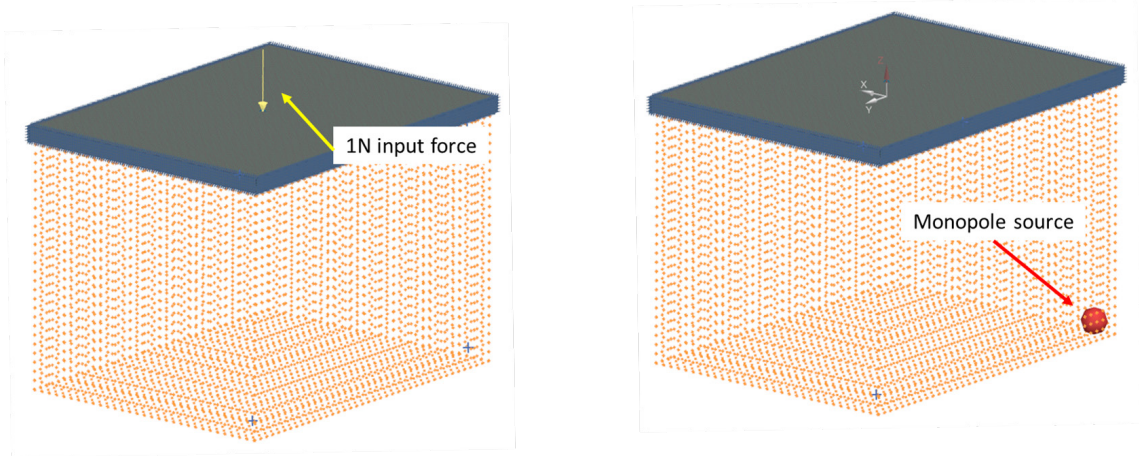


Figure 3-8 The simulation models used to study reciprocity. A 1N input force applied on the floor was used to simulate the radiated SPL at a particular microphone node (left), a monopole source was placed at the same microphone node in a separate simulation model and the acceleration at the previous force location was simulated

Simcenter 3D allows defining a monopole source using a sound power input and volume velocity can be calculated from sound power using [110]

$$W = \frac{\rho_o \omega^2 Q^2}{8\pi c}, \quad (3-4)$$

where, W is the sound power (watts), ρ_o is the density of air (kg/m^3), ω is the angular frequency (rad/sec), c is the speed of sound (m/s), and Q is the volume velocity (m^3/s). For the simulation model, a 1 W steady-state sound power for the entire frequency domain under study was modeled. The calculated volume velocity was differentiated to get volume acceleration (\dot{Q} in m^3/s^2) using

$$\dot{Q} = j\omega Q \quad (3-5)$$

Based on the reciprocity theory, the A/\dot{Q} FRF is the same as the direct P/F FRF. The non-reproducibility problems that affect the SPL measurements due to a non-diffuse sound field would have a similar effect on the reciprocal measurements for different Q source locations. This may lead to poor reproducibility with the reciprocity method. Two approaches can be followed to improve reproducibility – reduce the effect of room modes, or embrace the room modes in the measurement.

The effect of the room modes may be reduced if the Q source is placed in the near field of the ceiling and the contribution of the direct field would be high. To embrace the room modes, the Q source can be placed near a room corner where most of the room modes are excited. The following sub-sections provide details of the simulation model for these two approaches

3.2.3.1 *Q source placed near the ceiling*

The Q source in the simulation model was placed at the ceiling node and the driving point floor acceleration was simulated. This measurement was repeated for two cases – normal impedance boundary conditions (0.5 sec reverberation time) and free field boundary conditions (using AML surface). This was done to evaluate if the Q source placement near the ceiling gives similar results compared to a free-field model.

The ceiling Q source simulation was performed for five different assemblies – rectangular concrete, rectangular wood-joint, CS concrete, CS wood-joint, and BW concrete. For each case, the baseline performance FRF was developed by placing the Q source at randomly selected ceiling nodes and simulating the corresponding driving point floor acceleration. As each new random selection was made, the floor averaged A/\dot{Q} FRF was re-calculated with the new set of points and the RMS error was compared with the previous point selection. As the RMS error stabilized, it signaled that the number of measurement points were sufficient to represent the performance of the entire floor-ceiling structure. Twenty measurement points were used for all assemblies except the CS shape where twenty-three measurement points were used.

3.2.3.2 *Q source placed near the room corner*

The Q source was placed near a room corner and the baseline performance FRF was calculated as an average of the A/\dot{Q} FRFs of every floor node location. The measurement guidelines, along with the Q source placement guidelines are discussed in Chapter 4.

3.3 Evaluating reciprocal measurements in buildings

Four assemblies were evaluated for reciprocity. This section provides details on individual assemblies and the test procedure. In each case, direct measurements were made with an input source on the floor, and radiated SPL was measured in the receiving room. Reciprocal measurements were made using a Q source in the room below (at the microphone location from direct measurements) and measuring the floor acceleration (at the input force location). For simplicity, the microphone/ speaker location is referred to as ReSo (Receiver location turned to Source for reciprocal measurements), and the force/ acceleration location is referred to as SoRe (Source location turned to Receiver for reciprocal measurements).

The Siemens Q source used for this work (SN 13379) [114] has a built-in transducer to measure the volume acceleration. The calibration information for the Q source is unknown so some variability may be present. A Gaussian white noise signal was played from the Q source for frequencies from 20 Hz to 1024 Hz. The data acquisition parameters were the same as those defined in Section 3.1.3, with the exception that 50 averages were recorded and processed using a Hanning window with 50% overlap. The measurements were made using a combination of Siemens and National Instruments data acquisition systems, based on availability.

3.3.1 Test R1: Heavy concrete

A set of stacked classrooms with a similar top and bottom room layout were selected for this test. The floor structure is similar to floor HC2 defined in Table 3-1: 6 in reinforced concrete on a 1/2" metal sheet. Figure 3-9 (left) shows the direct test where a 12lb modal hammer (PCB 086D50) was used at the SoRe location and the SPL was measured at the ReSo location using an array microphone (PCB 130D21). Appendix A.7 validates the low-frequency performance of the array microphone. For the reciprocal test, the Q source was used at the ReSo location and the acceleration was measured at the SoRe location (PCB 356A16), shown in Fig. 3-9 (right). The test was conducted late at night to minimize the effect of background noise but no effort was made to remove or control flanking noise.

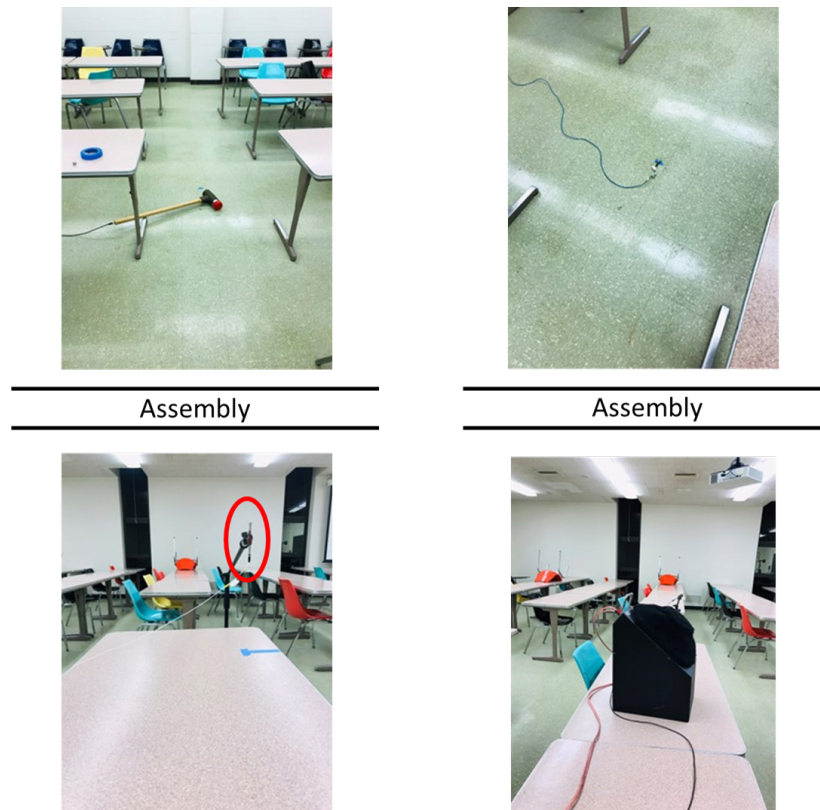


Figure 3-9 Field test R1 for reciprocity. In a stacked classroom configuration, a 12lb modal hammer was used at the SoRe location in the upstairs room and a microphone was used in the ReSo location downstairs (left). For reciprocal measurements, a Q source was placed at the ReSo location and the acceleration was measured at the SoRe location (right)

3.3.2 Test R2: Hollow core concrete

A precast hollow core concrete assembly with 50 mm diameter holes at 100 mm O.C. topped with a 65 mm thick concrete slab was used for this test. The top floor was a roof and the receiving room below was a 34 m³ office space with general room furnishings. A modal hammer, an impact ball, and the tapping machine were used as inputs at the SoRe

location for direct measurements and the Q source was placed at the ReSo location in the room below for reciprocal measurements. An exponential window was used for the microphone response with all three input methods. Figure 3-10 shows the setup for the direct test (left) and the reciprocal test (right). The additional accelerometers in the photo were not used for this work. The test was conducted after normal office hours but the structure was near a busy interstate highway and some effects due to background noise may be present.

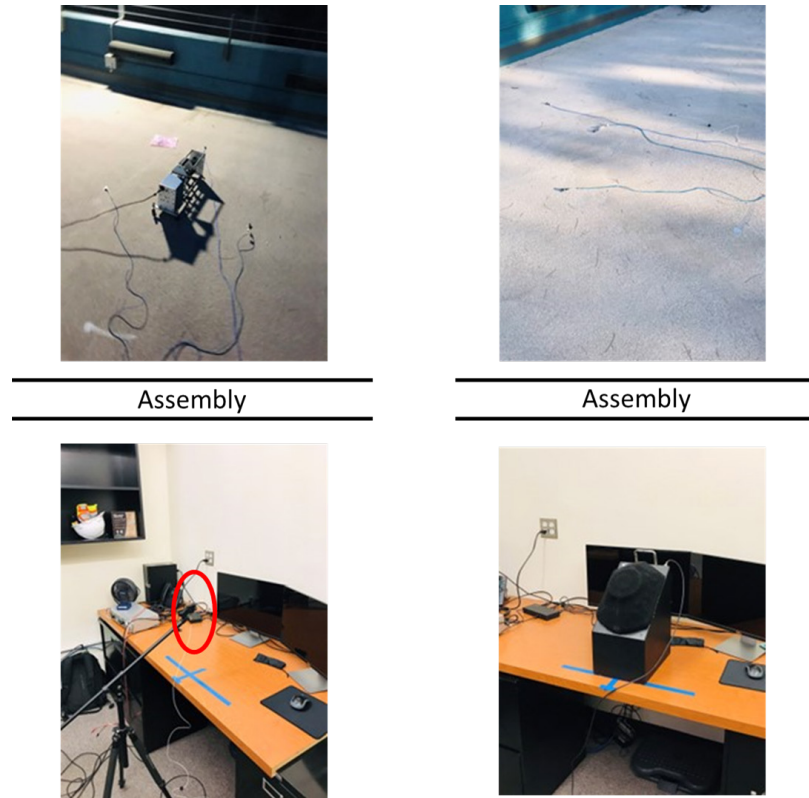
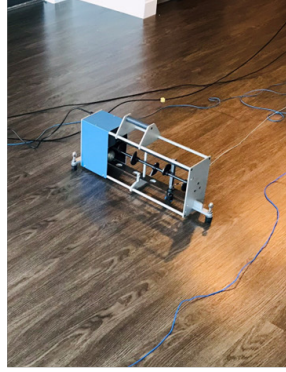


Figure 3-10 Field test R2 for reciprocity. The direct measurements using a force input at the SoRe location and the SPL at the ReSo location (left). The reciprocal measurements using a Q source at the ReSo location and the acceleration at the SoRe location (right)

3.3.3 Test R3: Wooden joist-framed assembly

This assembly consists of a Stone Plastic Composite (SPC) layer with a 1” gypsum floor topping, sound attenuation mat, wood sheathing, 2 × 12 wood framing with batt insulation, resilient channel, and a 5/8” gypsum ceiling board. Three SoRe locations were selected on the floor above and two ReSo locations in the room below for a total of six combinations. Figure 3-11 shows one such configuration for the direct measurements on the left and the reciprocal measurements on the right. A sine sweep signal was played through the Q source in addition to the white noise signal. For the force input, a modal hammer, a tapping machine, and an impact ball were used as inputs. The assembly was close to an intersection of two busy roads and some background noise may be present. An exponential window was used on the response channel for the tapping machine test.



Assembly



Assembly



Figure 3-11 Field test R3 for reciprocity. The setup for direct measurements is shown on the left and reciprocal measurements are shown on the right. This is one out of a total of six SoRe and ReSo combinations tested for this assembly

3.3.4 Test R4: Wooden joist-framed assembly

The assembly consists of a luxury vinyl plank flooring finish, 1” cast underlayment, sound attenuation mat, 3/4” plywood subfloor, floor truss, 1/2” resilient channels, and 5/8” gypsum board ceiling. A modal hammer, an impact ball, and a tapping machine were used at the SoRe location and a Q source was used at the ReSo location. One of the cables for the force transducers used for the impact ball force plate (see Section 3.1.1.2) broke during the experiment so the total input force could not be measured. Figure 3-12 shows the setup for direct measurements and reciprocal measurements on the left and right, respectively. Note that a photo of the microphone at ReSo location is not available.



Assembly



Assembly

N/A



Figure 3-12 Field test R4 for reciprocity. The setup for direct measurements is shown on the left but the photo of the microphone at ReSo location is not available. The setup for reciprocal measurements is shown on the right.

3.4 Overall proposed method testing

The simulation model was used to define the acceleration and Q source locations on the floor and the room, respectively, to improve the low-frequency measurement variability. The guidelines developed using the simulation model were evaluated for three real structures. This section provides details on individual assemblies and the test procedure. The direct and reciprocal measurements were made using the modal hammer, array microphones, Siemens Q source, and accelerometers as mentioned in Section 3.3. A sine sweep from 25 to 400 Hz was played from the speaker for 80% of the total acquisition time of 8 seconds. 50 averages were recorded with the Q source using a Tukey window on the accelerometer response channels.

The volume acceleration of the Q source was measured separately and the averaged autopower spectrum was used with the acceleration autopower spectra to calculate the Ratio of Powers Function (RPF). The RPF is given as

$$RPF = \frac{\sqrt{G_{aa}}}{\sqrt{G_{qq}}}, \quad (3-6)$$

42

where, G_{aa} is the acceleration autopower spectrum measured with the accelerometers and G_{qq} is the volume acceleration autopower spectrum measured with the Q source. The RPF measurement is easier than the FRF measurement for field tests as simultaneous measurements are not needed and a long BNC cable between the two floors, which may be difficult for field tests, is not required. We make the assumption that phase is less consequential than magnitudes with using the RPF instead of the FRF.

For all assemblies, a standard ASTM test was performed using a standard tapping machine (Scantek 211A SN 29653). A Sound Level Meter (SLM) (B&K 2250 SN 2551401) was scanned in the room below to calculate the ISR and LIR ratings. The details of the assemblies and the test procedure are presented in the following subsections.

3.4.1 Test O1: Heavy concrete

The same assembly as described for Test R1 (Section 3.3.1) is used here. The two rooms in a stacked configuration had approximately the same size and type of furnishings (classroom furniture). The standard tapping machine and the modal hammer used for the test are shown in Fig. 3-13 (a) and (b), respectively. The direct P/F FRFs and the reciprocal A/\dot{Q} RPFs were measured for two cases – Q source/microphone close to the ceiling (Fig. 3-13 (d) and (f)) and Q source/microphone near room corners (Fig. 3-13 (c) and (e)). All four room corners were studied as part of this work.

A ladder was used to place the speaker close to the ceiling and wooden spacers were used to gain height. In the configuration shown in Fig. 3-13 (d), the acoustic center of the speaker is approximately 170 mm (6-1/2”) from the ceiling but additional wooden spacers couldn't be added without making the setup unsafe.

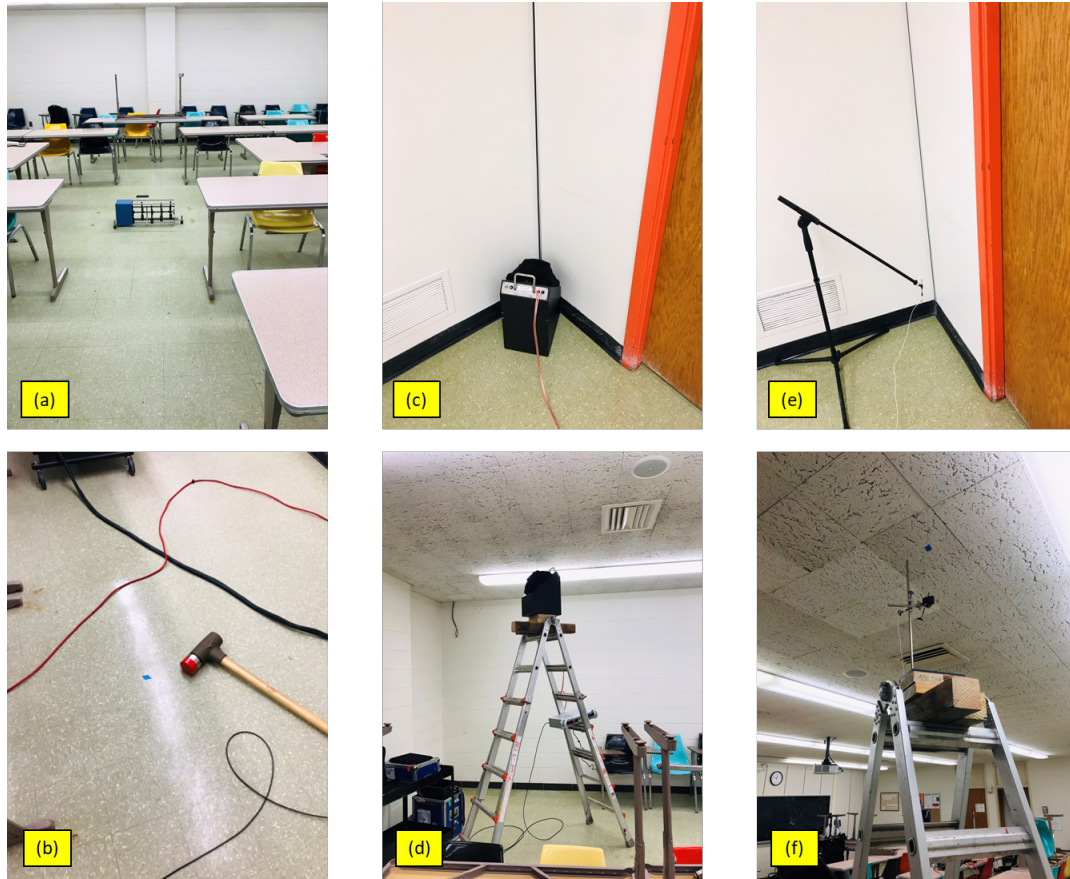


Figure 3-13 Field test O1 for the final proposed method. Two stacked classrooms were tested with a standard tapping machine (a), a modal hammer (b), a Q source near a room corner (c), a Q source near the ceiling on a ladder (d), a microphone at ReSo corner location (e), and a microphone at the ReSo ceiling location (f)

3.4.2 Test O2: Wooden joist-framed assembly

The assembly details of this residential house are unknown. Downstairs was an enclosed room and the upstairs space had an open floor plan consisting of a kitchen, dining room, and a large living room. The dining space was directly above the downstairs test room and had some heavy cupboards near the wall (Fig. 3-14 (b)). The downstairs and the upstairs spaces have slightly different areas.

The standard tapping machine and the modal hammer in the test space are shown in Fig. 3-14 (a) and (b), respectively. The Q source/ microphone close to a room corner is shown in Fig. 3-14 (c) and (e), respectively and the Q source/ microphone close to the ceiling is shown in Fig. 3-14 (d) and (f), respectively. A ladder with wooden spacers was used to place the speaker close to the ceiling. With a stable ladder setup, the acoustic center of the speaker was approximately 140 mm (5-1/2") from the ceiling. The test was conducted when the house was empty but the HVAC system and other home appliances were running normally.

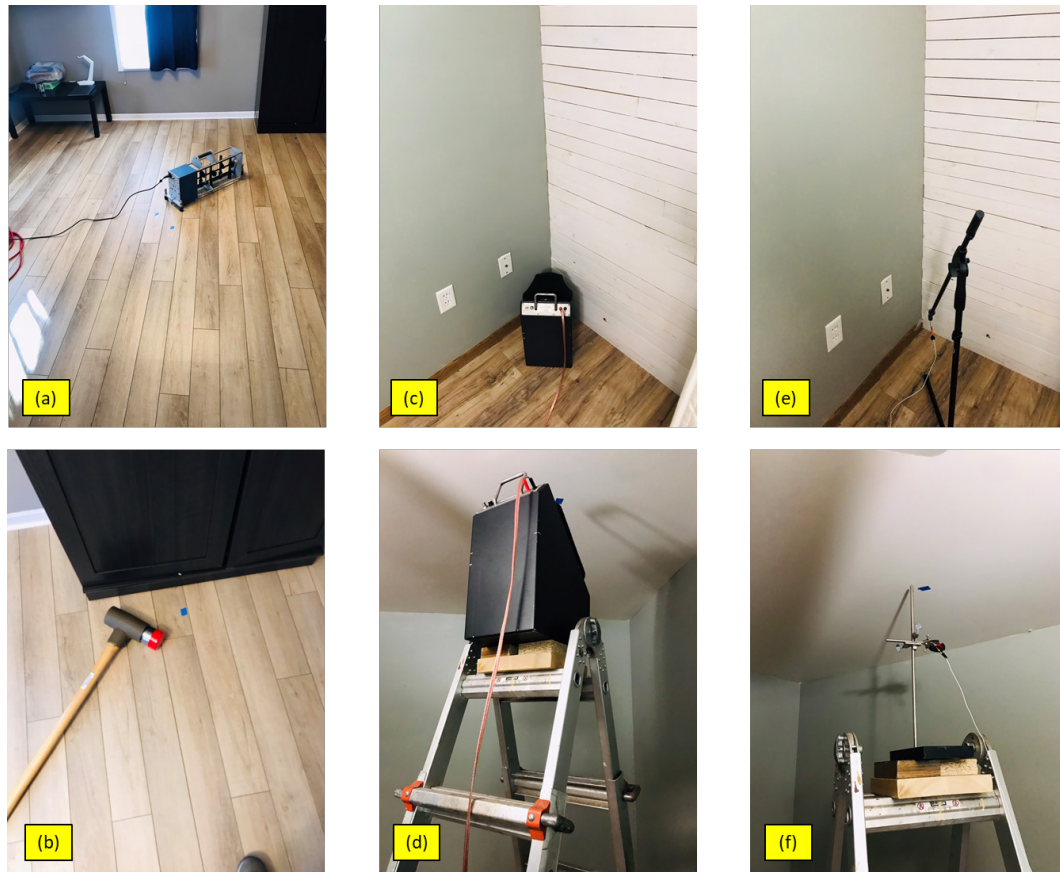


Figure 3-14 Field test O2 for the final proposed method. The downstairs room was slightly larger than the upstairs dining space which had an open floor plan with the kitchen and the living room. The figure shows the standard tapping machine (a), a modal hammer (b), the Q source near a room corner (c), the Q source near the ceiling on a ladder (d), a microphone at ReSo corner location (e), and a microphone at the ReSo ceiling location (f)

3.4.3 Test O3: Wooden joist-framed assembly with carpet finish

The downstairs and the upstairs rooms are carpeted and have slightly different surface areas and room volumes. The assembly is made of 12” manufactured joists (16” O.C.) with an OSB (Oriented Strand Board). The rest of the assembly details are unknown. The upstairs room has a high-pile carpet and the metal Velcro pieces (refer Appendix A.3) were used to mount the accelerometers in a non-destructive way for the reciprocal testing (Fig. 3-15 (b)). The house was occupied during the tests and the background noise and vibration may affect the data but the residents made an effort to minimize their effect on the measurements. The HVAC system and other home appliances were running normally.

The standard tapping machine is shown in Fig. 3-15 (a), the Q source/ microphone close to a room corner is shown in Fig. 3-15 (c) and (e), respectively and the Q source/ microphone close to the ceiling is shown in Fig. 3-15 (d) and (f), respectively. A ladder with wooden spacers was used to place the speaker close to the ceiling. With a stable ladder setup, the acoustic center of the speaker was at approximately 230 mm (9”) from

the ceiling which may lead to an increased contribution of reflected sound field on the ceiling.

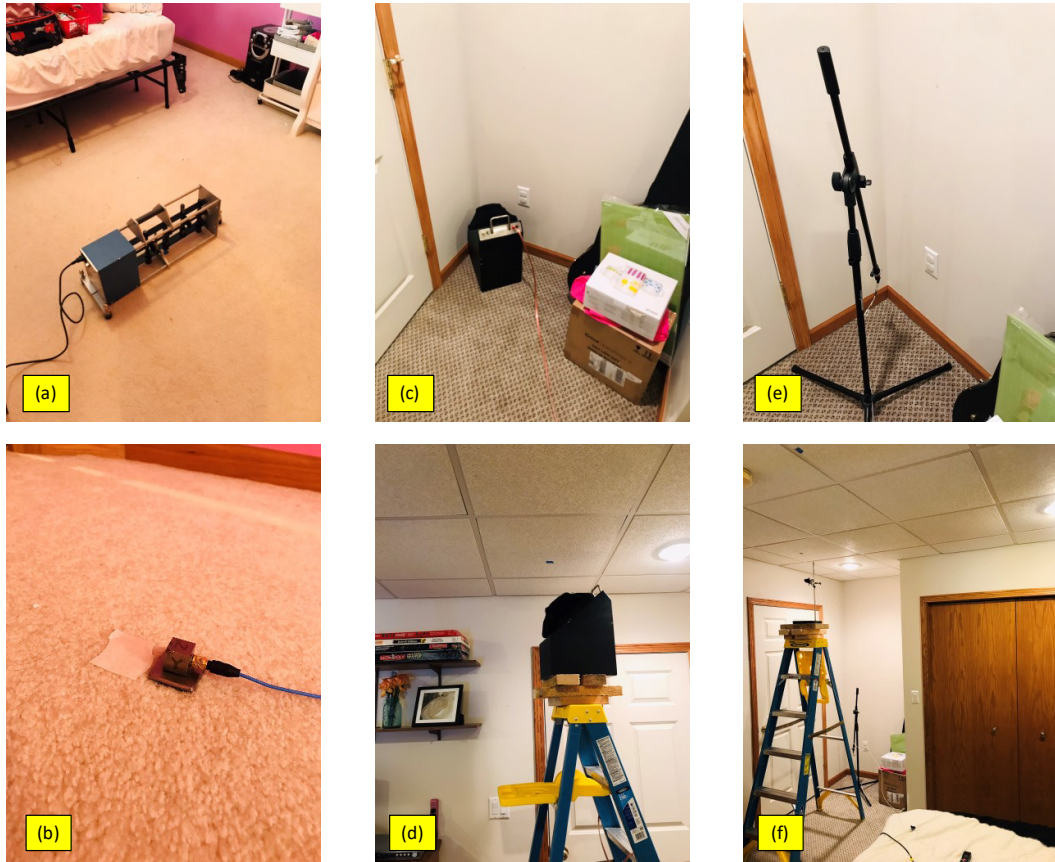


Figure 3-15 Field test O3 for the final proposed method. The downstairs room was smaller than the upstairs room and both rooms were carpeted. The standard tapping machine is shown in (a), the metal Velcro mount used for accels on the high-pile carpet (b), Q source near a room corner (c), Q source near the ceiling on a ladder (d), a microphone at ReSo corner location (e), and a microphone at the ReSo ceiling location (f)

4 Results

This chapter discusses the experimental and simulation results based on the research methods discussed in Chapter 3. The input force measurement results are first discussed that show that the peak-to-peak variation observed with the tapping machine impacts can be very high and FRF measurements are required to better evaluate the impact performance of floor-ceiling assemblies. The results of the simulations are later discussed to evaluate different measurement strategies. Sound Power measurement based on simulated intensity is discussed along with the reciprocal test method. The reciprocal method showed promise and was evaluated for real structures. The direct and reciprocal FRFs for real structures was compared.

The findings from the simulation model were used to develop the guidelines for accelerometer and the Q source placement on the floor and in the room (respectively). The final measurement method based on these results is proposed. This proposed method is used to evaluate the impact performance of three assemblies and the results are compared later in this Chapter. As a thumb rule, a 1 – 1.5 dB difference between two frequency curves is considered acceptable for this work. Class 1 type SLM used for the ASTM tests are allowed a tolerance of ± 1.1 dB for frequencies above 1000 Hz and ± 2.5 dB for frequencies above 20 Hz. Additionally, a 1 – 1.5 dB difference between two frequency curves may lead to a difference of approximately 1 ASTM ISR rating or 2 LIR ratings, as compared to the existing variation of 4 – 10 dB observed in the literature [32].

4.1 Input force measurement results

This section answers the research question whether the same input mechanism generates different force levels on different floors. If this is the case, then FRF measurements are needed to quantify the performance of floor ceiling assemblies. The force input levels from the tapping machine, the impact ball, and the modal hammer are compared in the time domain and the frequency domain. The force impulse values calculated from the time data for all the floors are also compared. The floor impedance measured using all three input methods is compared in Appendix A.8.

4.1.1 Time domain comparison

Figure 4-1 presents the time domain impact force values for the tapping machine on all the floors tested. All HC floors are plotted with blue lines, all LH floors with red lines, and green is used for the LC floors. The data plotted have been corrected for hammer head impedance (ref. Section 3.1.1.1). The input force levels for the HC floors were between 3500 – 5000 N and the force levels for all lightweight floors (LH and LC) were between 65 – 1000 N. Approximately 38 dB difference was observed between the maximum and minimum peak input levels recorded with the tapping machine.

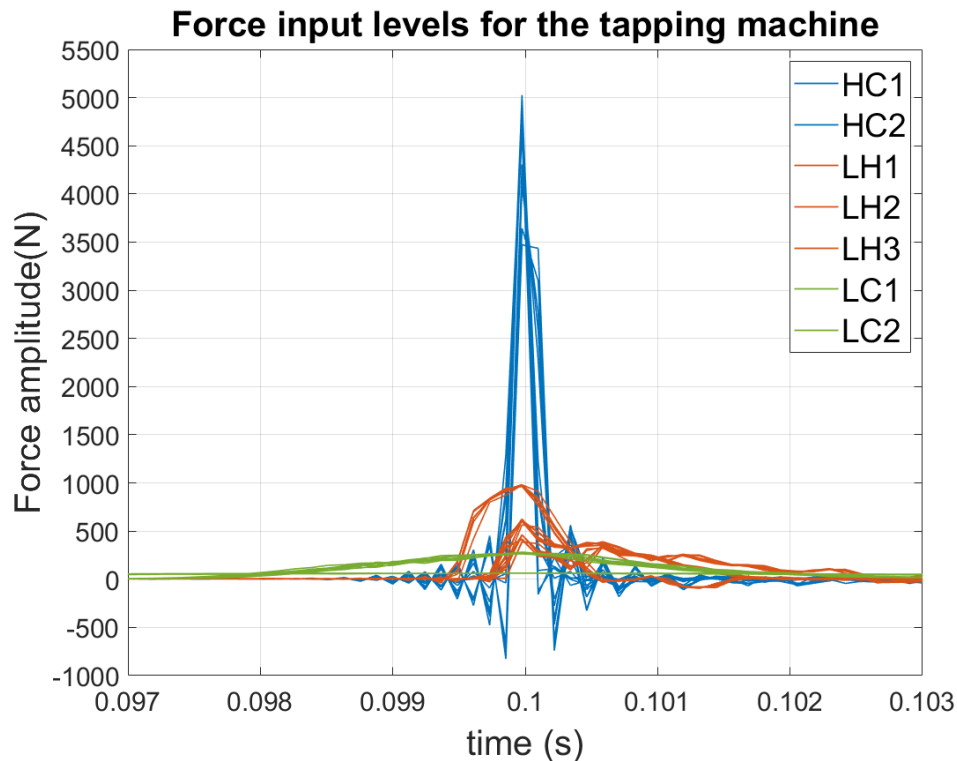


Figure 4-1 The time domain input force levels with the instrumented tapping machine (corrected for hammer head impedance) are shown using blue color for the HC floors, red color for the LH floors, and green color for the LC floors. Approximately 38 dB variation is observed between the highest and lowest impact levels on any floor tested

The time domain input force values due to the impact ball drops on all the floors are shown in Fig. 4-2. Same color scheme is followed as before (blue for HC, red for LH, and green for LC floors) and floors LH2 and LC2 were not tested with the impact ball. The peak input force for all the impacts on all the floors was between 1600 – 1850 N (approximately 1.5 dB variation). Floor LC1 showed some initial bounce in the time data because of the carpet tile, but in general, only minor differences in the peak force values were observed for all the floors, regardless of the type of construction. The duration of the impact for all the floors was very similar to each other.

The dashed black line in Fig. 4-2 is the approximate reference curve included in the ISO standards [77]. Recall that the standard impact ball should follow this defined curve, but it is unclear how these measurements are made. The measured peak force levels are approximately 1 – 2 dB higher than the ISO curve with an approximately 4.4 msec shorter impact duration.

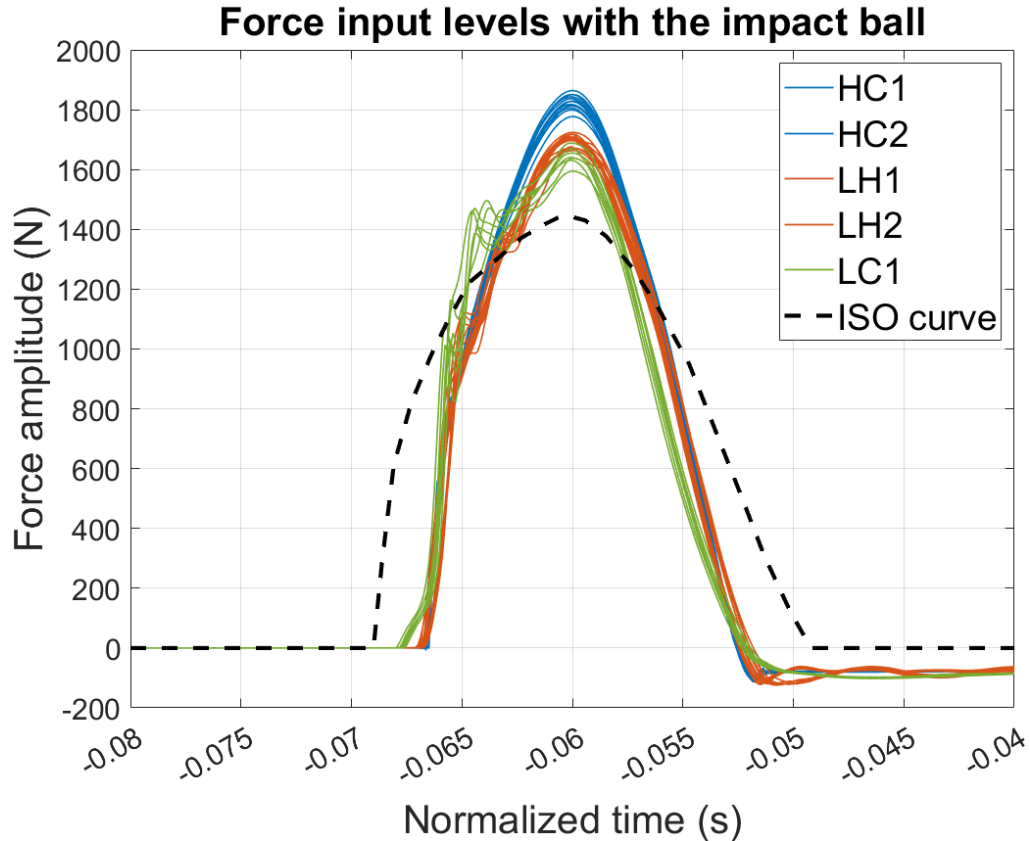


Figure 4-2 The time domain peaks from the ISO impact ball on all five floors tested showed minor differences in the time data (approximately 1.5 dB) and the LC1 floor with carpet tile showed some initial bounce in the time domain. The dashed black line shows the approximate input force curve defined in the ISO standards that compares well with measured data

A comparison of the tapping machine (Fig. 4-3 left), the modal hammer (Fig. 4-3 center), and the impact ball (Fig. 4-3 right) is shown using the same time scale (x-axis) and force scale (y-axis). Same color scheme as before is followed: blue for HC floors, red for LH floors, and green for LC floors. The tapping machine recorded the highest and the lowest peak force levels out of all the floors tested with any input source. This floor-to-floor variation was approximately 38 dB, while the impact ball showed the least floor-to-floor variation (approximately 1.5 dB). The variation with the modal hammer was approximately 22 dB. The lightweight and heavyweight floors were clearly separated for the tapping machine and the modal hammer, but not the impact ball. Lightweight floors with and without carpet didn't show any appreciable differences with the modal hammer, unlike the tapping machine. The duration of impact was the longest for the impact ball, followed by the modal hammer and the tapping machine. The frequency region excited by an impact correlates with the duration of impact and the longer duration corresponds to more low-frequency energy. Based on this time data comparison, we expect that the impact ball would have the highest low-frequency energy but a shorter excitation bandwidth.

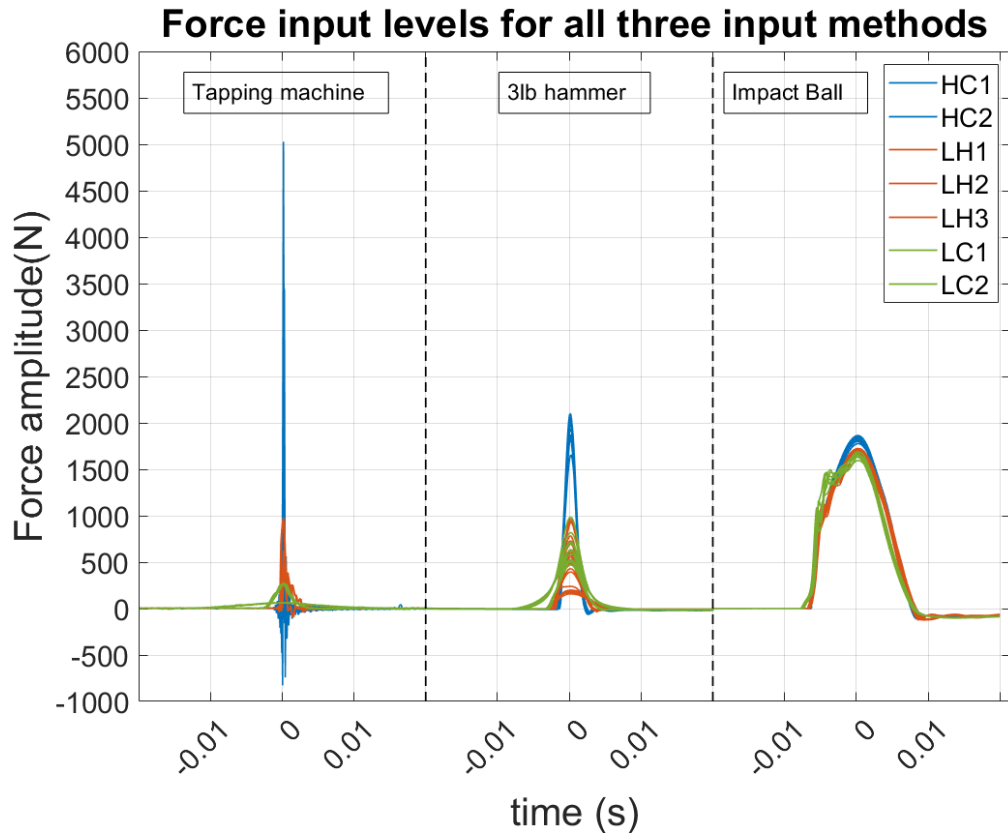


Figure 4-3 The time domain impact data for the tapping machine, the modal hammer, and the impact ball are compared. The tapping machine showed the minimum and maximum peak force levels for any floor with any input, causing the floor-to-floor variation to be 38 dB compared to 1.5 dB variation with the impact ball

4.1.2 Frequency domain comparison

In the frequency domain, the input force values for the tapping machine for all the floors (corrected for hammer head impedance) are compared in Fig. 4-4. Different colored solid lines are used to plot the data, please refer to the legend at the bottom left corner of the plot. The HC floors showed the widest frequency excitation with an almost flat frequency response for the bandwidth studied. The peak in otherwise flat spectra (between 2500 – 3000 Hz) occurred due to the hammer head impedance correction (see Appendix A.1). For the lightweight floors, the force spectra dropped by approximately 20 dB in the range of 70 – 1250 Hz based on the floor compliance. The floors may have a poor Signal to Noise Ratio (SNR) after that. Below 100 Hz, the frequency spectra values for all the floors were within 4 dB of each other (except floor LC2).

Input force values were also calculated from the literature. Material properties for a concrete floor and a hardwood floor (Table 3-2) were used to calculate the floor stiffness. The knowledge of the tapping machine (mass, free fall height, etc.), along with the stiffness of the floor was used to calculate a single impact pulse in the time domain, which was then converted to the frequency domain. All the calculations are based on VÉR

[52] and are plotted in Fig. 4-4. The dashed black line is the calculated spectra for a hardwood floor and the dotted black line is for a concrete floor. Overall, the shape of the analytical spectra compares well with the measurement data, but the amplitude values are slightly different, potentially because of differences in the material properties.

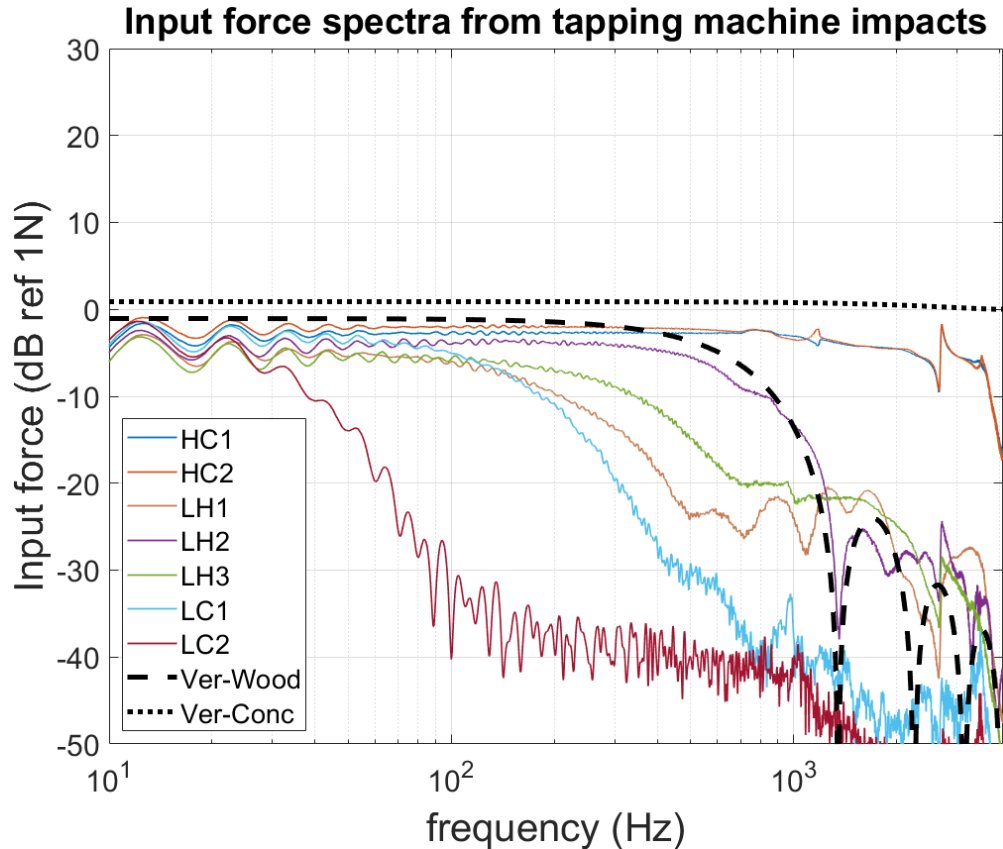


Figure 4-4 The input force spectra due to tapping machine impacts (corrected for the hammer head impedance) showed nearly flat spectra for the heavy floors, but the spectra dropped by more than 20 dB between 70 – 1200 Hz for the lightweight floors which may lead to poor SNR above this frequency range. Literature-based calculations [52] showed a similar shape of the spectra and the amplitude differences may exist due to differences in the assumed material properties

The force spectra for the floor LC2 dropped by more than 20 dB at 70 Hz which may lead to poor SNR. Figure 4-5 shows the input force on this floor on the top plot, and the coherence (for three floor accelerometers, see Section A.4) in the bottom plot. Poor coherence was observed after approximately 70 Hz and the values were consistently below 0.4. This showed that the floor had a poor SNR above 70 Hz with the tapping machine impacts. Recall that the lowest OTO band studied for the ASTM ISR rating is 100 Hz. For this particular floor, the tapping machine had poor SNR for the entire frequency bandwidth under study for the ASTM single number rating.

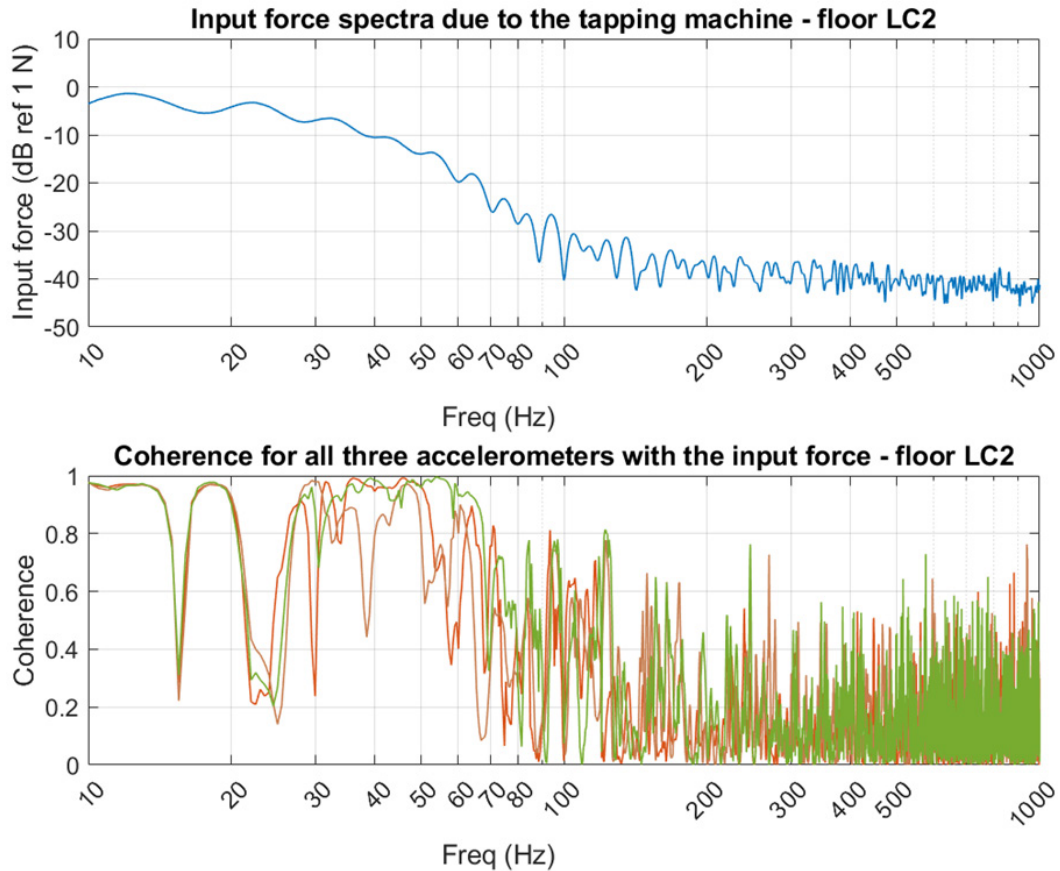


Figure 4-5 Tapping machine input force spectra for the floor LC2 (top) and the coherence for the three floor accelerometers (bottom) showed that the floor had poor coherence above approximately 70 Hz which will lead to poor SNR. This is below the minimum 100 Hz OTO band studied for the ASTM ISR rating (100 Hz)

Figure 4-6 shows the frequency domain input force for the impact ball. All the floors had similar frequency spectra levels below 100 Hz, regardless of the floor construction. This matches with the conclusions drawn from the time domain force plot (Fig. 4-2). This suggests that the impact ball may be a great source for frequencies below 100 Hz as the input force is approximately the same for all floors tested. However, the frequency spectra dropped by more than 35 dB at 100 Hz, suggesting that we have poor experimental SNR for all the floors above 100 Hz. The ISO standard [77] allows the test engineer to make measurements as high as 630 Hz with the impact ball. Experimental data showed that the frequency spectra dropped by approximately 45 dB at the 630 Hz OTO band, which led to poor measurement SNR.

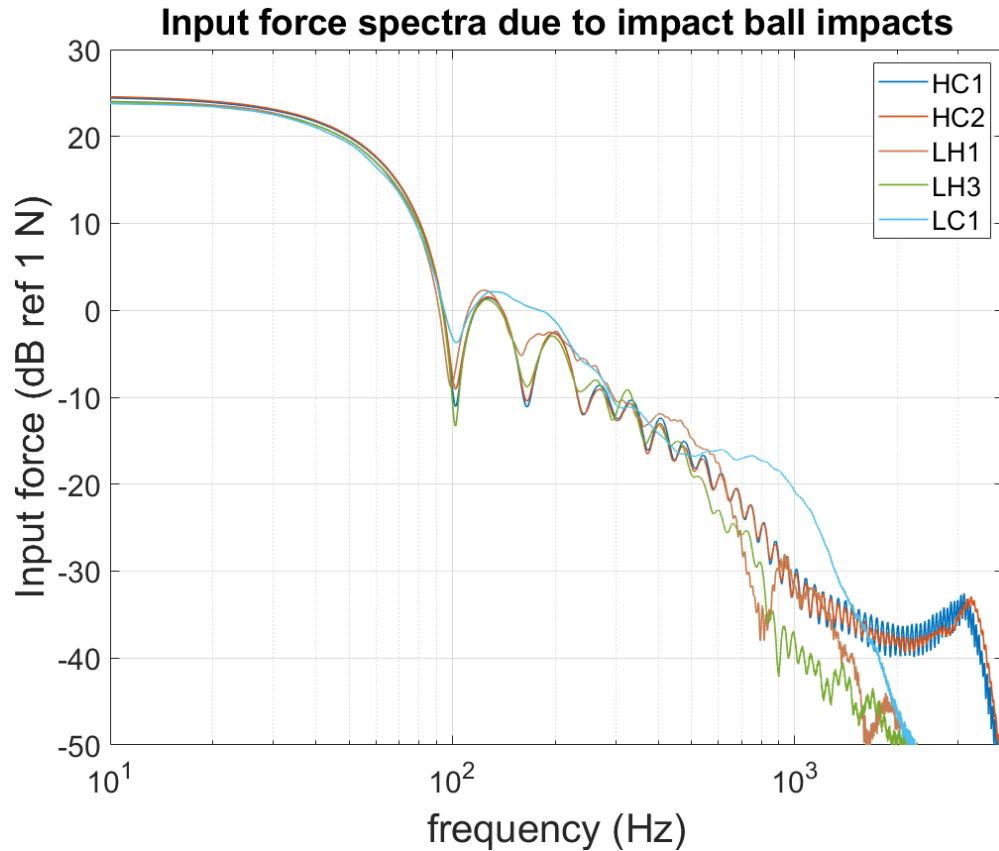


Figure 4-6 The frequency spectra values for the impact ball below 100 Hz were approximately the same regardless of the type of construction, but the spectra dropped by approximately 35 dB at 100 Hz, suggesting that all floors may have a poor SNR above this frequency

The frequency spectra for the tapping machine, modal hammer, and the impact ball are compared in Fig. 4-7 using solid lines, dashed lines, and dotted lines, respectively. Recall that the floors LH2 and LC2 were not tested with the impact ball. In low frequencies, the input force due to the impact ball was approximately 28 dB higher than the tapping machine but had the narrowest frequency excitation bandwidth out of the three. For the modal hammer, the low frequency force levels showed an approximate 11 dB variation from floor to floor. The modal hammer also showed a wider frequency excitation for most of the floors when compared to the impact ball. The tapping machine showed the lowest low-frequency force levels out of the three input methods.

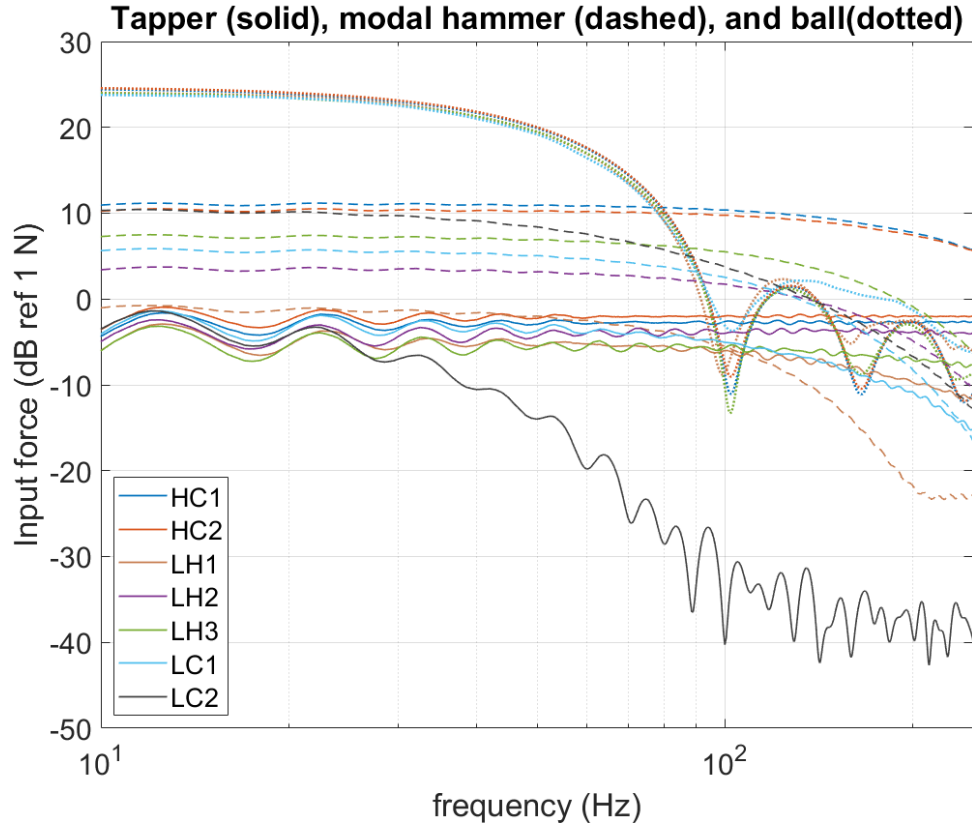


Figure 4-7 The frequency spectra of the three input methods – the tapping machine, the modal hammer, and the impact ball are shown using solid lines, dashed lines, and dotted lines respectively. The impact ball showed the highest low-frequency force levels and the tapping machine showed the lowest. Modal hammer recorded the highest variation from floor to floor, approximately 11 dB in low frequencies

4.1.3 Impulse comparison

The impulse is given as the area under the time-domain curve during the impact and can be calculated using

$$Impulse = \int_{t_{start}}^{t_{end}} f(t)dt, \quad (4-1)$$

where, $f(t)$ is the time domain input spectra (N), and t_{start} and t_{end} denote the start and end of the input force impulse. From the recorded time data, the start and end time of the impacts were manually selected for each average and the impulse was calculated, shown in Fig. 4-8. Due to the nature of the manual selection of the time window, some variability may exist but overall, the impulse from the impact ball (square markers) and the tapping machine (asterisk markers) were in a similar range. This is not the case for the modal hammer (circle markers), where the floor-to-floor variation was approximately 12 dB. This may be because the force input from the modal hammer is dependent on the user, but the impact ball and the tapping machine are standardized input methods where a

fixed mass falls freely from a fixed height. Due to the inherent differences in these input sources, the overall impulse values for the impact ball were approximately 27 dB higher than the tapping machine.

The impulse values from a standard tapping machine can be calculated from the literature [50, 51] using the momentum of the impact. The literature provides minimum and maximum bounds where the impulse from a tapping machine should lie for any floor tested. These bounds are presented with the dashed black lines in Fig. 4-8 and the calculated impulse from the tapping machine follows these minimum and maximum bounds.

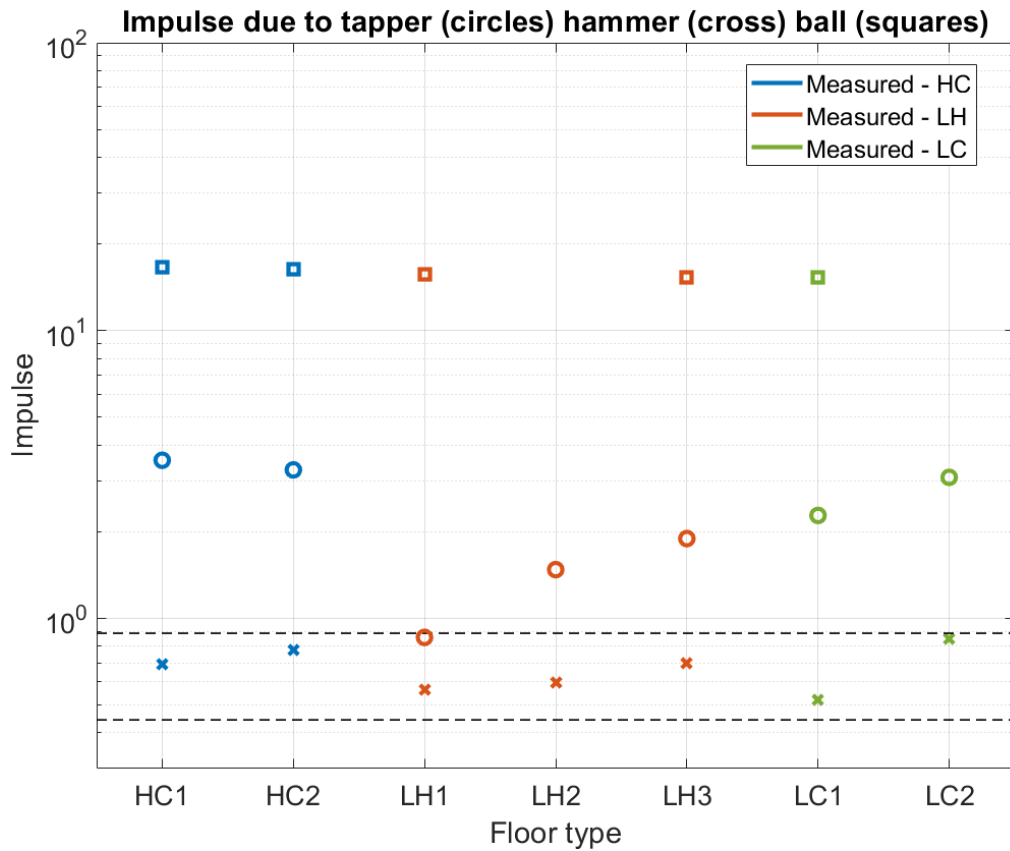


Figure 4-8 The time domain force impulse for the impact ball is shown with square markers, the modal hammer with circle markers, and the tapping machine with asterisk markers. The impact ball impulse values were approximately 27 dB higher than the tapping machine, but for both of the floors, the impulse values don't change significantly based on the type of floor. The tapping machine impulse also followed the minimum and maximum bounds according to the literature [50, 51]

From this section, it is clear that the peak-to-peak variation for the tapping machine is high and FRF measurements are needed to better evaluate the impact performance of floor-ceiling assemblies. The following sub-sections discuss the simulation results from the sound intensity test method and the reciprocity test method.

4.2 Exploring measurement ideas using the simulation model

This section uses the simulation model to compare the performance of different measurement ideas. Only the sound intensity and reciprocity methods are discussed here. The rest of the measurement methods are presented in Appendix A.6.

4.2.1 Sound Power based on simulated sound intensity

Appendix A.6.4 contains the complete results and discussion from the raw room intensity based sound power (L_w) compared with the free field L_w . Figure 4-9 compares the free field L_w (solid black) with the forward propagating L_w (solid blue) and the raw intensity based L_w (dashed red) for a room with 1.5 sec reverb time (left) and 0.5 sec reverb time (right). These two conditions represent a room with low and high absorption, respectively. The forward propagating L_w compared within 1 – 5 dB of the free field L_w in the 40 – 100 Hz OTO bands and the shape of the spectra were matched much better. The raw intensity L_w showed differences of approximately 1 – 15 dB for 1.5 seconds reverb time and 1 – 10 dB for the 0.5 seconds reverb time.

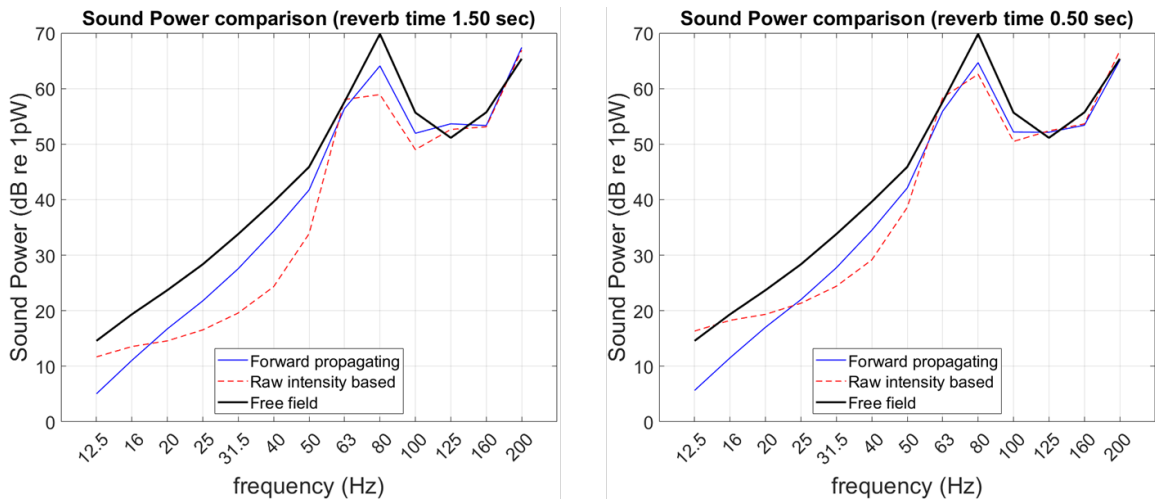


Figure 4-9 The free field L_w (solid black) compared with the forward propagating L_w (solid blue) and the raw intensity-based L_w (dashed red) for a model with 1.5 sec reverb time (left) and 0.5 sec reverb time (right). Forward propagating L_w shows an improvement of approximately 10 dB and 5 dB for 1.5 sec and 0.5 sec model, respectively, but still shows 1 – 5 dB difference from the free field L_w

Similar observations can be made for the simulation models with other room boundary conditions. Figure 4-10 shows the difference between free field L_w and raw intensity based L_w (left) and the difference with the forward propagating L_w (right) for six different reverberation times. 6 – 15 dB differences were observed between the 40 – 100 Hz OTO bands for the raw-intensity based L_w while 1 – 5 dB differences were observed with the forward propagating L_w . Additionally, the forward propagation L_w did not change significantly due to different room absorption conditions. This suggests that there

may be a limit to how close the free field L_w of the assembly can be predicted based on room intensity measurements. Additionally, a furnished room tested with this method would provide similar results when compared to an unfurnished room.

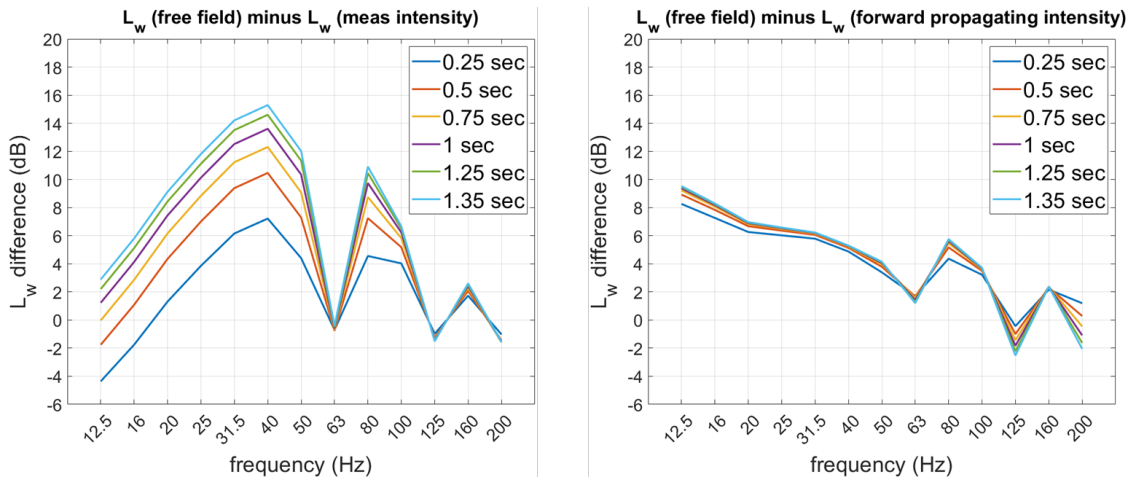


Figure 4-10 The difference between the free field L_w , the raw intensity L_w , and the forward propagating L_w (left and right, respectively) showed 6 – 15 dB differences with the raw intensity and 1 – 5 dB differences with the forward propagating intensity. The forward propagating intensity doesn't change significantly with room absorption

4.2.2 Reciprocity method simulation

The simulation model behaves linearly and it is expected that the reciprocity principle will hold. Figure 4-11 compares the FRFs obtained between a room microphone node with a force input on the floor (P/F) and floor acceleration with a Q source input (A/\dot{Q}) represented with a solid blue line and a dashed red line, respectively. Note that the room location for the microphone/ Q source and floor location for the force/ acceleration are unchanged for both cases. The magnitude (top) and phase (bottom) of the FRFs showed a perfect comparison, proving that the reciprocity principle works for this simulation model. The plot shows the data for only one combination of floor and room locations, but a similar comparison was observed for other simulation points.

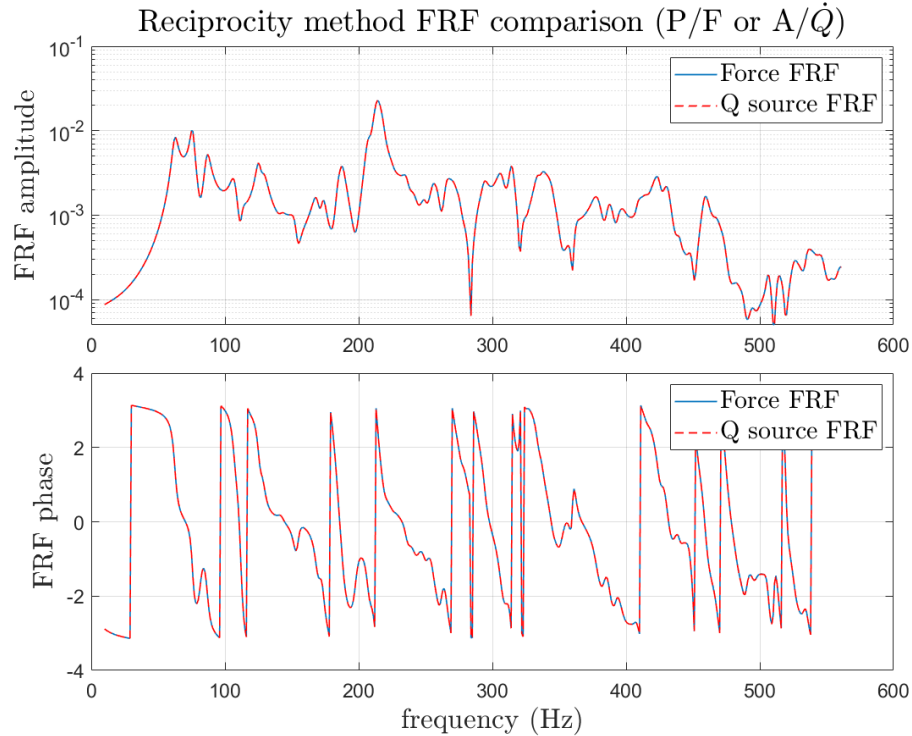


Figure 4-11 Reciprocity comparison in the simulation model. Solid blue is the direct P/F FRF between a room microphone location and floor force location and dashed red is the reciprocal A/\dot{Q} FRF between the same two floor and room locations using a Q source in the room. Both show a perfect comparison of magnitude (top) and phase (bottom)

4.2.3 Comparing the intensity and reciprocity simulation results

The forward propagating sound intensity method showed that measurements between 1 – 2 dB can be made for rooms irrespective of the room absorption. Even though the measured values were 1 – 5 dB different when compared with the free-field sound power, the reproducibility of the method can be high. However, this test method in the field requires a significant amount of time, which may not be acceptable to the acoustic industry or the building residents. Additionally, the input source needs to be stationary so that discrete point intensity measurements can be made. For these reasons, this test method was not evaluated for future tests.

Reciprocity method shows a perfect comparison with the direct FRF in the simulation model. A Q source can be placed in the room below and the floor acceleration can be easily measured. The test time would not change significantly but some initial training may be required. However, this test method is promising and it was explored further. Note that the simulation model is linear but the real structures may not be linear. It is important to evaluate the reciprocal measurements for real structures, as discussed in the next section.

4.3 Evaluating reciprocal measurements for real

structures

The floor assemblies can be non-linear [21, 22, 60] and the direct and reciprocal FRFs were compared for four real structures detailed in Section 3.3. Similar to the automotive industry [115], less than 3 dB differences between the direct and reciprocal FRFs were considered acceptable for this work.

4.3.1 Test R1: Heavy Concrete Assembly

Figure 4-12 compares the direct (blue) and the reciprocal (red) FRFs obtained using a modal hammer and the Q source, respectively. The difference between the two is shown using bar plots along the y-axis on the right. Less than 2 dB difference was observed from 50 – 100 Hz OTO bands and approximately 3 dB for the entire frequency range from 20 – 400 Hz OTO bands. This shows that reciprocal measurements can be used to get the floor impact performance FRF. Some reasons for the difference between the two measurements may be the effect of background noise due to the intermittent operation of the building elevator, or some flanking effects due to the routing of the cable under the door. Additionally, calibration information for the Q source was unavailable and the transducer sensitivity provided by the manufacturer was used.

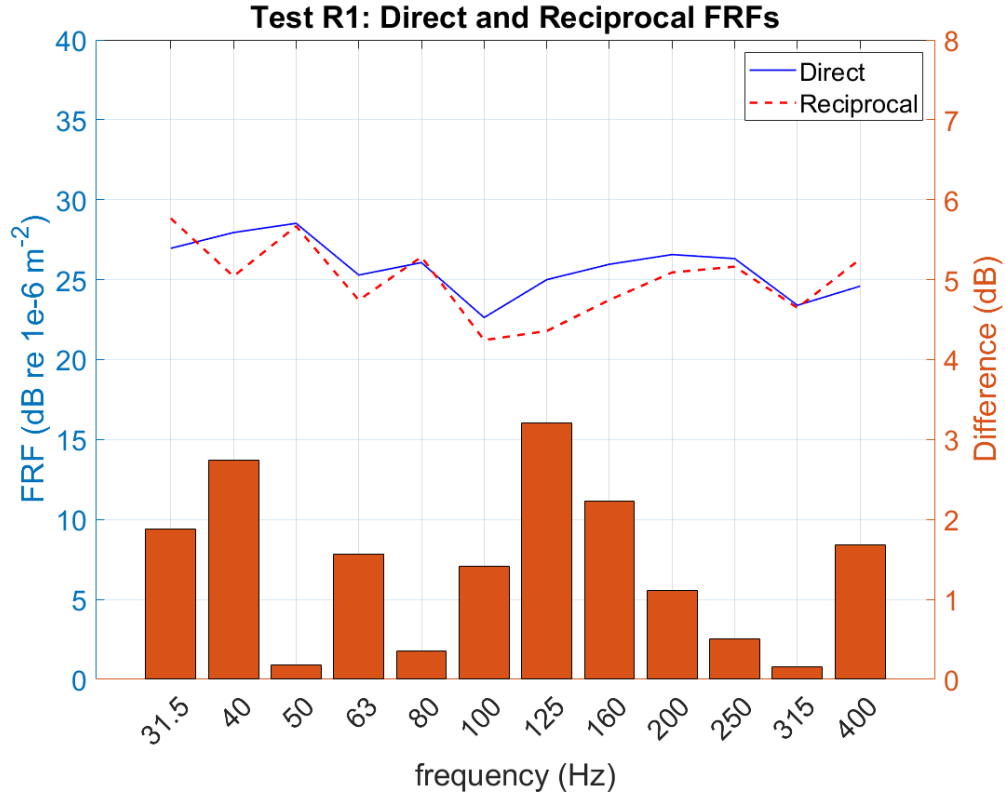


Figure 4-12 The solid blue line represents the hammer P/F FRF and the dashed red line represents the A/\dot{Q} FRF using the Q source speaker. Less than 2 dB variation was observed in the low-frequencies of interest from 50 – 100 Hz OTO bands

4.3.2 Test R2: Hollow Core Concrete

The direct P/F and reciprocal A/\dot{Q} FRFs for Assembly R2 are shown in Fig. 4-13 where the solid blue, dotted red, dash dot magenta, and dashed black lines represent the modal hammer, the impact ball, the tapping machine, and the Q source with white noise. The difference between the direct modal hammer and the impact ball FRFs with the Q source reciprocal FRF was less than 1 dB above the 25 Hz OTO band. The tapping machine shows higher differences in low-frequencies – approximately 5 dB at 25 Hz. However, the difference between the tapping machine and the Q source FRF from 50 – 100 Hz OTO bands was less than 2 dB. The reciprocal method can be used to predict the floor performance FRF for this assembly.

Note that with the Q source, the SNR of the floor acceleration signal was poor. This may be because of the proximity of the assembly to a busy interstate highway that may cause building vibrations. Additionally, the roof under test had two air conditioner units that could not be switched off for the test. The measured floor acceleration with the speaker is compared to the background acceleration levels in Appendix A.9.1.

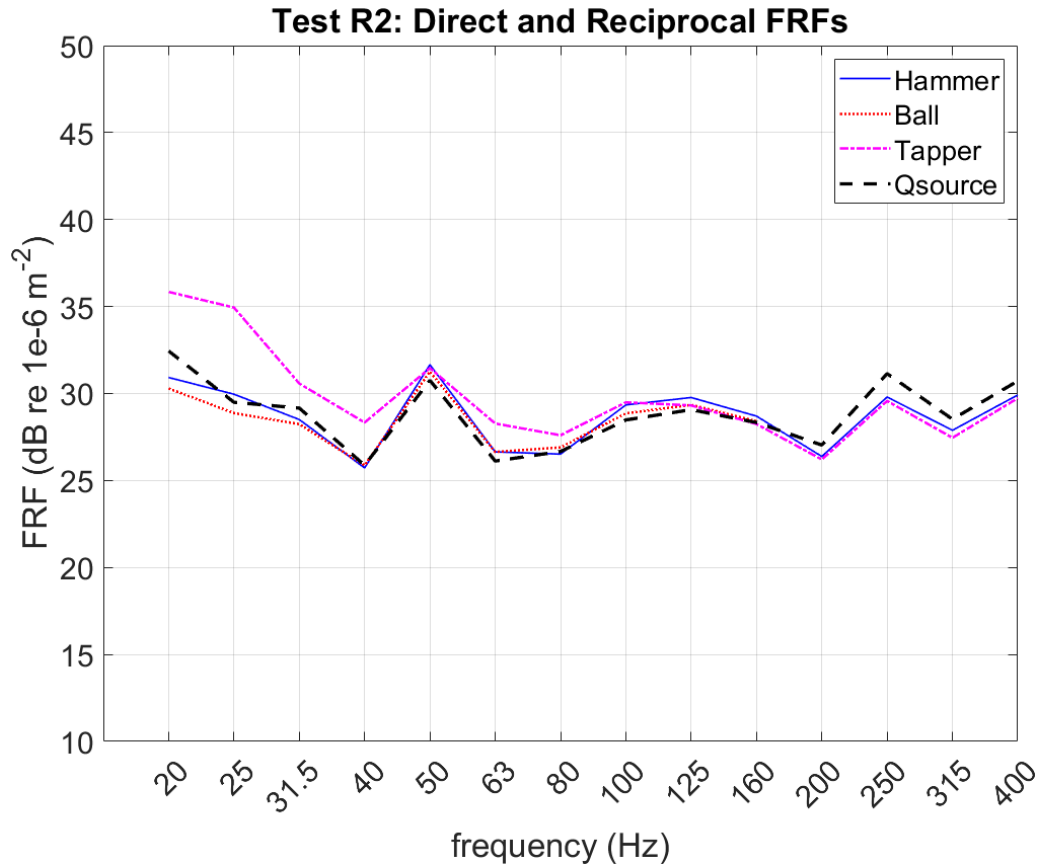


Figure 4-13 The hammer and the impact ball P/F FRFs compare within 1 dB with the reciprocal A/\dot{Q} FRF above 25 Hz but the tapping machine shows approximately a 5 dB difference at 25 Hz. This may be because the tapping machine impacts the same floor differently when compared with the modal hammer and the impact ball. The background noise from the nearby interstate may also affect the measurements and details are discussed in Appendix A.9.1

The measurement coherence for all three input sources and the reciprocal Q source are shown in Fig. 4-14 on the left and right, respectively. The hammer, ball, and tapper coherence are shown using solid blue, dashed red, and dotted black lines, respectively. The tapping machine shows poor coherence below 100 Hz that may explain the higher FRF differences observed in Fig. 4-13. The modal hammer and the impact ball show good coherence (close to 1) in the low frequencies. For the Q source (right), the coherence is poor (below 0.5) below 60 – 70 Hz. This may be because of background vibration in the ceiling (see Appendix A.9.1). However, the reciprocal and direct FRFs (with the modal hammer and the impact ball) still show a good comparison in that frequency range (see Fig. 4-13). The Q source can be used to get the performance FRF of the floor-ceiling assembly.

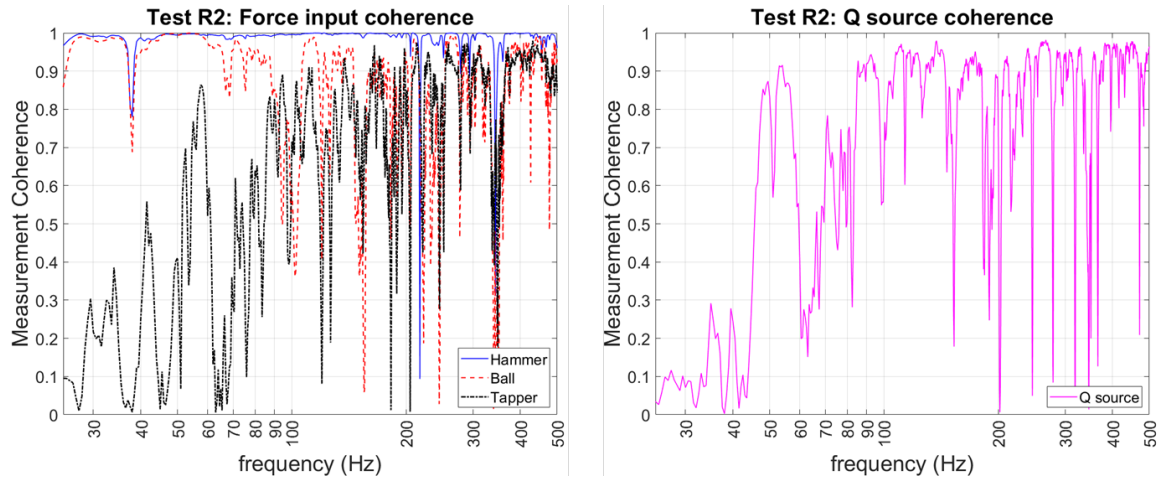


Figure 4-14 Test R2: Measurement coherence with all the force input methods (left) and the Q source (right) shows that the tapping machine has poor coherence below approximately 100 Hz for this floor but the impact ball and the modal hammer have good low-frequency coherence. Additionally, the Q source has poor coherence below 100 Hz but the measurement FRF shows good comparison with the modal hammer data. Poor coherence may be due to background vibration in the floor but the effect on the measurement FRF is not significant

4.3.3 Test R3: Wood Joist-framed Assembly

Figure 4-15 compares the direct and the reciprocal FRFs for one of the six floor/room combinations for assembly R3. The other five combinations are plotted in Appendix A.9.2. In Fig. 4-15, the direct FRFs measured with the hammer, the impact ball, the tapping machine, and the reciprocal FRF measured with the Q source are shown with a solid blue line, dotted red line, dash dot magenta, and dashed black line, respectively. All four FRFs compare within 2 dB of each other below 160 Hz. Note that the impact ball data are only plotted below 100 Hz because of poor SNR (Appendix A.9.3). The tapping machine shows less than 1 dB difference from the reciprocal measurements below 160 Hz but the difference increases with higher frequencies. The modal hammer and the impact ball compare within 1 dB of each other but show a variation of 1 – 2 dB from the reciprocal measurements. For the modal hammer and the impact ball, the user has to stand near the impact location during the test, which is not the case for the tapping machine or the Q source acceleration measurements. This may mass load the lightweight wood structure and potentially cause some of the differences presented here.

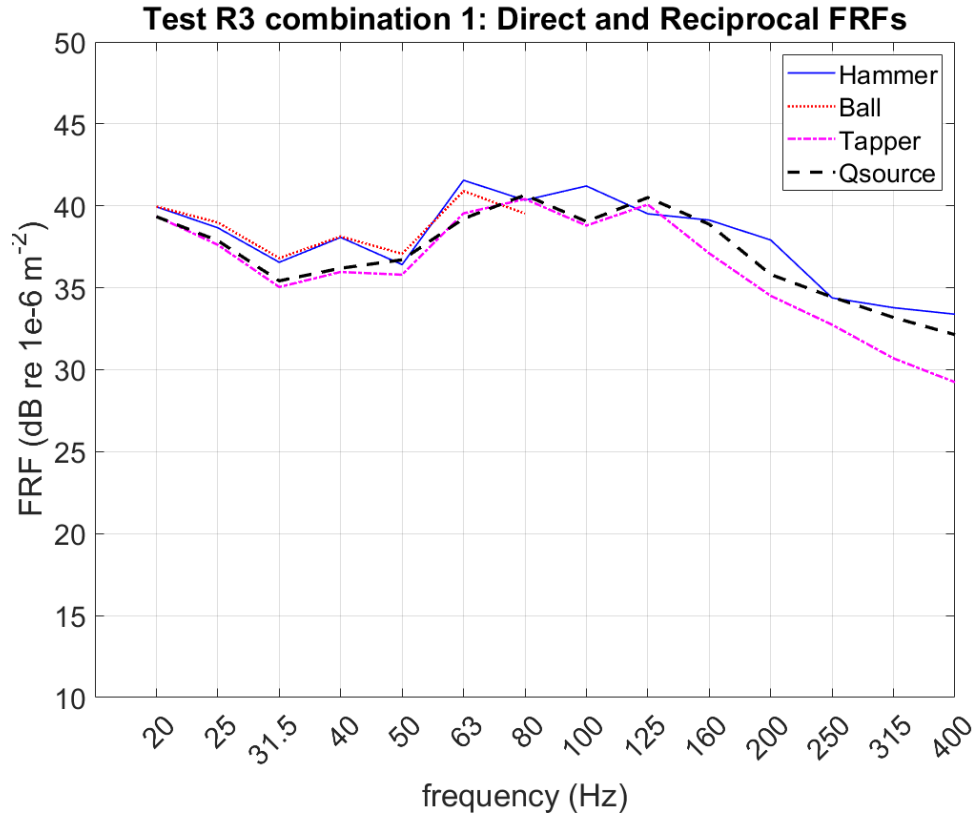


Figure 4-15 The direct FRFs obtained with the modal hammer, the impact ball, and the tapping machine, compared with the reciprocal FRF obtained with the Q source for one of the six floor/room combinations show that all FRFs compare within 2 dB of each other below 160 Hz. The comparison was slightly better for the tapping machine (less than 1 dB) below 160 Hz as compared to the modal hammer and the impact ball.

In addition to the white noise, a sine sweep signal was also played through the Q source for all six combinations. The FRFs obtained using the sine sweep and white noise are within 0.5 dB of each other and are compared in Appendix A.9.3.

4.3.4 Test R4: Wooden Joist-framed Assembly

Figure 4-16 shows a comparison of the direct FRFs with a modal hammer (solid blue), impact ball (dotted red), tapping machine (dash dot magenta), and the reciprocal Q source (dashed black) FRF. The tapping machine and the impact ball FRFs compare within 2 dB of the reciprocal FRF above 20 Hz but the comparison with the impact ball is limited only to 80 Hz due to poor SNR. Recall that the input force from the impact ball could not be measured due to equipment limitations, but Section 4.1 shows that the time and frequency spectra from the impact ball are similar regardless of the construction of the floor. The measured force autopower spectrum for the impact ball from assembly R2 was used to calculate the P/F FRF and compared with the reciprocal FRF. That may explain some of the differences between the two.

For the modal hammer, less than 2 dB difference was observed below 400 Hz except at the 100 Hz OTO band where an approximately 4.5 dB difference was observed. For this test, the refrigerator could not be unplugged during the test and it would intermittently turn on based on its internal temperature. This may cause some of the differences in the FRFs. The hammer test is much shorter than the Q source test so intermittent refrigerator noise may affect the hammer measurements more as compared to the Q source. The measurement coherence for the Q source is poor in the 100 Hz OTO band as shown in Appendix A.9.4. A comparison of the measured acceleration and SPL values with the background levels is also shown in Appendix A.9.4. Additionally, the calibration data for the Q source is unknown which may cause some differences when compared with the direct measurements too.

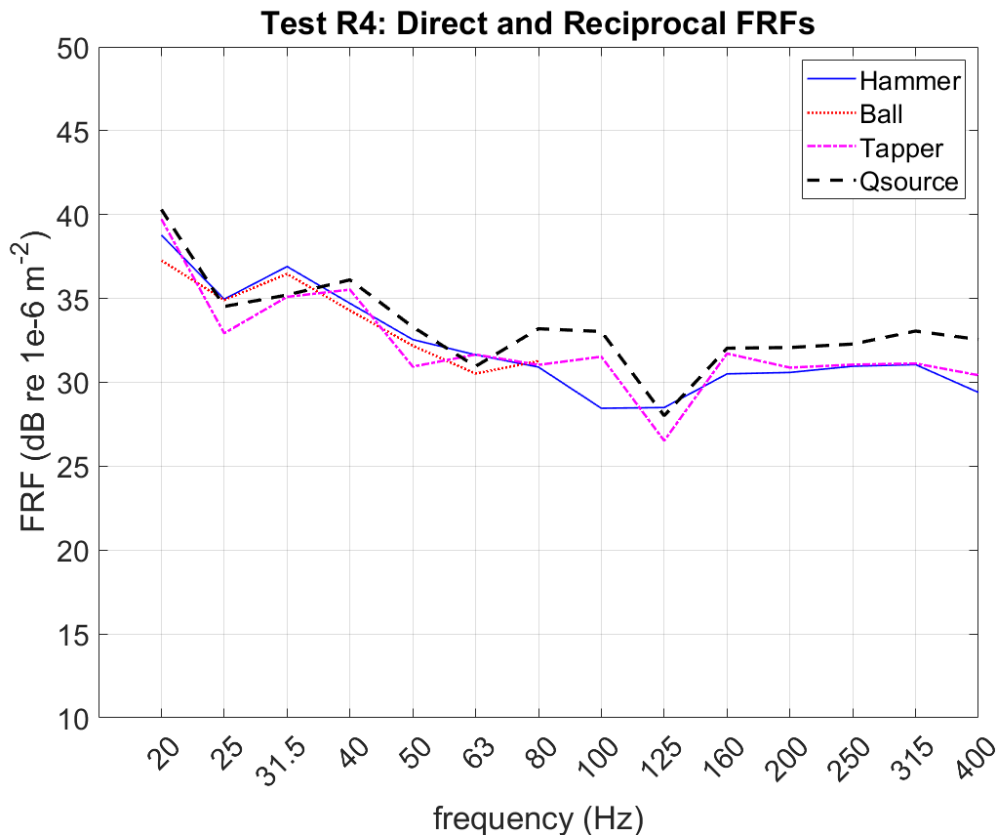


Figure 4-16 The direct P/F FRFs obtained using the modal hammer (solid blue), impact ball (dotted red), and the tapping machine (dash dot magenta) are compared with the reciprocal A/\dot{Q} FRF obtained with a Q source (dashed black). Less than 2 dB differences are observed for all cases above 25 Hz but the modal hammer shows approximately 4.5 dB difference with the reciprocal FRF in the 100 Hz OTO band

It is evident from this section that the reciprocal test method can be used to get the impact performance of floor-ceiling assemblies. But just like the direct measurements, the reciprocal measurements would suffer from non-reproducibility issues due to the room non-diffuse field (see Section 3.2.3). The simulation model was used to develop a Q

source and accelerometer placement strategy, as discussed in the next section. The measurement method proposed based on the simulation model showed significantly lower measurement variability as compared to the existing method, and was used to evaluate the impact performance of three real structures.

4.4 Proposed reciprocity-based measurement method

This section discusses the development of a measurement method to answer the research question of improving measurement reproducibility in low frequencies. Two cases were explored – the Q source placed near the ceiling and the Q source placed near the room corner (see Section 3.2.3). This section details the learnings from the simulation model for these two approaches and develops the final measurement guidelines to be followed for any test structure.

For the case when the Q source is placed near the ceiling, Fig. 4-17 shows the RMS error as random measurement locations were selected on the floor/ceiling on the CS shaped concrete floor. The RMS error values are normalized based on the highest value and the random locations selected are plotted in the top right corner with red dots. The RMS error stabilized after approximately 16 measurement locations showing that the number of locations selected are sufficient to represent the performance of the entire floor-ceiling assembly. This is considered as the baseline which would be compared to the final measurement method for the simulation model. For the CS shaped floor, twenty-three locations were used and for the rectangular and BW floor, twenty locations were used to get the baseline FRF.

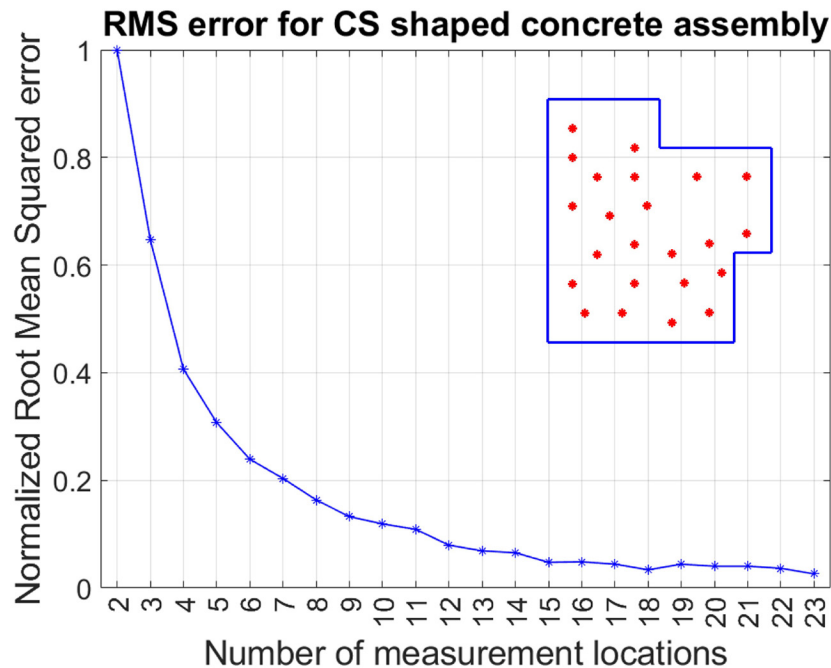


Figure 4-17 The normalized RMS error as random Q source locations were selected near the ceiling for the CS shaped concrete floor. The error stabilized after approximately 16

locations, signaling that the number of locations were sufficient to represent the performance of the entire floor

Total test time is a high priority for field tests and testing twenty-three random floor locations would not be a practical solution for the industry. The simulation model was used to identify measurement combinations that would provide similar results as the baseline with a significantly reduced number of measurement locations. Two combinations were successful – five measurement locations aligned as a cross along the floor/ceiling, or three measurement locations aligned along a room diagonal.

Figure 4-18 shows the cross and the diagonal location configuration for a rectangular shaped floor on the left and right, respectively. For the cross configuration, the area is divided into five equal segments with one measurement point each (blue cross mark). All five measurement locations have an equal spatial contribution. For the diagonal measurements, two outer cross points are ignored so the spatial contribution of the other two outer points is twice that of the inner location. The overall FRF is calculated using the following steps:

1. Multiply the FRF of the two outer diagonal points by 2
2. Take a mean of the magnitude of the three FRFs
3. Multiply the average by a factor of (3/5) for spatial averaging.

For all the assemblies evaluated in this work, the results from the cross and the diagonal configuration were similar and only the diagonal configuration is discussed in the rest of this work.

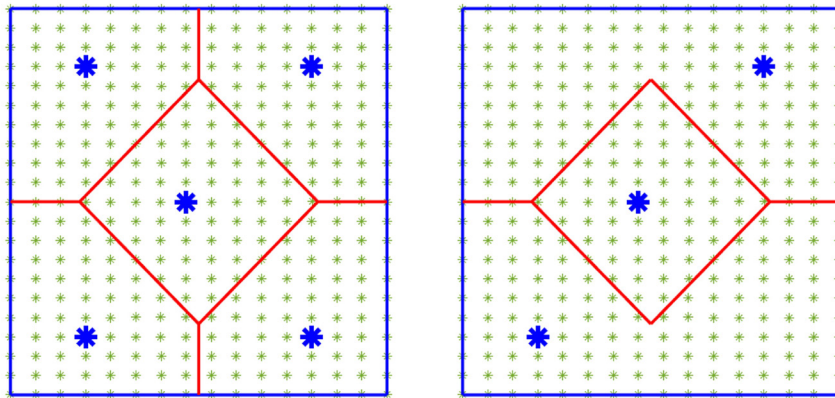


Figure 4-18 Floor measurement strategy using the cross configuration (left) and the diagonal configuration (right). All five points for the cross configuration have the same spatial contribution but the two outer points for the diagonal configuration have twice the spatial contribution as compared to the inner point. Both configurations gave similar results and only the diagonal points are discussed in the rest of this work

The measurement points are selected at 17%, 50%, and 83% of the length of the longest room diagonal so that most of the floor space can be represented. This combination of points was selected because they are non-integer multiples of each other and the chance

of a floor mode missing all three measurement points is low. Additionally, 17% and 83% translate to two-thirds the length of half of the room diagonal length. Most of the low order floor modes in low frequencies would not have a node at the two-thirds distance so the chance of recording most of the floor modes is high. The numbers 17 and 83 are also transferrable, meaning that the dimensions can be measured from either side of the diagonal and the final results would be the same.

Figure 4-19 shows two options to pick a room diagonal (solid cyan) and measurement points (black cross marks) for the CS shaped room. The Q source locations for both cases are shown using red cross marks. The left plot shows the longest room diagonal and the right shows a shorter diagonal for a room corner. The diagonal on the right does not cover most of the floor surface area and would be a poor choice to pick a room corner or diagonal measurement locations. Note that the measurement points may not be located precisely on the diagonal due to the grid size of the model and the closest available points were selected.

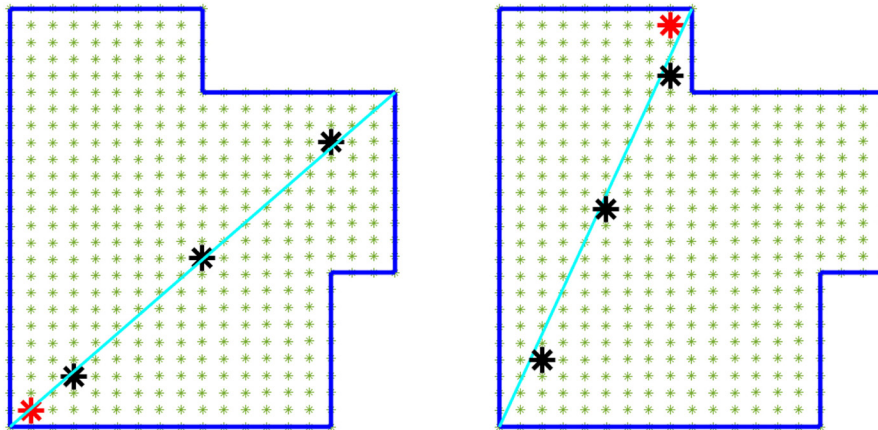


Figure 4-19 Two room diagonal selections (solid cyan) and the associated measurement points (black cross marks) are shown for the CS shaped assembly. The diagonal on the left is the longest room diagonal, but the diagonal on the right is a short diagonal and does not cover most of the floor surface. This would be a poor choice to select measurement locations

The diagonally measured FRFs were compared to the baseline FRFs for the case of the Q source placed near the ceiling and near the room corner. These two cases are individually discussed in the following sub-sections.

4.4.1 Developing measurement guidelines for the Q source placed near the ceiling

A/\dot{Q} FRF in the free-field condition (red) is compared to the FRF with the room impedance boundary conditions (blue) when the Q source is placed near the ceiling in Fig. 4-20. The two FRFs showed a difference of approximately 1 – 4 dB in the non-diffuse region from 40 – 100 Hz OTO bands. The room reflection condition also showed

a drop in the spectra at the 20 Hz OTO band which was not observed in the free field. Placing the Q source close to the ceiling did not remove the effect of room modes completely.

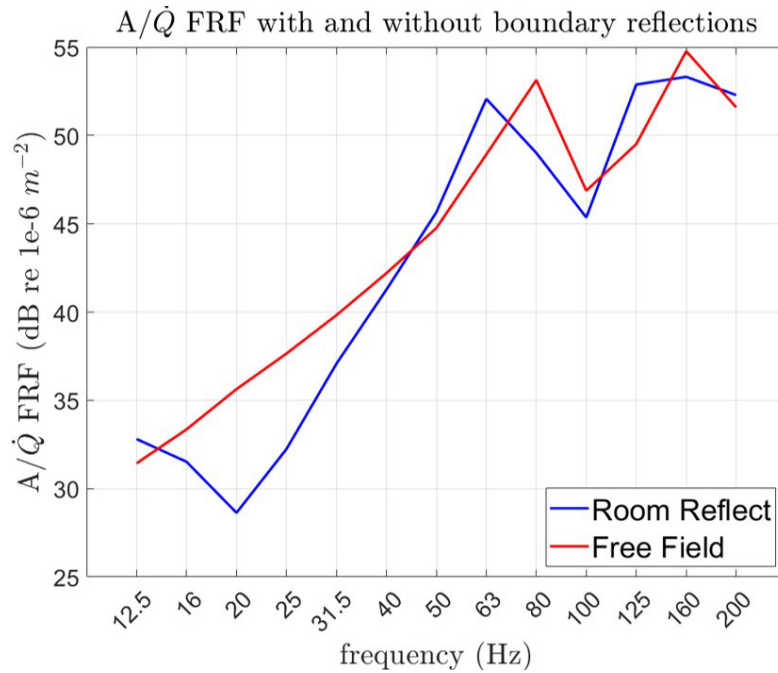


Figure 4-20 The A/Q FRF when the Q source was placed close to the ceiling with the room impedance conditions (solid blue) and the free field conditions (solid red) showed a difference of approximately 1 – 4 dB from the 40 – 100 Hz OTO bands. The room impedance FRF showed a drop in spectra at 20 Hz which was not observed in the free field data

The diagonally measured FRFs and the baseline FRFs for the rectangular concrete and wood-joint assemblies are compared in Fig. 4-21 left and right plots, respectively. Both assemblies showed a difference of approximately 1 – 2.3 dB between the diagonal and baseline FRFs from 40 – 100 Hz OTO bands. Three measurement points along a diagonal can closely represent the performance of the entire floor assemblies in these cases.

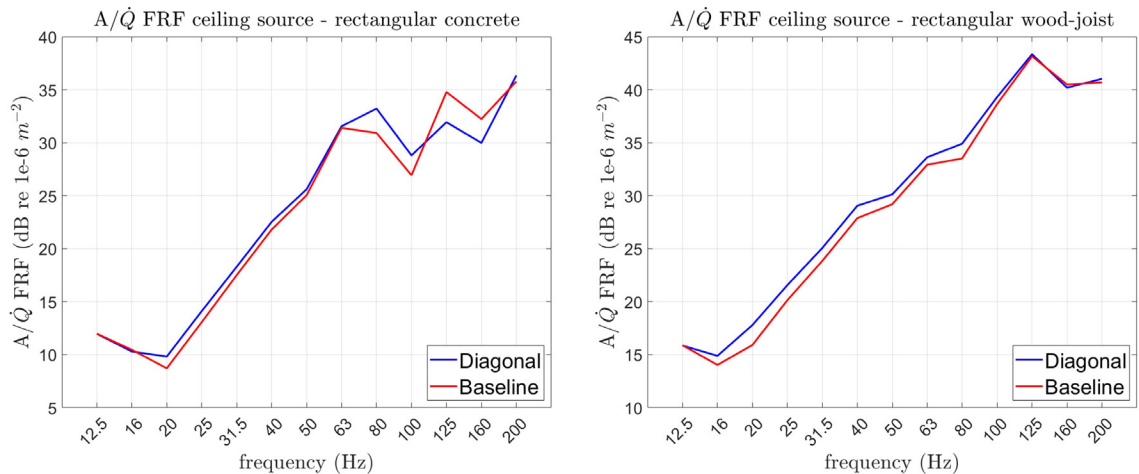


Figure 4-21 The diagonally averaged FRF (blue) compared with the baseline A/Q FRF (red) for the rectangular concrete (left) and the wood-joint (right) assembly. Both pairs of FRFs compare within 1 – 2.3 dB in the non-diffuse region from 40 – 100 Hz OTO bands

Field tests may also include test rooms with a coupled space, such as a dining room, a reading nook, a closet, etc. (such as the CS shaped assembly). The diagonal in such a room could be defined based on the entire floor space (including the coupled space) or only the main floor space (excluding the coupled space). For the CS wood-joint floor, Fig. 4-22 compares the baseline (solid red) with the diagonal FRF for the entire floor (solid blue) and only the main floor space (dashed blue). The sketch of the selected diagonal and the measurement points is also available in Fig. 4-22. All three FRFs showed a comparison of 1 – 1.5 dB below the 100 Hz OTO band. This variation increases slightly with frequency. Only the main floor space can be used to predict the performance of the entire floor structure. The CS concrete and BW concrete showed similar results (see Appendix A.10).

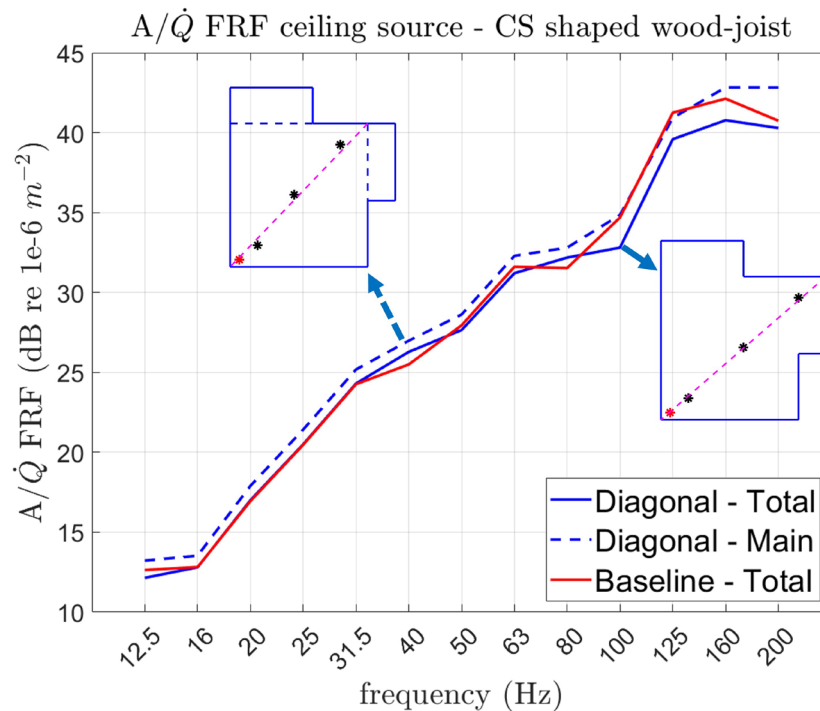


Figure 4-22 The baseline FRF (solid red) compared with the diagonal FRF over the entire floor (solid blue) and only the main floor space ignoring the coupled spaces (dashed blue) showed a difference of approximately 1 – 1.5 dB below the 100 Hz OTO band for the CS shaped wood joist floor. Only the main floor space can be used to predict the floor performance

For the case of the Q source placed near the ceiling, three measurement points aligned along the room diagonal can be sufficient to represent the impact performance of the entire floor. The next sub-section discusses the simulation results for the Q source placed near the room corner and compared the results to the ceiling placement case.

4.4.2 Developing measurement guidelines for the Q source placed near a room corner

As the Q source is placed near a room corner, the diagonal points were selected and analyzed using the same guidelines as previously discussed. The comparison for the rectangular concrete and the wood-joint assemblies is shown in Fig. 4-23 left and right, respectively. Both FRF pairs compared within 1 dB of each other below 125 Hz OTO bands. For these assemblies, using three diagonal measurement points can sufficiently represent the performance of the entire floor.

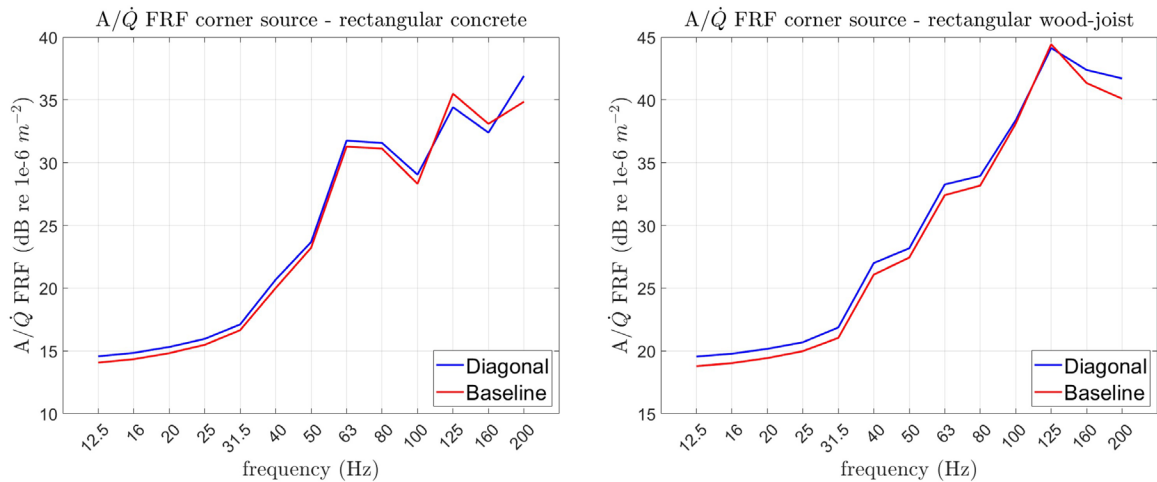


Figure 4-23 The diagonal FRF compared with the baseline when the Q source is placed near the corner for the rectangular concrete and wood-joint assembly showed that both pairs of FRFs compared within 1 dB for frequencies below 125 Hz OTO band.

The effect of the coupled spaces can also be evaluated for the corner Q source case. For the CS shaped wood joist assembly, Fig. 4-24 shows the comparison between the baseline (solid red), the diagonal FRF of the entire floor (solid blue), and the diagonal FRF from only the main floor (dashed blue). All three FRFs compared within 1 – 1.5 dB from 40 to 100 Hz OTO bands and the diagonal FRFs slightly overpredicted the baseline FRF. Note that some differences may exist because of the inaccuracy of finding the diagonal points because of the floor mesh size. The CS and BW concrete floors showed a similar comparison (see Appendix A.10)

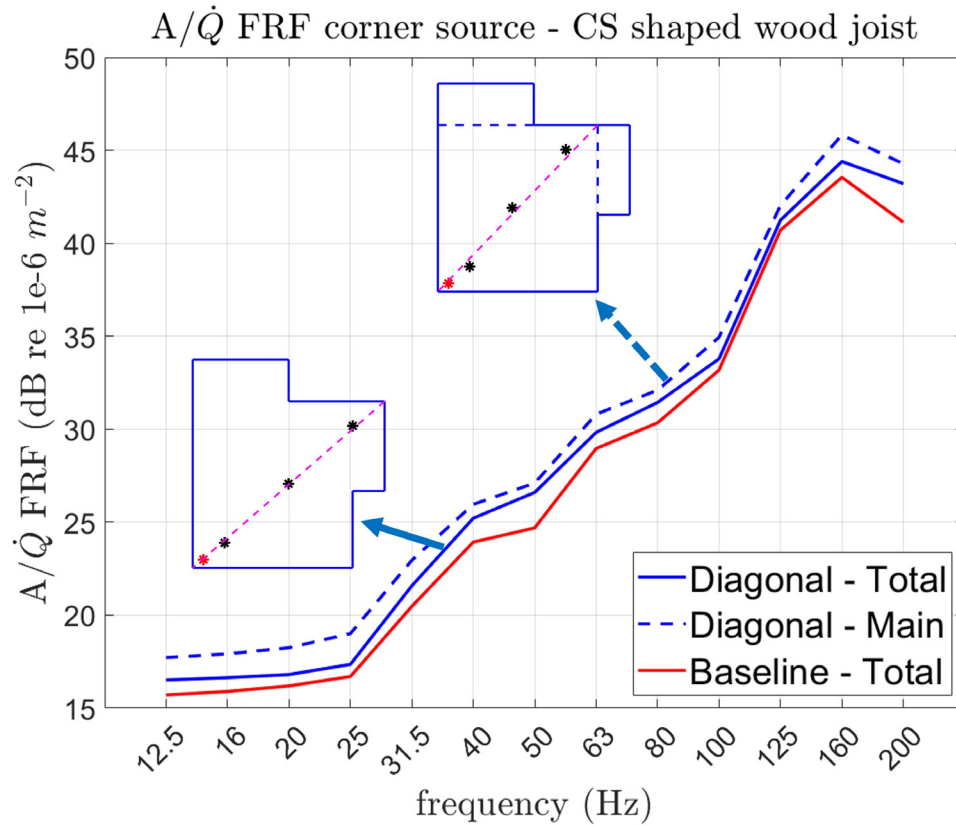


Figure 4-24 The diagonal and the baseline FRFs (solid red) compared for the CS shaped wood-joist floor by including the coupled spaces (solid blue) or excluding the coupled spaces (dashed blue) showed approximately 1 – 1.5 dB difference in the 40 – 100 Hz OTO bands

For the simulation model, the accuracy of finding the diagonal points may be compromised based on the grid size. Similarly for a field test, finding a diagonal point accurately may be challenging due to human error or other environmental factors. A simulation study was conducted to quantify the error in the diagonal FRF based on the error in finding the “accurate” diagonal point. For the rectangular concrete assembly with the corner Q source location, all possible combinations using all available points in different radii (250 mm to 550 mm) from the original locations were simulated. Figure 4-25 shows an example of such a selection for 450 mm radius in the bottom left corner. The red cross marks are the original diagonal locations, the magenta line is the 450 mm radius circle from the diagonal locations, and black cross marks are all available options that can be selected for that radius. Diagonal FRFs for all possible combinations of measurement locations were compared with the reference FRF (three original diagonal locations) and the error is plotted in Fig. 4-25 from 40 – 100 Hz OTO bands. A standard deviation of less than 0.5 dB was observed if the measurement points can be selected within 250 mm (approximately 10 inches) of the suggested guidelines from 40 – 100 Hz OTO bands. The standard deviation increases as the measurement tolerance radius increases, as expected.

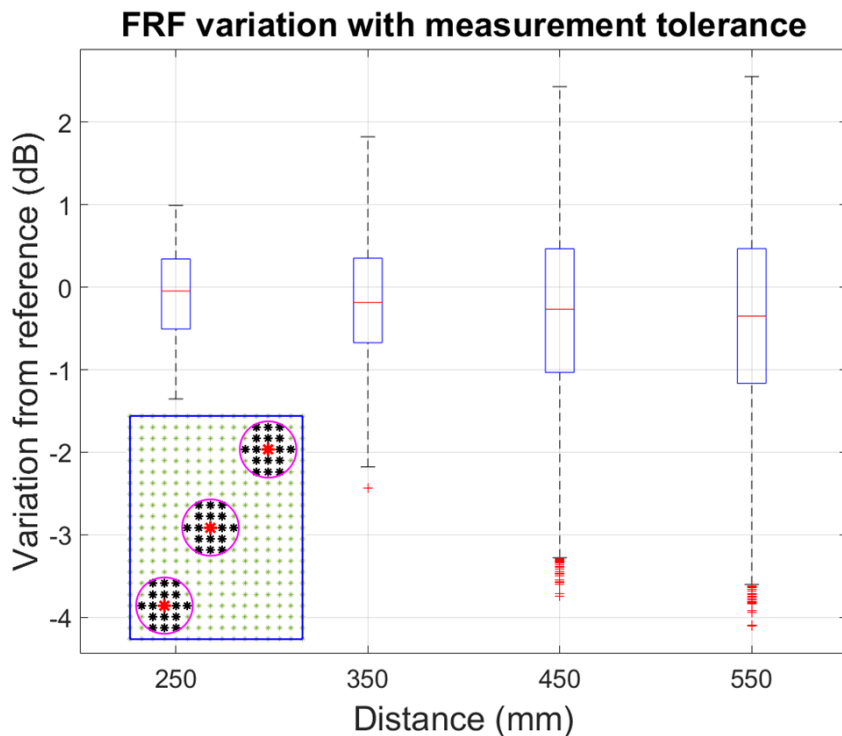


Figure 4-25 The standard deviation observed if any point combination is picked for different radii around the diagonal locations is shown. A standard deviation of less than 0.5 dB was observed if the measurements are made within 250 mm (approx. 10 in) of the proposed diagonal locations. An example of selecting all available measurement locations within 450 mm radius of the diagonal locations is shown in the bottom left corner

The Q source placed near all four corners in a perfect rectangular room would give the same diagonal FRF but this may not be the case if the room has coupled spaces such as the CS or the BW shaped assembly. Figure 4-26 shows the four diagonal FRFs obtained using the four room corners for the CS shaped concrete floor. The color of the curve and the corner (see the top left side of the plot) are matched in the figure. In the non-diffuse region from 40 – 100 Hz OTO bands, the four diagonal FRFs varied by approximately 2 – 4 dB. This variation may be reduced by averaging results from multiple room corners.

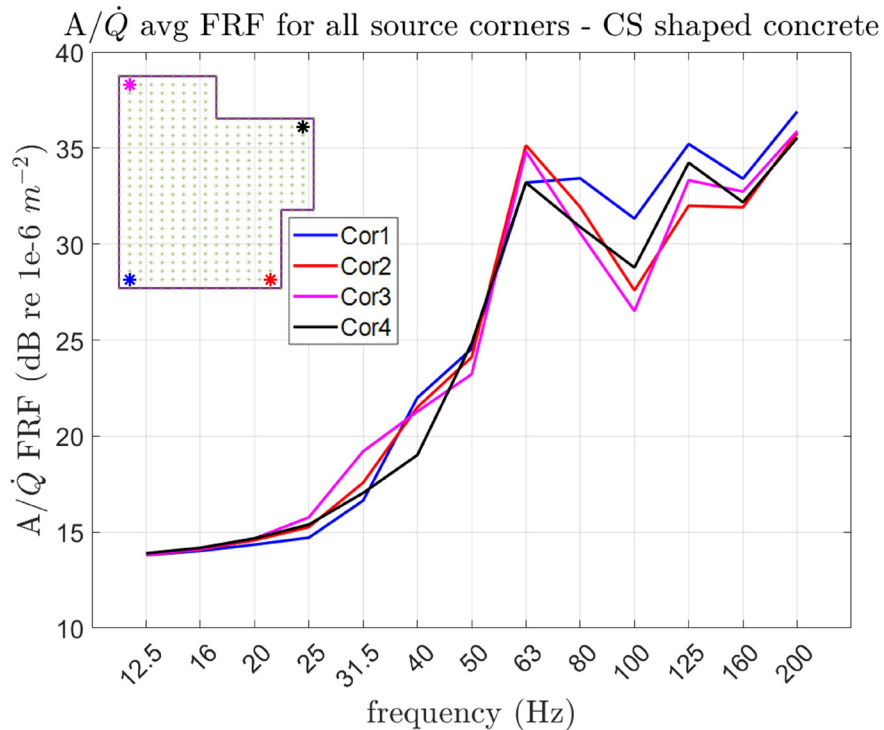


Figure 4-26 Four diagonal FRFs for all four corners in the CS shaped room assembly showed an approximate 2 – 4 dB variation in the 40 – 100 Hz OTO bands. Multiple corners may be needed to reduce this variation

Averaging the results by placing the Q source near two room corners can reduce measurement variation as shown in Fig. 4-27 for the CS shaped floor (left) and the BW shaped floor (right). All possible corner combinations were selected and corners along the same room diagonal were avoided. For each combination, at least one corner in the main room area was selected (an inside corner). The top-left side of Fig. 4-27 shows all corner options for both assemblies using red dots and the solid black line is the averaged FRF from all corner options in each case. Less than 1 dB standard deviation was observed between all corner combinations for the CS assembly and less than 0.5 dB standard deviation was observed for the BW assembly in the 40 – 100 Hz OTO bands.

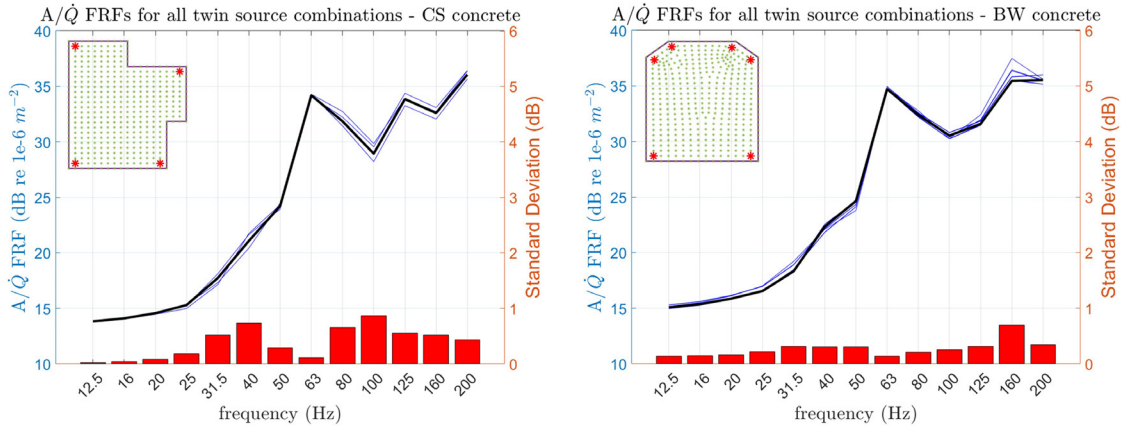


Figure 4-27 The standard deviation (right axis) between all corner combinations for the Q source placement showed less than 1 dB deviation for the CS floor (left) and less than 0.5 dB variation for the BW floor (right) in the 40 – 100 Hz OTO bands

4.4.3 Comparing the simulated FRF from the ceiling and the corner placement

The A/Q FRFs from the ceiling Q source location and the corner Q source location for the CS shaped concrete and wood-joint assemblies are shown in Fig. 4-28 (left and right, respectively). Approximately 1 – 2 dB difference was observed between the two floor performance FRFs measured using two different methods. Other simulation assemblies showed similar results. This indicates that comparable FRFs can be obtained if the Q source is placed near the corner or near the ceiling.

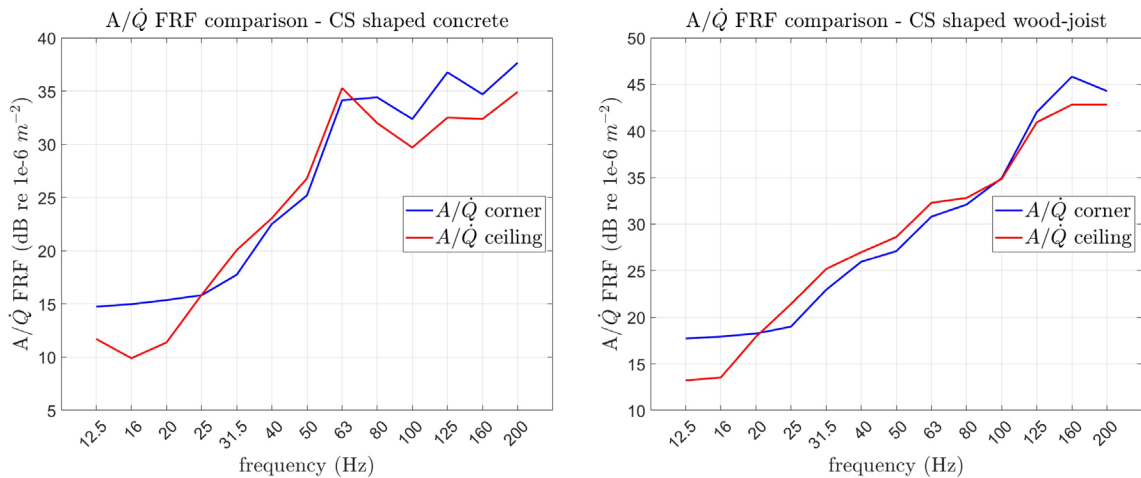


Figure 4-28 A/Q FRFs obtained using ceiling Q source and corner Q source placement for CS shaped concrete and wood-joint assemblies (left and right, respectively) showed a difference of approximately 1 – 2 dB in the 40 – 100 Hz OTO band non-diffuse region. Similar performance FRFs can be achieved using either Q source placement guidelines

The conclusions from the simulation model have been used to define the final measurement guidelines in the next sub-section

4.4.4 Proposed measurement guidelines based on the simulation model

The simulation model shows that the ceiling and corner diagonal FRFs provide very similar results. For ceiling testing, additional equipment such as a tall ladder may be needed to place the Q source as close to the ceiling as possible. For all three diagonal measurement locations, the ladder needs to be moved to the new location, which often means bringing the Q source down, moving the ladder, and placing the source on the ladder again. This involves lifting a heavy Q source while climbing a ladder and may significantly increase the test time. Additionally, it may be difficult to place the Q source near the center of the ceiling because of constraints such as ceiling fans, light fixtures, fire alarms, etc. Some variability may exist due to the speaker location inaccuracy.

Alternatively, for the corner measurements, the Q source can easily be placed near two room corners and the acceleration on the diagonal locations can be measured simultaneously. This reduces the total test time and doesn't put the operator at considerable risk by carrying a heavy Q source up a tall ladder multiple times.

All the models simulated have the same ceiling and floor surface area (like a stacked configuration) but for field tests, the room above and below may have different surface areas (for example a bedroom and a small office room located directly below a large open floor living room). In such a case, only the common floor space between the two should be considered. In the example above, the impact performance of the same floor-ceiling assembly (living room) could be perceived differently for the bedroom or the small office room so these cases will be studied individually by considering the common floor space in each case.

The single number rating calculated based on the proposed measurement method is named Low-frequency Impact Response Rating (LIRR) and is calculated similarly to the ASTM LIR rating [39] using the sum of values in the 50 – 80 Hz OTO bands as given below

$$LIRR = 130 - 2 * 10 \log_{10} \left(\sum_{f=50}^{f=80} 10^{FRF(f)/10} \right), \quad (4-2)$$

where, $FRF(f)$ is the measured FRF (or, RPF) in the f (Hz) frequency band. The number '130' is an arbitrary selection made to get the LIRR numbers in a similar range as compared to the ASTM LIR ratings.

For any test assembly, follow the following steps:

1. Identify the common floor space shared by the upstairs and the downstairs room
2. Identify the two longest floor diagonals in the common floor space

3. Identify the measurement locations at approximately 17%, 50%, and 83% of the diagonal length
4. Place the Q source near one of the corners along the diagonal. Avoid corners with obvious flanking or leakage paths (flanking noise transmission is not considered in this research for simplicity)
5. Measure the A/\dot{Q} FRFs at the three diagonal accelerometer locations. Alternatively, RPFs can be measured to avoid simultaneous measurements.
6. Multiply the outer diagonal points' FRF (or, RPF) by 2 and average the magnitude of all three FRFs (or, RPFs)
7. Multiply the average A/\dot{Q} FRF (or, RPF) by (3/5) to account for spatial averaging
8. Repeat steps 4 – 7 for the second room diagonal
9. Take an average of the two diagonal FRFs (or, RPFs).
10. Calculate the LIRR single number rating proposed in Eq 4-2.

The test rooms may often have a coupled space such as a closet, dining nook, reading corner, etc. The upstairs residents would spend much more time walking on the main floor space as compared to the coupled spaces like a closet. The ASTM test method includes the coupled spaces since the radiated sound field from the assembly entering the coupled spaces needs to be accounted for. For the reciprocal method, the coupled spaces can be ignored while evaluating the three diagonal measurement locations for the accelerometers.

These measurement guidelines were used to evaluate the impact performance of three structures, as detailed in the next section.

4.5 Evaluating the impact performance using the proposed test method

Three assemblies as defined in Section 3.4 were tested based on the proposed method and the standard ASTM test method. Recall that to avoid running a long BNC cable between the two rooms, the volume acceleration of the Q source and the floor acceleration were not measured simultaneously. The A/\dot{Q} RPFs were recorded to calculate the LIRR ratings that were compared to the standard ASTM single-number ratings. The floors are ranked based on their FRF performance and subjective response and the LIRR method shows an improved floor performance ranking.

4.5.1 Test results based on the proposed method

In addition to the proposed Q source location (near two room corners), all four corners were evaluated and the Q source was also placed close to the ceiling. This was done to compare the two RPFs even though corner measurements are easier to perform in the field. The results for all three assemblies are compared in this section and the additional plots are shown in Appendix A.11.

4.5.1.1 Test O1: Heavy concrete

The rooms were in a stacked configuration with a similar room size upstairs and downstairs. The heavy concrete assembly was tested with the Q source at five locations near the ceiling in the cross configuration (ref Fig. 4-18). The cross averaged RPF (from all points) and the two diagonal averaged RPFs compared within 1.5 dB below 400 Hz (see Appendix A.11.1). This showed that only three measurement locations along the room diagonal can be used to get the floor performance RPF. Both room diagonals had the same length and one of them was selected as the ‘final’ ceiling averaged RPF.

The Q source was also placed near the four room corners and the acceleration was measured at five floor locations aligned in the cross configuration. In each case, the diagonal RPFs were within 1 dB of the cross configuration (see Appendix A.11.1) confirming the conclusions from the simulation model. Only the diagonal FRFs were considered for the rest of this test. There are four possibilities for selecting any two corners in the room to get the corner averaged diagonal RPF. The four RPFs show a maximum standard deviation of 1 dB below 400 Hz (see Appendix A.11.1). Two corners were randomly selected to get the ‘final’ corner averaged RPF. The corner and the ceiling averaged RPFs are compared in Fig. 4-29 using solid blue and solid red lines, respectively.

The two RPFs show a difference of approximately 2 – 3 dB below 100 Hz OTO band but the shape of the spectra is similar. Recall that the Q source distance from the ceiling was approximately 170 mm due to the ladder height restrictions. This distance may lead to a lower impact SPL at the ceiling for the same measured Q output, which may lead to a lower floor acceleration and a lower A/\dot{Q} RPF when compared to the corner location. Figure A-31 in Appendix A.10 shows that the effect of the distance of the Q source from the ceiling cannot be corrected in post-processing.

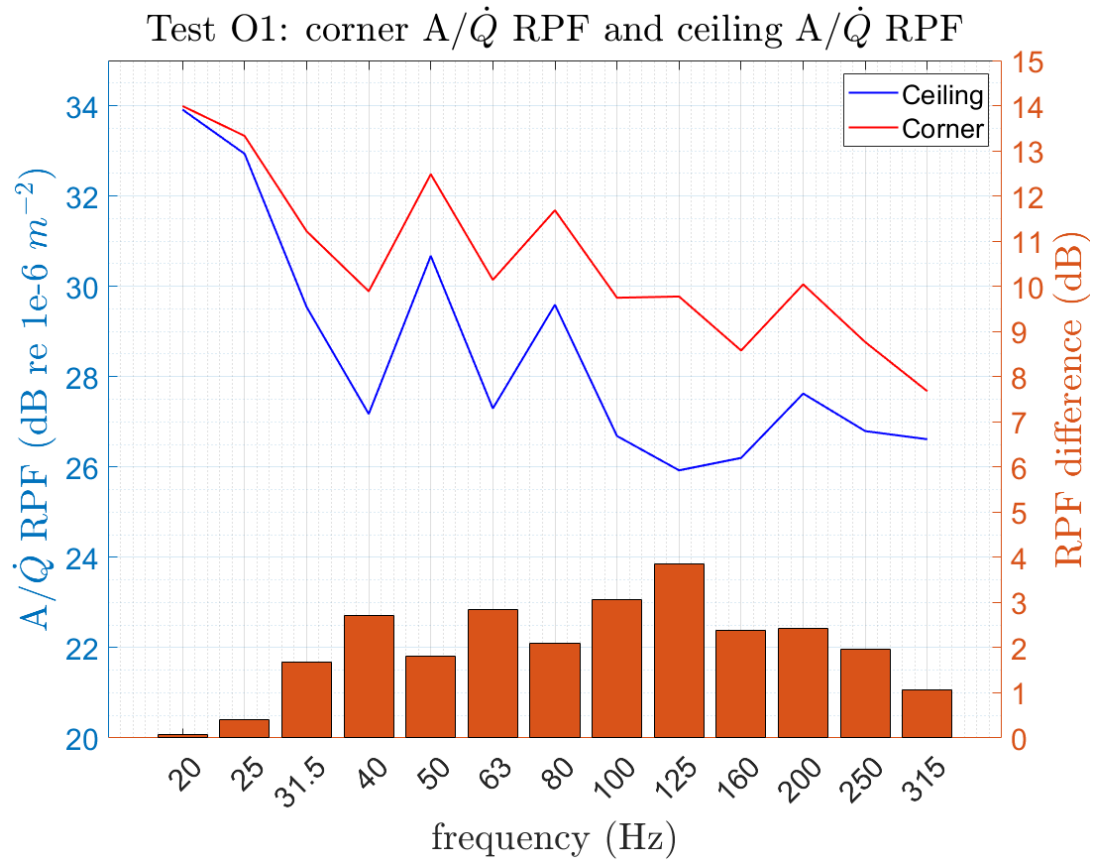


Figure 4-29 Test O1: The corner Q source RPF (red) compared with the ceiling Q source RPF (blue) shows a difference of approximately 2 – 3 dB below 100 Hz OTO band. Some differences may be explained due to the distance between the Q source and the ceiling (170 mm) which will lead to a reduced floor acceleration for the same measured speaker Q value

A modal hammer with microphones in the receiving room was also used to get the direct FRFs. The ‘average’ corner and ceiling direct FRFs were obtained the same way as the reciprocal RPFs and the two are compared in Fig. 4-30. The comparison for the ceiling Q source/ mic location is shown on the left, and the corner placement results are shown on the right. FRF/RPF pairs showed a maximum difference of approximately 1 dB from 31.5 Hz to 160 Hz OTO bands and the difference increased with frequency. This shows that the reciprocity theorem is applicable to this structure and the Q source can be used to get the impact performance of the floor. For this assembly, the diagonal RPF obtained using two random corner Q source locations has been used as the ‘final’ performance RPF.

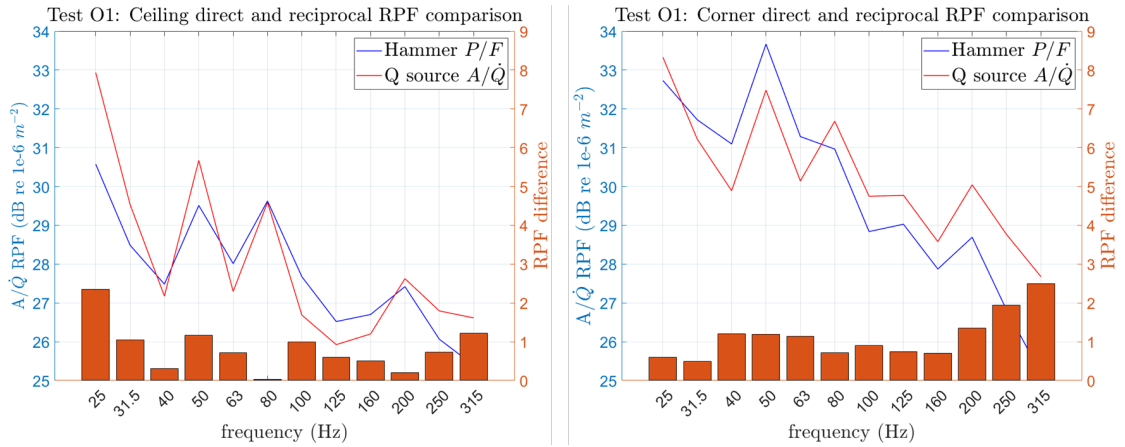


Figure 4-30 Test O1: The direct FRFs measured using a modal hammer and the reciprocal RPFs measured using the Q source for the ceiling locations (left) and the corner locations (right) showed a difference of approximately 1 dB from 31.5 to 160 Hz OTO bands. The reciprocity theory is applicable and the Q source can be used to get the impact performance of the floor

4.5.1.2 Test O2: Wooden joist-framed assembly

The downstairs room (blue lines in Fig. 4-31) is an enclosed room with furnishings such as a mattress, a desk, a cupboard, and some computer monitors. The upstairs floor has an open floor plan with a dining space just above the downstairs room under test (red lines in Fig. 4-31). The dining space is open to the kitchen on one side and the living room on the other (dotted red lines). Natural partitions such as the kitchen countertop and the wall between the kitchen and the living room were used to mark the ‘test space’ and the common area between the upstairs and downstairs room was used to get the room diagonals (solid cyan lines) and the measurement locations (magenta cross marks). The Q source was placed near all four room corners (black cross marks).

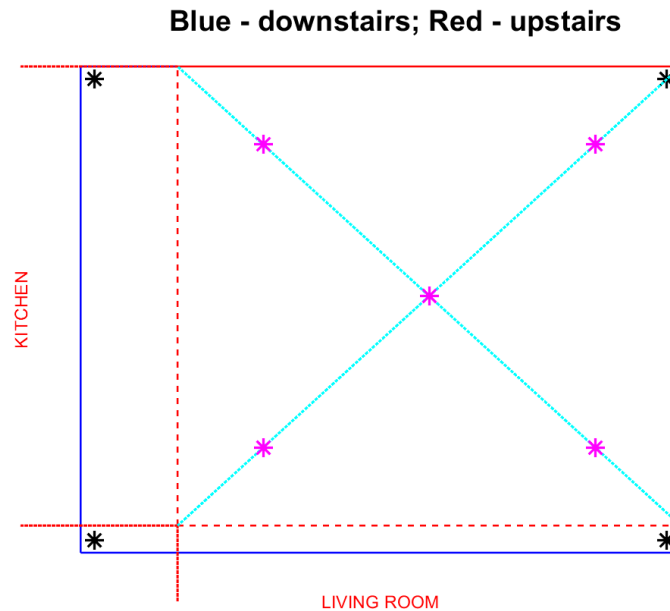


Figure 4-31 Test O2: The upstairs dining space (red) and the downstairs room (blue) have different floor areas. The upstairs space is open to the kitchen on one side and the living room on the other. The test area was selected based on the natural partitions in the house such as a kitchen counter and the wall between the kitchen and the living room (dashed red lines). The measurement locations (magenta cross marks) were selected based on the common area between the upstairs and the downstairs space

For assembly O2 with the Q source placed near the ceiling, the cross averaged RPF and the two diagonally averaged RPFs compared within 1.5 dB below 100 Hz and the variation increases with frequency (see Appendix A.11.2). Both room diagonals have the same length and one of them was selected to get the ‘final’ ceiling RPF.

With the Q source placed near the corners, the A/\dot{Q} RPFs from the cross configuration are within 1 dB of the diagonal RPFs (see Appendix A.11.2) and only the diagonal arrangement is used for this section. The four total two-corner combinations showed less than 1 dB standard deviation below 400 Hz. Two corners were randomly selected to get the ‘final’ corner RPF and is compared with the ceiling RPF in Fig. 4-32 using the solid red and the solid blue lines, respectively. Both RPFs compare within 1.5 dB in the 50 – 125 Hz OTO band range. The Q source is approximately 140 mm from the ceiling due to the ladder height restrictions and may explain some of the differences observed here.

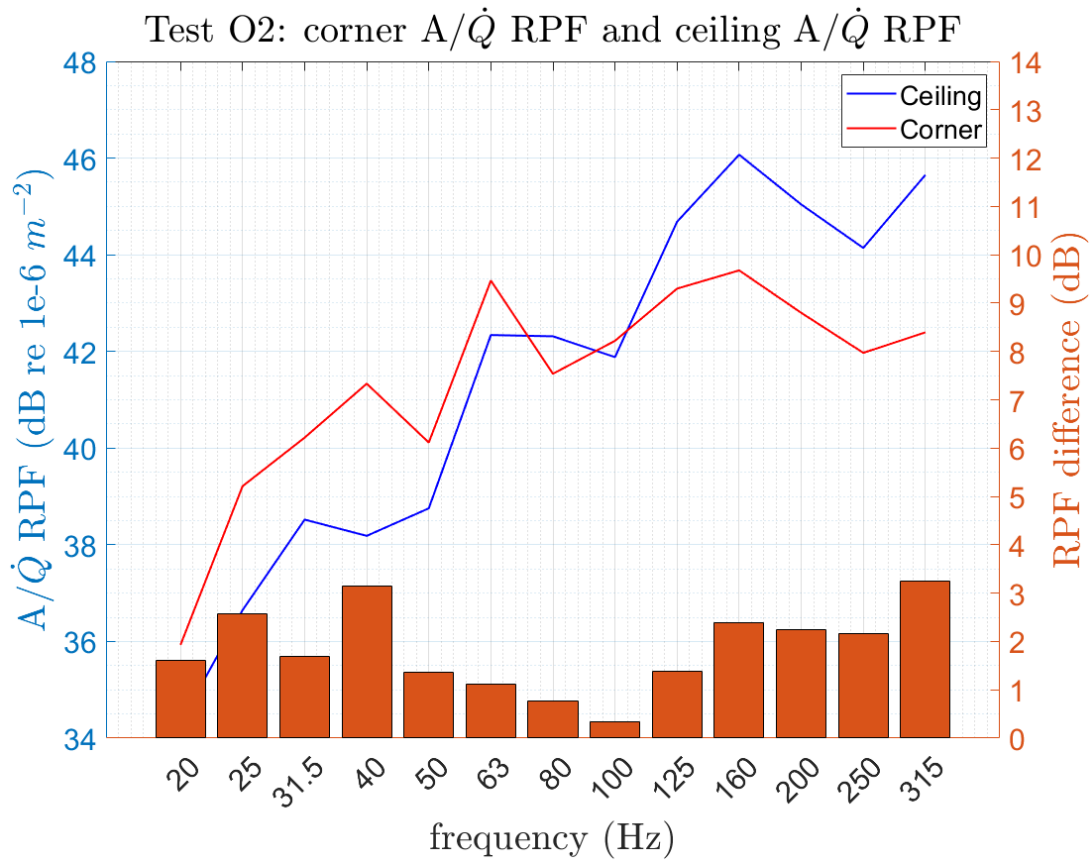


Figure 4-32 Test O2: The corner Q source RPF (red) compared with the ceiling Q source RPF (blue) shows less than 1.5 dB difference in the 50 – 125 Hz OTO bands. Some differences may be explained due to the distance between the Q source and the ceiling (140 mm) which will lead to reduced floor acceleration for the same measured speaker Q value

A modal hammer with microphones in the receiving room was also used to get the direct FRFs. The ‘average’ corner and ceiling direct FRFs were obtained the same way as the reciprocal RPFs and the two are compared in Fig. 4-33. The comparison for the ceiling Q source/ mic location FRF/RPFs is shown on the left, and the corner placement results are shown on the right. The ceiling data show a maximum difference of approximately 1.5 dB above 50 Hz and the corner data show a maximum difference of approximately 2 dB above 50 Hz. Recall that the automotive industry generally considers up to 3 dB differences between the direct and reciprocal FRF/RPFs as acceptable. The reciprocity theory is applicable and the Q source can be used to get the impact performance of the floor. For this assembly, the diagonal RPF obtained using two random corner Q source locations has been used as the ‘final’ performance RPF.

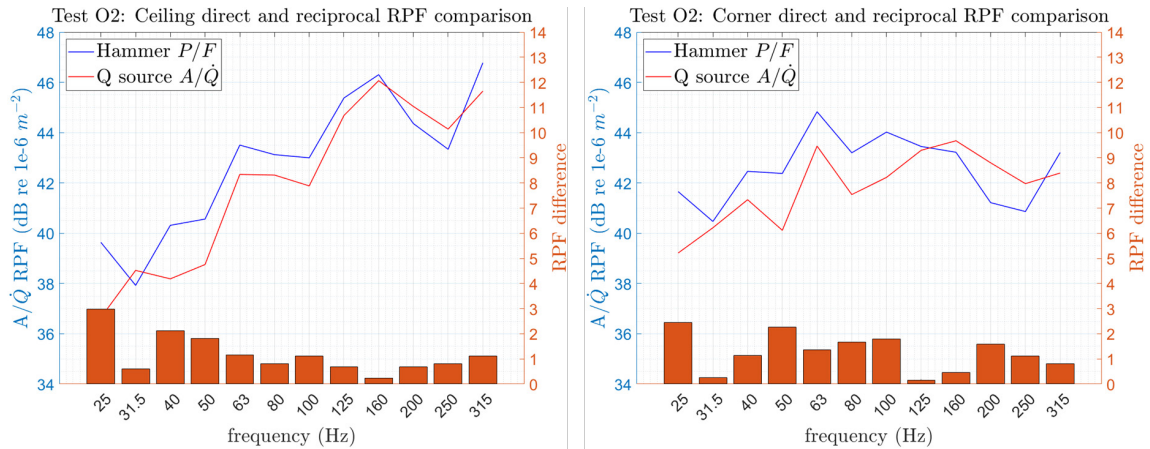


Figure 4-33 Test O2: The direct FRFs measured using a modal hammer and the reciprocal RPFs measured using the Q source for the ceiling locations (left) show a maximum difference of approximately 1.5 dB above 50 Hz. For the corner locations (right), the maximum difference observed is approximately 2 dB above the 50 Hz OTO band.

4.5.1.3 Test O3: Wooden joist-framed assembly with carpet finish

The downstairs room (blue lines in Fig. 4-34) has a closet (dashed lines) and a coupled space (bottom left corner) and the room size is different than the upstairs room (red lines in Fig. 4-34). The common floor space between the two rooms was selected as the ‘test space’ used to draw the two room diagonals (cyan lines) and the five measurement locations in the cross configuration (magenta cross marks). The Q source was placed at the four room corners (black cross marks), including the corner near the thin wooden closet door. Note that the Q source was also placed near the corner in the coupled space (black cross mark at the bottom left corner in Fig. 4-34) even though the coupled space was not used to get the measurement locations.

Blue - downstairs; Red - upstairs

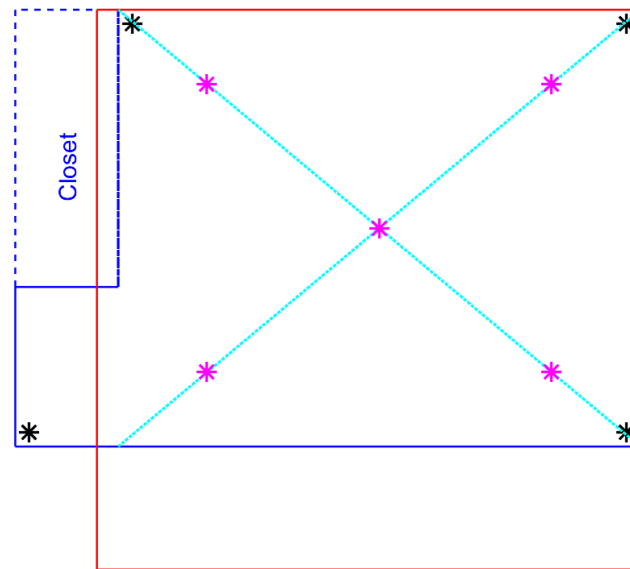


Figure 4-34 Test O3: The upstairs room (red) and the downstairs room (blue) with a coupled space (bottom left corner) have different room sizes. The common floor space was used to get the five cross configuration measurement locations (magenta cross marks). The Q source was placed near all the room corners (black cross marks)

The house was inhabited by a family with young children and the residents tried to stay in the other side of the house during the test. Some variability due to children running or jumping and people talking may be present in the measurement data. The HVAC system was also running normally so some effect of background noise may be present.

Both rooms were carpeted and a metal piece with Velcro (see Section 3.1.1.2) was used to mount the accelerometers in a non-destructive manner on the floor. To verify this mounting method, the reciprocity of the test assembly was evaluated as shown in Fig. 4-35. Solid blue and solid red lines are used to represent the direct FRFs and reciprocal RPFs, respectively. The left and right plots compare the reciprocity of the overall ceiling and the overall corner FRF/RPFs. A good comparison is observed below 40 Hz but approximately 2 – 3.5 dB difference is observed from 50 – 80 Hz. This may be because of improper mounting strategy used for the accelerometers with the metal Velcro piece.

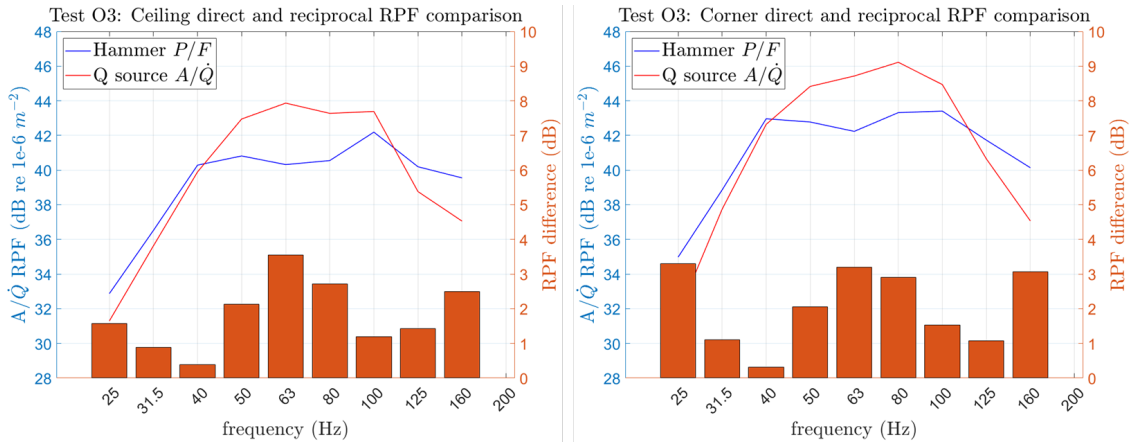


Figure 4-35 Test O3: The direct FRFs and reciprocal RPFs compared for the overall ceiling and overall locations show a difference of approximately 2 – 3.5 dB from 50 – 80 Hz which may be due to accelerometer mounting issues on the carpet with the metal Velcro piece

The narrowband spectra for the direct FRFs and the reciprocal RPFs (blue and red curves, respectively) for the ceiling and corner locations are compared in Fig. 4-36 (left and right, respectively). The reciprocal RPFs followed the profile of the curve but showed higher amplitude from approximately 40 to 100 Hz frequencies. This may be because of the accelerometer mounting method used for this test.

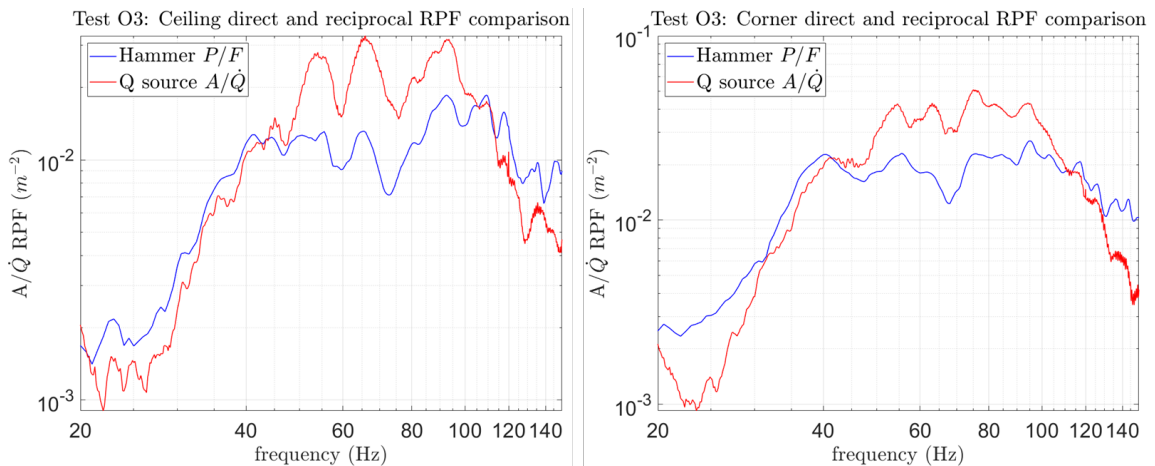


Figure 4-36 Test O3: The narrowband spectra comparison for the direct FRFs and the reciprocal RPFs showed that the reciprocal RPFs followed the general shape of the curve but showed higher amplitudes from 40 to 100 Hz which may be because of the metal Velcro mounting method used for the accelerometers

During an impact with the modal hammer for the direct FRF measurements, the carpet fibers will compress (for the area under impact) and may create a more direct path for the force. This may not be the case for a sound energy impact on the ceiling using a Q source. For the Q source, the measured acceleration may be dependent solely on the quality of the grip from the Velcro hook side with the carpet fibers, which may be the

reason for the error we see. The metal Velcro mounting method was previously discussed in Appendix A.3 and was used to mount the force transducers for the impact ball force plate (Section 3.1.1.2) with success. Just like a modal hammer, an impact ball drop would also compress the carpet fibers, creating a more direct path for the force and may be the reason why we had success using such a mounting method previously.

To check the test variability, one of the accelerometer metal Velcro mounts was removed and re-applied at the same location without changing the Q source location in the room below. Figure 4-37 compares the acceleration autopower spectra from the three tests and shows that the reproducibility is poor above 50 Hz. The metal Velcro mounting method was not successful and the reciprocal A/\dot{Q} RPFs measured for this assembly may be incorrect. Only direct P/F FRFs would be used for the rest of this section for this assembly.

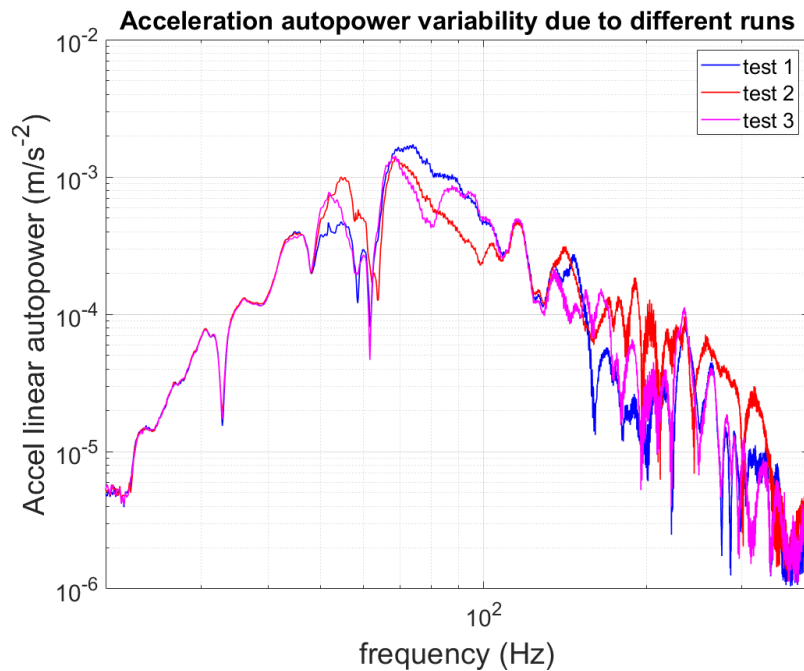


Figure 4-37 Test O3: The metal Velcro mount for the accelerometer was removed and re-applied at the same location without changing the Q source location to check the mount reproducibility. High variation was observed above 50 Hz and the metal Velcro mounting method was not successful for this assembly

The microphone was placed near the ceiling for all five measurement locations as the hammer impacts were made at the ‘driving point’ floor locations. Appendix A.11.3 compares the cross FRF with the two diagonal FRFs where less than 1 – 2 dB differences were observed. One of the diagonals was used as the ‘final’ averaged ceiling FRF.

Microphones were also placed near the room corners for hammer impacts at the five cross locations. The cross FRFs compared within 0.5 dB of the diagonal FRFs (see Appendix A.11.3) and only the diagonal configuration was used for this section. The four

total combinations of two-mic corners showed less than 1.3 dB standard deviation (Appendix A.11.3). Two corners were randomly selected to get the ‘final’ corner FRF which is compared with the ceiling FRF in Fig. 4-38 using the solid red and the solid blue line, respectively. Approximately 2 – 3 dB differences were observed which may be because of the 230 mm distance between the microphone location and the ceiling. Higher distance between the mic and the ceiling would lead to a reduced measured SPL for the same amount of measured input force level which would lead to a lower FRF value. The acoustic center of the Q source on the ladder could not be placed closer than 230 mm from the ceiling and the microphone was placed at the same location to test reciprocity.

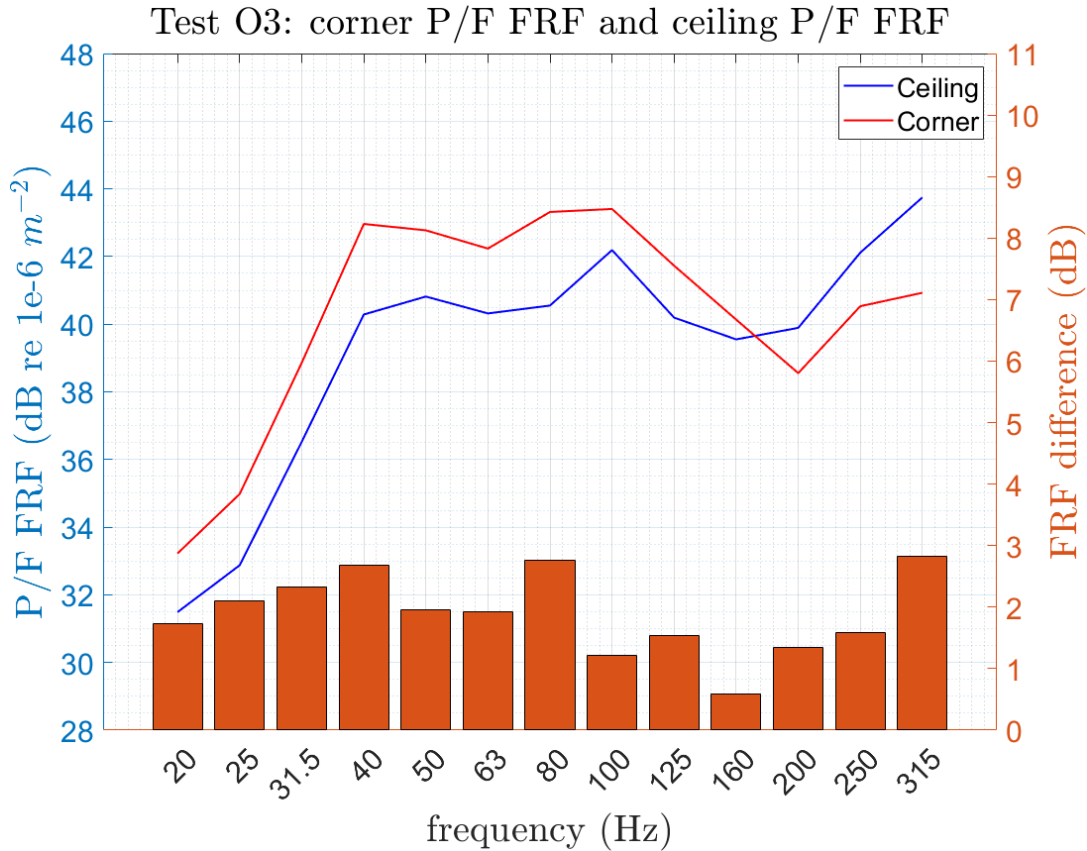


Figure 4-38 Test O3: The corner direct *P/F* FRF (red) compared with the ceiling FRF (blue) shows a difference of approximately 2 – 3 dB. Some differences may be explained due to the distance between the microphone and the ceiling (approximately 230 mm) which will lead to a reduced measured SPL for the same measured input force levels

4.5.2 Comparison between the existing and proposed single number performance ratings

The ASTM ISR and LIR ratings were calculated using the standard test method and the LIRR rating was calculated using the proposed method. This section compares all the single number ratings.

4.5.2.1 Calculation of LIRR rating

The corner FRF/RPFs from all three assemblies are compared in Fig. 4-39 where the reciprocal RPFs are used for assemblies O1 and O2, and direct FRF is used for assembly O3 (due to accelerometer mounting issues). Assembly O1 (concrete) significantly outperformed assemblies O2 and O3 (wood-joist structures). Assemblies O2 and O3 had similar performance for most of the frequency spectra but floor O2 had slightly better performance in lower frequencies from 40 to 100 Hz OTO bands. Similar observations were made from the ceiling FRF/RPFs (Appendix A.11.4)

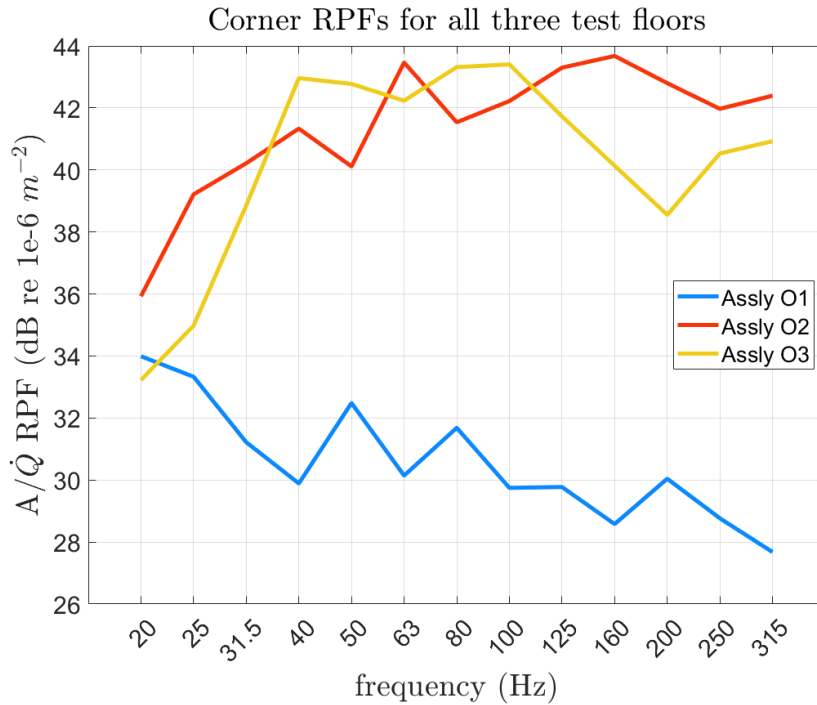


Figure 4-39 Corner RPFs compared for all floors based on the proposed measurement method showed that assembly O1 significantly outperformed the other two and assembly O2 slightly outperformed assembly O3 in low and high frequencies. This is in line with the conclusions from the adjusted tapping machine based P/F FRFs (Fig. 4-41)

The final ratings (using Eq 4-2) based on the proposed method using the corner and the ceiling placements are compared in Table 4-1. For both cases, assembly O1 significantly outperforms assemblies O2 and O3, which show a similar rating to each other. The ceiling LIRR is approximately 1 – 5 points higher than the corner LIRR which is more pronounced for assemblies O1 and O3 as compared to assembly O2. This may be because of the distance of the Q source (or, the microphone) from the ceiling and only the corner case is considered as the final rating.

Table 4-1 Proposed LIRR ratings for the corner and the ceiling Q source placement

	LIRR (corner)	LIRR (ceiling)
Assembly O1	57	62
Assembly O2	37	38
Assembly O3	35	39

4.5.2.2 Calculation of standard ASTM ISR and LIR ratings

The standard tapping machine was used for all three assemblies and Fig. 4-40 compares the averaged radiated SPL measured using the scanning measurement method for all cases. Assembly O2 (joist-framed with hardwood finish) had the loudest response with the tapping machine impacts below 800 Hz, with a maximum difference of 33 dB at 160 Hz compared to O1 (concrete). Assembly O3 (joist-framed with carpet finish) showed a louder response than O1 below 80 Hz with the tapping machine impacts but assembly O1 was louder above 80 Hz. The SPL for assembly O1 was approximately flat for the entire measurement bandwidth which was not the case for wood-joist floors (O2 and O3). Based on this curve, it is expected that floor O1 would have the highest LIR rating, followed by O3 and O2, and floor O3 would have the lowest ISR rating.

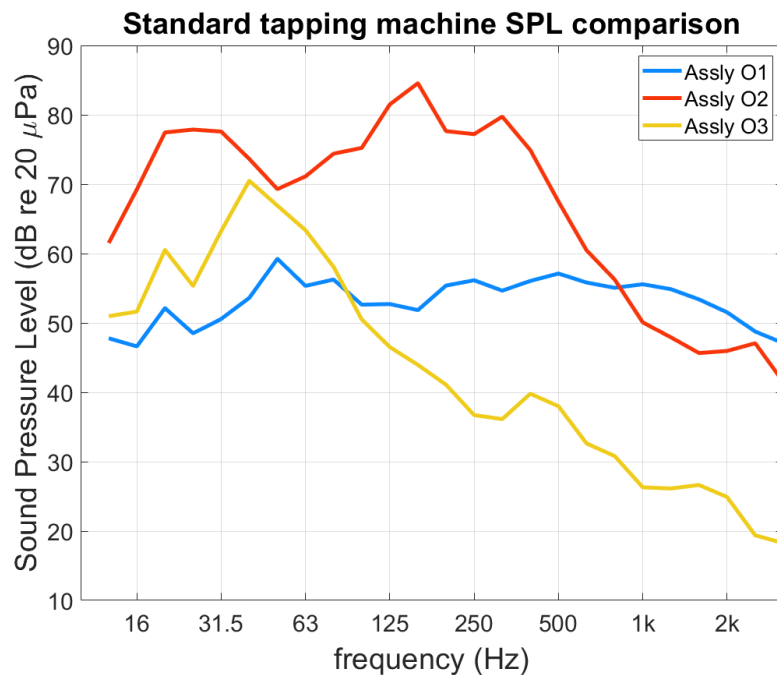


Figure 4-40 The average ASTM scanning SPL for all three test assemblies show that assembly O2 was the loudest below 800 Hz and assembly O3 was louder than O1 below 100 Hz and quieter above 100 Hz

The ASTM LIR and ISR ratings were calculated and tabulated in Table 4-2. Floor O1 has the highest LIR rating followed by floors O3 and O2. This is similar to the conclusions drawn from Fig. 4-40. Floor O2 has a significantly lower ISR rating as expected from Fig. 4-40. Floor O3 has a better ISR rating as compared to floor O1 even though the low-

frequency energy is higher for this floor. ISR looks at frequencies above 100 Hz so the effect of low-frequency energy doesn't show up in the ISR rating.

Table 4-2 ASTM ISR and LIR ratings obtained for the three test floors

	ASTM ISR	ASTM LIR
Assembly O1	52	66
Assembly O2	35	36
Assembly O3	69	52

4.5.2.3 Comparing the standard and the proposed method ratings

Recall that the input force frequency spectra for the tapping machine is highly dependent on floor compliance (Section 4.1.2). The measured SPL from the tapping machine can be corrected with the force autopower spectra measurements to get *P/F* RPFs. Note that the force autopower spectra from the tapping machine were measured on different floors and not on floors O1, O2, or O3, and with a single impact instead of continuous impacts with five hammers.

Floors HC2, LH2, and LC2 were found to be the most similar in construction and floor finishes compared to floors O1, O2, and O3, respectively. The single impact force values for these floors (Fig. 4-4) were used to calculate the *P/F* RPFs. The processed RPFs are shown in Fig. 4-41. Assembly O1 performs significantly better than assemblies O2 and O3 and the two wood-joint assemblies perform very similarly for most of the frequency bandwidth (in contrast to the ASTM ISR rating where a 34 point difference was observed). From 40 to 100 Hz OTO bands, assembly O3 shows approximately 2 – 7 dB worse performance as compared to assembly O2. This is in complete contrast to the LIR rating observed with the measured SPL where assembly O3 outperformed assembly O2 by 16 LIR points.

This is in line with the subjective response of the author where the low-frequency thuds were more annoying for floor O2 than floor O3. SPL based comparison with the tapping machine fails to quantify this behavior. An FRF-like measurement method can improve the rank order of floor performance with the subjective reaction.

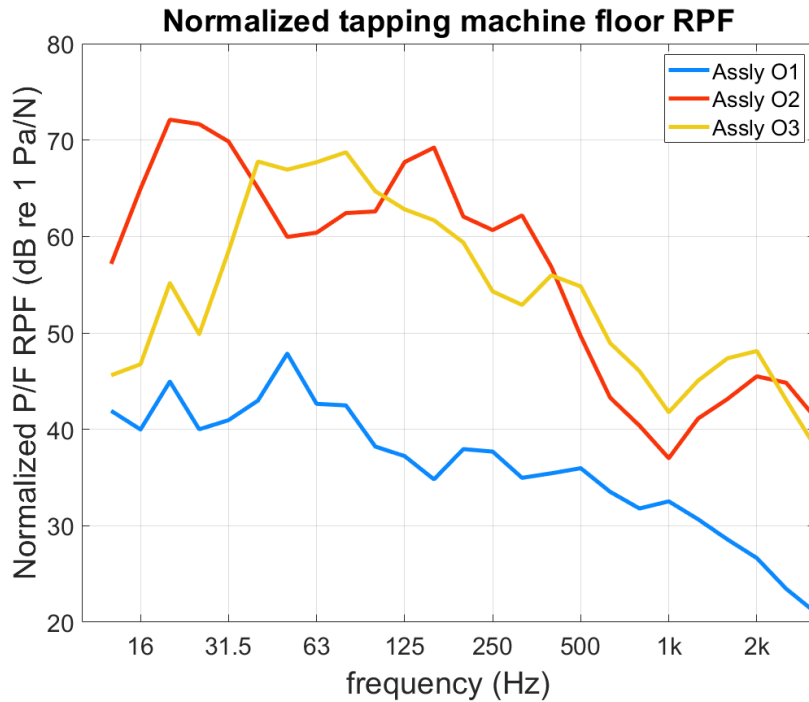


Figure 4-41 *P/F* RPF calculated using the measured SPL with the tapping machine and measured force. The SPL was measured using continuous impacts using 5 hammers and the force autowpowers were measured previously on different floors (with a similar construction) using a single impact. Assembly O3 underperforms by approximately 2 – 7 dB in the 40 – 100 Hz OTO bands as compared to assembly O2 which is in contrast with the LIR rating where O3 rated 16 points higher than floor O2

The proposed LIRR ratings for the three assemblies are compared with the standard ASTM ISR and LIR ratings in Table 4-3. The LIRR ratings match closely with the subjective reaction of the author and the *P/F* RPF from the standard ASTM tests where assembly O1 outperforms the other two and assembly O2 slightly outperforms O3.

Table 4-3 Proposed LIRR ratings compared with standard ASTM ratings

	ASTM ISR	ASTM LIR	LIRR
Assembly O1	52	66	57
Assembly O2	35	36	37
Assembly O3	69	52	35

5 Discussion

The input force due to an impact depends on the combined impedance of the impacted surfaces. If the impedance of one of the two objects is much higher than the other, the overall impedance is controlled by the object with the lower impedance. The tapping machine impactor is made of hardened steel [77] which has a much higher impedance than the floors under test, especially lightweight joist-framed floors. Therefore, the impact force from the tapping machine varies widely based on the type of floor. A 38 dB variation was observed from the seven floors tested for this work.

The ISO impact ball is made of rubber [77] and the impedance of rubber is much lower than the floor-ceiling assemblies. The input force is generally controlled by the impedance of the rubber ball, which remains unchanged for all floors tested. Therefore, less than 1.5 dB variation was observed in the peak level input forces with the impact ball. However, the impact ball fails to excite the floors above 100 Hz and is not a part of the ASTM standards.

The force from the footstep impacts also depends on the overall impedance of the foot and the floor assembly. With hard-heeled shoes, the input force will be dependent on the compliance of the floor (similar to the tapping machine) and for barefoot impacts, the input force may have low variation for all the assemblies (similar to the impact ball). Footsteps also suffer from inherent variability from one person to another. With such a variation, it becomes important to scale the output with the input to get an FRF-like quantity to quantify floor-ceiling assemblies.

An FRF-like measurement would also account for the tapping machine input force variability. However, currently, there is no provision in the standards to measure the input force from the tapping machine and an FRF measurement cannot be made. A reciprocity-based measurement method is presented in this work. The guidelines for this method are defined in Section 4.4.4

Note that the wood joists used in the simulation model are spaced at 19" O.C., but the 16" O.C. assemblies are more common for real structures. The joist span used in the simulation model was selected such that an integer joist spacing could be used throughout the simulated floor, which was not possible with the 16" O.C. design choice. The conclusions drawn in this work using the 19" O.C. simulation model should be valid for the 16" O.C. real structures as the narrower joist span (16" versus 19") shifts the local modes of the assembly to higher frequencies. It is expected that results for varying joist spacing will not differ significantly from the results shown here.

The Q source in the downstairs room can be set up with a stand-alone signal generator. The volume acceleration autopower spectrum can be measured separately and can be used with the measured floor acceleration autopower spectra to get the A/\dot{Q} RPFs. A long BNC cable would not be required between the upstairs and downstairs room and only three acquisition channels would be needed for the three diagonal locations for the test. A white noise or a sine sweep signal will give good precision. Currently, this method is

only limited to floors with a hard surface finish since a methodology to mount accelerometers on carpet floors has not been developed.

A normal speaker (non-Q source speaker) may be used for the test if it acts as a monopole in lower frequencies. The sound power of the speaker can be measured in an anechoic chamber and the monopole relationship can be used to calculate the volume acceleration relationship with the input signal level. During the test, speaker \dot{Q} can be calculated based on the measured input signal level. This was not explored for this work and is part of the future scope.

Note that according to the reciprocity principle, the guidelines discussed above can be followed to get a P/F floor performance FRF if a known input force is used. The disadvantage of direct versus reciprocal measurements is that the hammer force needs to be acquired simultaneously with the microphone signals and a long BNC cable would be required to connect the transducers in the upstairs and the downstairs room. A data acquisition system with at least four input channels is required. For carpet floors, the accelerometer mounting method has not been developed yet so direct P/F FRF may be required to evaluate the performance of such floors.

It is important to discuss the overall cascading error of the proposed measurement method. If the measurement points are selected within 250 mm (approximately 10 inches) of the recommended locations, less than 0.5 dB errors can be expected. The test data from three structures showed that approximately 1 dB error may exist based on the random room corners selected for the Q source placement. The overall variability of the test method is approximately 1 – 1.5 dB if different test engineers select different room corners or different floor measurement locations (within 10 inches). This is a significant improvement when compared to the 4 – 10 dB variation observed in the literature [32].

The existing ASTM ISR rating is based on the radiated SPL measurements and an FRF-like quantity between the output SPL and input force is not calculated. The RPF results from the proposed method in their current state cannot be compared with the old ASTM data. The number '130' used to calculate the LIRR rating is selected to get the numbers in a similar range as the LIR rating but a direct conversion between the two cannot be established currently. Over time, however, as more assemblies are tested with the proposed method and the existing ASTM method, patterns will emerge that will allow the researchers to develop a relationship between the two. This was not included in this work and is considered part of the future research goals.

An infinite number of assembly combinations may exist in the field (based on the layout of the rooms, coupled spaces, room dimensions, floor construction, etc.) and it is impossible to cover all our bases for this work. Three field assemblies and five simulation assemblies were studied but it is recommended that the field test engineer take copious notes while performing the test. The Q source and the floor accelerometer locations should be clearly marked in the final report so that the variability of the test method can be low. A detailed report is preferred but a separate 'overview' report might be needed at times to communicate with the clients.

6 Conclusions and Future Scope

The tapping machine showed a 38 dB variation in the peak force levels for the seven floor-ceiling assemblies tested. This force variation is not accounted for in the current ASTM standards or the building codes. For one of the seven floors, a poor signal to noise ratio was observed above 70 Hz. Recall that the lowest frequency OTO band studied for the ASTM ISR rating defined in the building codes is 100 Hz and this floor was poorly excited for the entire bandwidth. The impact ball showed a 1.5 dB variation in peak force levels for all the floors tested but it's a poor impactor for frequencies above 100 Hz.

The simulation model showed that the forward propagating intensity method can reduce the effects of the reflected sound field on the measured surface but the results are still approximately 1 – 5 dB different when compared to a free-field assembly sound power. Additionally, the intensity method involves specialized equipment (intensity probe), long test times (to measure the intensity at discrete points near the ceiling), and may suffer from higher measurement variability (based on operator error for discrete point measurements). Most of the field tests are meant to be fast to reduce the inconvenience for the residents and the intensity method may not be a practical choice of measurements. Therefore, the intensity method was not explored any further.

The reciprocity method can be used to get the floor performance FRF similar to the automotive industry. A total of nine tests on four floor-ceiling assemblies showed that the reciprocal and the direct FRFs show a good comparison in the low-frequencies.

Three measurement points aligned along the room diagonal provide reciprocal RPFs within 1 – 2 dB of the baseline and can be used to represent the performance of the entire floor. Measurement guidelines are defined in the main text and if the acceleration is measured within approximately 250 mm (10 inches) of the accurate points, a 0.5 dB maximum error can be expected. The Q source for the measurements can be placed near the ceiling or near a room corner to get similar performance RPFs but corner measurements are preferred as they require reduced test time and effort. The Q source is placed near two room corners and the diagonal RPF results are averaged. Reproducibility errors of 1 – 1.5 dB can be expected for the proposed method based on user error (picking Q source corners or acceleration measurement locations) as compared to 4 – 10 dB error from the literature with the current measurement method in low-frequencies. Note that an uncertainty analysis was not performed since it requires the same assembly to be tested multiple times. It was considered out of scope of the current research but will be considered for future work.

In the future, the applicability of using a non-Q source speaker will be evaluated if the speaker can be assumed to behave as a monopole source in low frequencies. Non-destructive accelerometer mounting strategy on carpet floors will also be developed for reciprocal testing. As more assemblies are tested, patterns will be identified to relate the existing ASTM ISR and LIR ratings to the proposed LIRR rating. A subjective evaluation would be conducted to relate the resident annoyance due to footstep noise for different assemblies with the LIRR rating rank order. The effect of room absorption and

furnishings will also be evaluated with the corner reciprocal measurements and a potential reverberation-time normalization procedure will be developed.

7 Reference List

1. Anthes, E., *The Great Indoors*. 2020: Farrar, Straus, and Giroux.
2. Systems, C.f.S. *U.S. Cities Factsheet*. 2020; Available from: <https://css.umich.edu/factsheets/us-cities-factsheet>.
3. Smith, A., *A review of the effects of noise on human performance*. Scandinavian Journal of Psychology, 1989. **30**(3): p. 185-206.
4. Ronsse, L.M. and L.M. Wang, *Relationships between unoccupied classroom acoustical conditions and elementary student achievement measured in eastern Nebraska*. The Journal of the Acoustical Society of America, 2013. **133**(3): p. 1480-1495.
5. Rasmussen, B. and O. Ekholm. *Is noise annoyance from neighbours in multi-storey housing associated with fatigue and sleeping problems?* in *23rd International Congress on Acoustics-ICA 2019*. 2019. Deutsche Gesellschaft für Akustik (DEGA eV).
6. Broyles, J.M., M.R. Shepherd, and N.C. Brown, *Modified acoustic transmission metrics for early-stage design exploration using a computational case study of heavyweight floors* ☆. Applied Acoustics, 2022. **196**: p. 108865.
7. Blazier Jr, W.E. and R.B. DuPree, *Investigation of low-frequency footfall noise in wood-frame, multifamily building construction*. The Journal of the Acoustical Society of America, 1994. **96**(3): p. 1521-1532.
8. US_EPA. *EPA to Launch Noise Control Program*. [Electronic] 1972 Sept 14, 2016; Available from: <https://archive.epa.gov/epa/aboutepa/epa-launch-noise-control-program.html>.
9. US_EPA. *EPA Identifies Noise Levels Affecting Health and Welfare*. 1974 Sept 14, 2016; Available from: <https://archive.epa.gov/epa/aboutepa/epa-identifies-noise-levels-affecting-health-and-welfare.html>.
10. Control, U.S.-O.o.N.A., *Information on levels of environmental noise requisite to protect public health and welfare with an adequate margin of safety*. 1974: US Government Printing Office.
11. Council, I.C., *2021 International Building Code, in Section 1206 Sound Transmission*. 2020, ICC: Washington DC.
12. Bodlund, K., *Alternative reference curves for evaluation of the impact sound insulation between dwellings*. Journal of sound and vibration, 1985. **102**(3): p. 381-402.
13. Gerretsen, E., *A new system for rating impact sound insulation*. Applied Acoustics, 1976. **9**(4): p. 247-263.
14. Watters, B.G., *Impact-Noise Characteristics of Female Hard-Heeled Foot Traffic*. The Journal of the Acoustical Society of America, 1965. **37**(4): p. 619-630.
15. Jeon, J.Y., et al., *Review of the Impact Ball in Evaluating Floor Impact Sound*. Acta Acustica united with Acustica, 2006. **92**(5): p. 777-786.
16. Tachibana, H., et al., *Development of new heavy and soft impact source for the assessment of floor impact sound insulation of buildings*. INTER-NOISE and NOISE-CON Congress and Conference Proceedings, 1998. **1998**(4): p. 1227-1230.

17. Jeon, J.Y., P.J. Lee, and S.-i. Sato, *Use of the standard rubber ball as an impact source with heavyweight concrete floors*. The Journal of the Acoustical Society of America, 2009. **126**(1): p. 167-178.
18. ASTM_E989-21, *Standard Classification for Determination of Single-Number Metrics for Impact Noise*. 2021, ASTM International: West Conshohocken, PA.
19. ASTM_E492-09, *Standard Test Method for Laboratory Measurement of Impact Sound Transmission Through Floor-Ceiling Assemblies Using the Tapping Machine*. 2016.
20. ASTM_E1007-21, *Standard Test Method for Field Measurement of Tapping Machine Impact Sound Transmission Through Floor-Ceiling Assemblies and Associated Support Structures*. 2021.
21. Olynyk, D. and T.D. Northwood, *Assessment of Footstep Noise through Wood-Joist and Concrete Floors*. The Journal of the Acoustical Society of America, 1968. **43**(4): p. 730-733.
22. Mariner, T. and H. Hehmann, *Impact-Noise Rating of Various Floors*. The Journal of the Acoustical Society of America, 1967. **41**(1): p. 206-214.
23. Shi, W., C. Johansson, and U. Sundback, *A comparison of the characteristics of different impact force with a standard tapping machine*. INTER-NOISE and NOISE-CON Congress and Conference Proceedings, 1995: p. 739-742.
24. Lietzen, J., et al., *Evaluation of impact sound insulation of intermediate floors on the basis of tapping machine and walking*. INTER-NOISE and NOISE-CON Congress and Conference Proceedings, 2013. **247**(8): p. 729-735.
25. Warnock, A., *Low-frequency impact sound transmission through floor systems*. INTER-NOISE and NOISE-CON Congress and Conference Proceedings, 2000. **2000**(9): p. 1-10.
26. Amiryarahmadi, N., W. Kropp, and K. Larsson, *Identification of Low-Frequency Forces Induced by Footsteps on Lightweight Floors*. Acta Acustica united with Acustica, 2016. **102**(1): p. 45-57.
27. Nordby, K.S., *Tapping machine use and data interpretation*. INTER-NOISE and NOISE-CON Congress and Conference Proceedings, 1989: p. 611-616.
28. Byrick, W.R., *Field Measured Variation of Low Frequency Impact Noise in a Wood Frame Building*. INTER-NOISE and NOISE-CON Congress and Conference Proceedings, 2017. **254**(2): p. 388-393.
29. LoVerde, J.J. and D.W. Dong, *A dual-rating method for evaluating impact noise isolation of floor-ceiling assemblies*. The Journal of the Acoustical Society of America, 2017. **141**(1): p. 428-440.
30. Olynyk, D. and T. Northwood, *Subjective Judgments of Footstep-Noise Transmission through Floors*. The Journal of the Acoustical Society of America, 1965. **38**(6): p. 1035-1039.
31. Ljunggren, F., C. Simmons, and K. Hagberg, *Correlation between sound insulation and occupants' perception—Proposal of alternative single number rating of impact sound*. Applied Acoustics, 2014. **85**: p. 57-68.
32. Oliva, D., et al., *Measurement of low frequency noise in rooms*. Finnish Institute of Occupational Health, Helsinki, 2011.

33. Hopkins, C. and P. Turner, *Field measurement of airborne sound insulation between rooms with non-diffuse sound fields at low frequencies*. Applied Acoustics, 2005. **66**(12): p. 1339-1382.
34. Barnard, A., et al. *Evaluation of Receiving Room Diffusivity and the Effect on Low Frequency Impact Insulation Class*. in *INTER-NOISE and NOISE-CON Congress and Conference Proceedings*. 2018. Chicago, Illinois, USA.
35. Girdhar, S., *Improved low-frequency impact insulation class measurements based on comparison techniques*, in *Open Access Master's Report*. 2019, Michigan Technological University.
36. Simmons, C., *Uncertainty of room average sound pressure levels measured in the field according to the draft standard ISO 16283-1*. Noise Control Engineering Journal, 2012. **60**(4): p. 405-420.
37. Schoenwald, S. and S. Pedersoli. *Applicability of measurement method according to ISO 16283 in small rooms at low frequencies*. in *INTER-NOISE and NOISE-CON Congress and Conference Proceedings*. 2016. Institute of Noise Control Engineering.
38. Pedersen, S., H. Møller, and K.P. Waye, *Indoor Measurements of Noise at Low Frequencies — Problems and Solutions*. Journal of Low Frequency Noise, Vibration and Active Control, 2007. **26**(4): p. 249-270.
39. ASTM_E3207-21, *Standard Classification for Determination of Low-Frequency Impact Noise Ratings*. 2021: West Conshohocken, PA.
40. Reiher, H., *Über den Schallschutz durch Baukonstruktionsteile (Sound Isolation by Building Construction Elements)*. Beih. Ges.-Ing, 1932. **2**(11): p. 2-28.
41. Bausch, W., *Schalldämmungs-Messungen in Laboratorium und in fertigen Gebäuden (Sound Isolation Measurements in the Laboratory and in Finished Buildings)*. Beih. Ges.-Ing, 1939. **2**(20): p. 1-33.
42. Schultz, T.J., *Impact Noise Rating and Testing*. Architectural Science Review, 1981. **24**(3): p. 77-83.
43. Gösele, K., *Trittschall-Entstehung und Dämmung*. Acta Acustica united with Acustica, 1956. **6**(1): p. 67-72.
44. Gösele, K., *Zur Dämmung von Gehgeräuschen*. Vol. 80. 1959: Ges.-Ing. 1-4.
45. Brandt, O., *European Experience with Sound-Insulation Requirements*. The Journal of the Acoustical Society of America, 1964. **36**(4): p. 719-724.
46. Fasold, W., *Untersuchungen über den Verlauf der Sollkurve für den Trittschallschutz im Wohnungsbau*. Acta Acustica united with Acustica, 1965. **15**(5): p. 271-284.
47. Cremer, L., *Der Sinn der Sollkurven*. Schallschutz von Bauteilen (Berlin, Wilhelm Ernst & Sohn), 1960: p. 1-9.
48. Warnock, A.C.C., *Low frequency impact sound transmission through floor systems*. INTER-NOISE and NOISE-CON Congress and Conference Proceedings, 1992. **1992**(2): p. 743-748.
49. Long, M., *Architectural acoustics*. Second ed. 2014: Elsevier.
50. Rabold, A., et al., *Modelling the Excitation Force of a Standard Tapping Machine on Lightweight Floor Structures*. Building Acoustics, 2010. **17**(3): p. 175-197.

51. Cremer, L. and M. Heckl, *Körperschall: Physikalische Grundlagen und technische Anwendungen (Structure-borne Sound: Structural vibrations and sound radiation at audio frequencies)*. 1996, Berlin, Heidelberg, New York: Springer.
52. Vér, I.L., *Impact Noise Isolation of Composite Floors*. The Journal of the Acoustical Society of America, 1971. **50**(4A): p. 1043-1050.
53. Scholl, W. and W. Maysenhölder, *Impact Sound Insulation of Timber Floors: Interaction between Source, Floor Coverings and Load Bearing Floor*. Building Acoustics, 1999. **6**(1): p. 43-61.
54. Brunskog, J. and P. Hammer, *The Interaction Between the ISO Tapping Machine and Lightweight Floors*. Acta Acustica united with Acustica, 2003. **89**(2): p. 296-308.
55. Brunskog, J. and P. Hammer, *Prediction of impact noise of lightweight floors, including the tapping machine*. INTER-NOISE and NOISE-CON Congress and Conference Proceedings, 1999. **1999**(4): p. 347-352.
56. Qian, C., et al., *Calibration of the ISO tapping machine for finite-element prediction tool on a wooden-base floor*. Building Acoustics, 2019. **26**(3): p. 157-167.
57. Guigou-Carter, C., M. Villot, and J. Kouyoumji. *Analytical and Experimental Study of Wood Floorings*. in *Forum Acusticum*. 2005.
58. Kimura, S. and K. Inoue, *Practical calculation of floor impact sound by impedance method*. Applied Acoustics, 1989. **26**(4): p. 263-292.
59. Brunskog, J. and P. Hammer, *Prediction Model for the Impact Sound Level of Lightweight Floors*. Acta Acustica united with Acustica, 2003. **89**(2): p. 309-322.
60. Lindblad, S., *Impact sound characteristics of resilient floor coverings. a study on linear and nonlinear dissipative compliance*. 1968, Dissertation. Division of Building Technology, Lund Institute of Technology
61. Wittstock, V., *On the Spectral Shape of the Sound Generated by Standard Tapping Machines*. Acta Acustica united with Acustica, 2012. **98**(2): p. 301-308.
62. Qian, C., et al., *Description and Calibration of the ISO Tapping Machine in Numerical Impact Sound Predictive Tools*. INTER-NOISE and NOISE-CON Congress and Conference Proceedings, 2018. **258**(4): p. 3262-3271.
63. Caniato, M., et al., *Acoustic of lightweight timber buildings: A review*. Renewable and Sustainable Energy Reviews, 2017. **80**: p. 585-596.
64. Brunskog, J. and P. Hammer, *Prediction Models of Impact Sound Insulation on Timber Floor Structures; A Literature Survey*. Building Acoustics, 2000. **7**(2): p. 89-112.
65. Mariner, T., *Technical problems in impact noise testing*. Building Research, 1964. **1**: p. 53-60.
66. Olsson, J. and A. Linderholt, *Force to sound pressure frequency response measurements using a modified tapping machine on timber floor structures*. Engineering Structures, 2019. **196**: p. 109343.
67. Schultz, T.J., *Alternative test method for evaluating impact noise*. The Journal of the Acoustical Society of America, 1976. **60**(3): p. 645-655.

68. Nordstedt, J.R., *Comparison between different methods for impact testing of floors*. The Journal of the Acoustical Society of America, 1979. **65**(2): p. 418-424.
69. Scholl, W., *Impact Sound Insulation: The Standard Tapping Machine Shall Learn to Walk!* Building Acoustics, 2001. **8**(4): p. 245-256.
70. Lietzén, J., et al. *Measurements of impact force excitation on wooden floors*. 2018. Euronoise.
71. Lietzén, J., et al., *Impact force excitation generated by an ISO tapping machine on wooden floors*. Applied Acoustics, 2021. **175**: p. 107821.
72. Dodd, G. and B. Yen, *Measuring Ln without using a tapping machine?* INTER-NOISE and NOISE-CON Congress and Conference Proceedings, 2014. **249**(2): p. 4826-4831.
73. Inoue, K., M. Yasuoka, and H. Tachibana. *New heavy impact source for the measurement of floor impact sound insulation of buildings*. in *Proceedings of inter-noise*. 2000.
74. Park, S. and H. Kim, *Development of Analytical Impact Force Models for Floor Impact Vibration and Acoustic Numerical Analysis*. Applied Sciences (2076-3417), 2016. **6**(5): p. 120.
75. Späh, M., et al., *Subjective and Objective Evaluation of Impact Noise Sources in Wooden Buildings*. Building Acoustics, 2013. **20**(3): p. 193-213.
76. Olsson, J. and A. Linderholt, *Measurements of low frequency impact sound frequency response functions and vibrational properties of light weight timber floors utilizing the ISO rubber ball*. Applied Acoustics, 2020. **166**: p. 107313.
77. ISO, *16283-2: Acoustics — Field measurement of sound insulation in buildings and of building elements — Part 2: Impact sound insulation*. 2018.
78. Scholl, W., J. Lang, and V. Wittstock, *Rating of Sound Insulation at Present and in Future. The Revision of ISO 717*. Acta Acustica united with Acustica, 2011. **97**(4): p. 686-698.
79. Hamme, R.N., *Sound transmission through floor-ceiling structures: I. Evolution of new impact test method*. 1965, Geiger and Hamme Laboratories, Anne Arbor, MI.
80. Paley, S. *The Anatomy of an IIC Rating*. in *INTER-NOISE and NOISE-CON Congress and Conference Proceedings*. 2016. Institute of Noise Control Engineering.
81. Öqvist, R., F. Ljunggren, and R. Johnsson, *Walking sound annoyance vs. impact sound insulation from 20 Hz*. Applied Acoustics, 2018. **135**: p. 1-7.
82. Scholl, W., J. Lang, and V. Wittstock, *Revision of ISO 717: Future single-number quantities for sound insulation in buildings*. Proceedings Euronoise, Prague, 2012.
83. ISO, *717-2: Acoustics -- Rating of sound insulation in buildings and of building elements -- Part 2: Impact sound insulation*. 2013.
84. Rasmussen, B., M. Machimbarrena, and P. Fausti, *COST Action TU0901— Building acoustics throughout Europe*. Volume 1: Towards a common framework in building acoustics throughout Europe, 2014.
85. ISO, *19488: Acoustics — Acoustic classification of dwellings*. 2021, ISO.
86. ASTM_E3222-20, *Standard Classification for Determination of High-frequency Impact Sound Ratings*. 2020: West Conshohocken, PA.

87. Dong, W., J.L. Verde, and S. Girdhar, *Measurement of low frequency impact insulation*. The Journal of the Acoustical Society of America, 2020. **148**(4): p. 2513-2513.
88. Uosukainen, S., *On the use of the Waterhouse correction*. Journal of Sound and Vibration, 1995. **186**(2): p. 223-230.
89. Garg, N., et al., *Measurement uncertainty in airborne sound insulation and single-number quantities using sound pressure and sound intensity approached*. Noise Control Engineering Journal, 2016. **64**(2): p. 153-169.
90. Girdhar, S. and A. Barnard, *Improved low-frequency sound measurements for impact insulation class (IIC) rating using a comparison technique*. Noise Control Engineering Journal, 2020. **68**(1): p. 72-86.
91. Girdhar, S. and A. Barnard, *Predicting Sound Power Response from a Simply Supported Rectangular Panel for Impact Insulation Class (IIC) Test*. INTER-NOISE and NOISE-CON Congress and Conference Proceedings, 2019. **260**(1): p. 53-68.
92. Fahy, F., *The reciprocity principle and applications in vibro-acoustics*. Recent Developments in Air-and Structure-Borne Sound and Vibration, 1992. **2**: p. 611-618.
93. Skudrzyk, E., *Die Grundlagen der Akustik*. 1954, Vienna: Springer-Verlag.
94. Ver, I.L. *Some uses of reciprocity in acoustic measurements and diagnosis*. in *INTER-NOISE and NOISE-CON Congress and Conference Proceedings*. 1985. Institute of Noise Control Engineering.
95. ten Wolde, T., *On the Validity and Application of Reciprocity in Acoustical, Mechano-Acoustical and other Dynamical Systems*. Acta Acustica united with Acustica, 1973. **28**(1): p. 23-32.
96. Van Der Linden, P. and K. De Meester, *Airborne source strength measurements on the basis of pressure indicator inversion applied to an engine valve cover*. Proceedings of the 4th ICSV, St-Petersburg, 1996.
97. P.J.G. van der Linden and J.K. Fun, *Using Mechanical-Acoustic Reciprocity for Diagnosis of Structure Borne Sound in Vehicles*. 1993, SAE International.
98. Dom, S., et al., *Transfer path analysis: accurate load prediction beyond the traditional mount stiffness and matrix inversion methods*. 2014, SAE Technical Paper.
99. Van der Auweraer, H., et al., *Transfer path analysis in the critical path of vehicle refinement: the role of fast, hybrid and operational path analysis*. 2007.
100. Shuang, L., et al. *Application of multiple-references Transfer Path Analysis on the vibration at steering wheel under road excitation*. in *2014 IEEE Conference and Expo Transportation Electrification Asia-Pacific (ITEC Asia-Pacific)*. 2014.
101. Wyckaert, K. and L. Van Laere, *Operational Analysis, Transfer Path Analysis, Modal Analysis-Tools to Understand Road Noise Problems in Cars*. JOURNAL-SOCIETY OF AUTOMOTIVE ENGINEERS OF JAPAN, 1996. **50**: p. 69-74.
102. Siemens. *What is the acoustic quantity called Q*. 2019 [cited 2022; Available from: <https://community.sw.siemens.com/s/article/what-is-the-acoustic-quantity-called-q>].

103. Girdhar, S., et al., *Measuring the force due to standard tapping machine and floor impedance for ASTM standards*. INTER-NOISE and NOISE-CON Congress and Conference Proceedings, 2021. **263**(6): p. 767-777.
104. Girdhar, S., et al., *Input force and floor impedance measurement for the standard tapping machine and the standard impact ball*. Noise Control Engineering Journal, 2023. **71**(1): p. 57-74.
105. Piezotronics, P. *Impact Hammer | 086D20*. Available from: <https://www.pcb.com/products?model=086d20>.
106. ToolBox, T.E. *Concrete Properties*. 2008 [cited 2021; Available from: https://www.engineeringtoolbox.com/concrete-properties-d_1223.html].
107. ToolBox, T.E. *Wood, Panel and Structural Timber Products - Mechanical Properties*. 2011 [cited 2022; Available from: https://www.engineeringtoolbox.com/timber-mechanical-properties-d_1789.html].
108. Marburg, S., *Discretization Requirements: How many Elements per Wavelength are Necessary?*, in *Computational Acoustics of Noise Propagation in Fluids - Finite and Boundary Element Methods*, S. Marburg and B. Nolte, Editors. 2008, Springer Berlin Heidelberg: Berlin, Heidelberg. p. 309-332.
109. Marburg, S., *Six boundary elements per wavelength: Is that enough?* Journal of Computational Acoustics, 2002. **10**(01): p. 25-51.
110. Hambric, S.A., S.H. Sung, and D.J. Nefske, *Engineering Vibroacoustic Analysis: Methods and Applications*. 2016: John Wiley & Sons.
111. Barnard, A.R., *Development of Supersonic Intensity in Reverberant Environments (SIRE) with applications in underwater acoustics*. 2010.
112. Hambric, S. and A. Barnard, *Tutorial on Wavenumber Transforms of Structural Vibration Fields*. INTER-NOISE and NOISE-CON Congress and Conference Proceedings, 2018. **258**(7): p. 1-12.
113. Williams, E.G., *Fourier acoustics: sound radiation and nearfield acoustical holography*. 1999: Academic press.
114. Siemens. *Qsources: Acoustic and Structural Exciters*. 2019; Available from: <https://community.sw.siemens.com/s/article/qsources-acoustic-and-structural-exciters>.
115. ten Wolde, T., J.W. Verheij, and H.F. Steenhoek, *Reciprocity method for the measurement of mechano-acoustical transfer functions*. Journal of Sound and Vibration, 1975. **42**(1): p. 49-55.
116. Mooney, C.Z., *Monte carlo simulation*. Vol. 116. 1997: Sage publications.
117. Kroese, D.P. and R.Y. Rubinstein, *Monte Carlo methods*. WIREs Computational Statistics, 2012. **4**(1): p. 48-58.
118. Kroese, D.P., et al., *Why the Monte Carlo method is so important today*. Wiley Interdisciplinary Reviews: Computational Statistics, 2014. **6**(6): p. 386-392.
119. Piezotronics, P. *Model 130D21 ICP microphone with integral preamplifier*. [cited 2023 02/14/2023]; Available from: https://www.pcb.com/contentstore/docs/PCB_Corporate/Vibration/products/Manuals/130D21.pdf.

A APPENDIX – Additional details from various sections of the document

This appendix contains additional information as referred to in the main section of this document.

A.1 Hammer-head impedance correction for the instrumented tapping hammer

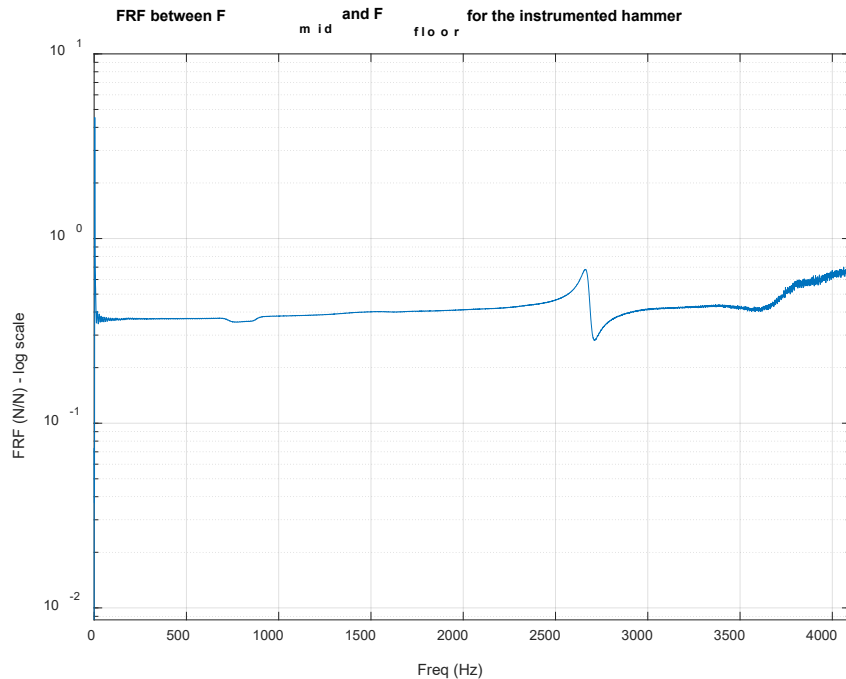


Figure A-1 FRF measured between force transducer location (F_{mid}) and impact tip location (F_{floor}) for the instrumented hammer measured using a modal hammer impact on the tip in free-free boundary conditions. The FRF is fairly flat at frequencies below 2000 Hz and was used to correct the measured input force spectrum from the force transducer.

A.2 Impact-to-impact variation with continuous drops from the instrumented tapping hammer

The tapping machine with a single instrumented hammer was placed on a heavy concrete floor (floor HC2) and allowed to run freely with a frequency of 2 Hz. The time domain data measured from the impacts is shown in Fig. A-2 (corrected for hammer head impedance). Approximately 3 dB variation is observed between peak levels from one impact to another (approximately, 3500 N to 5000 N). To avoid this variability in the measured impact data, only a single impact in the measurement time window was used.

The smaller, secondary peak that can be observed after each impact of the tapping machine may be the noise in the measurement system. The force transducer might be

measuring some force as the cam attached to the tapping machine motor hits the hammer shaft after the impact to raise it back to the standard height before the next impact. This is not a part of the force injected into the floor which was verified by a high speed camera during impacts on a concrete and a wood surface. For the tests with single hammer impact, a force window was used to avoid this noise in the system.

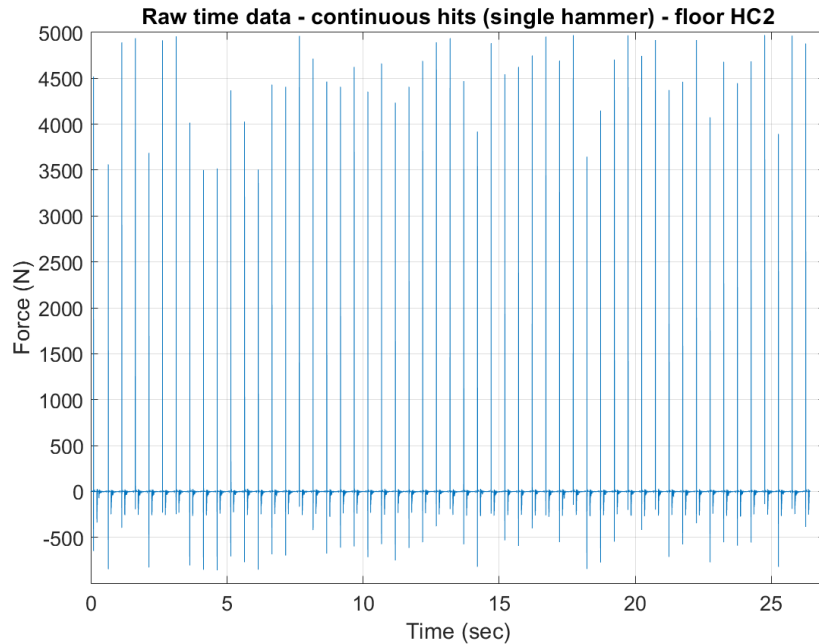


Figure A-2 The time domain impact data from the single instrumented tapping hammer shows an approximately 3 dB variation from one impact to another. To avoid this variation, only a single impact was used in the measurement window. The secondary peak in the time data after the main impact is noise in the system and was removed by using a force window.

For the same floor, a single impact measurement was measured and converted to the frequency domain. This frequency spectra is compared to the continuous impact spectra in Fig. A-3, using a solid blue line for single impact, and solid red line for continuous impacts. As expected, higher overall levels are observed with continuous impacts since more impacts are present in the measurement window. Additionally, the variation in the red curve may be due to the second additional impact force of the cam hitting the hammer shaft during rebound.

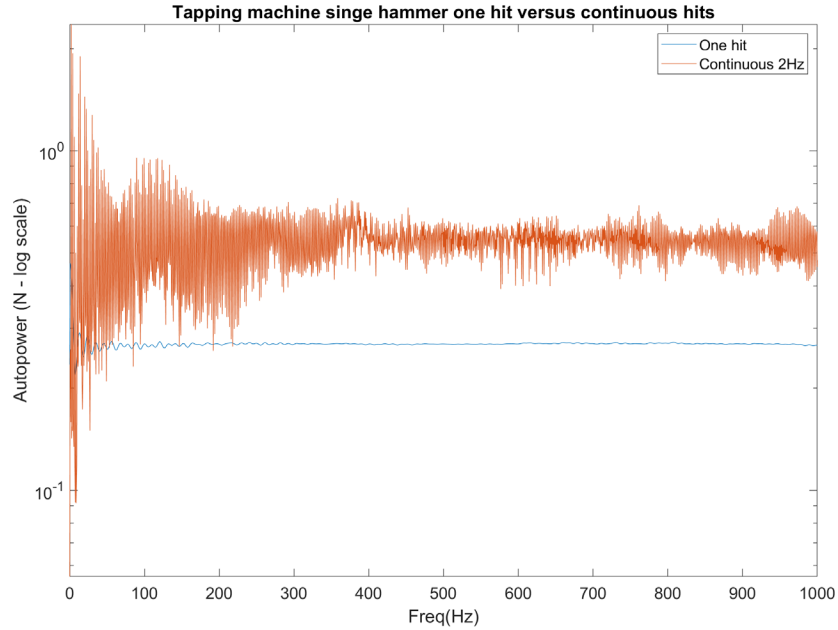


Figure A-3 The frequency spectra from a single impact test (solid blue) compared to the frequency spectra from a continuous impact test (solid red) shows high variation with the continuous data. The higher levels for the red curve are also observed as a greater number of impacts are present in the measurement window.

A.3 Non-destructive accelerometer mounting on carpet

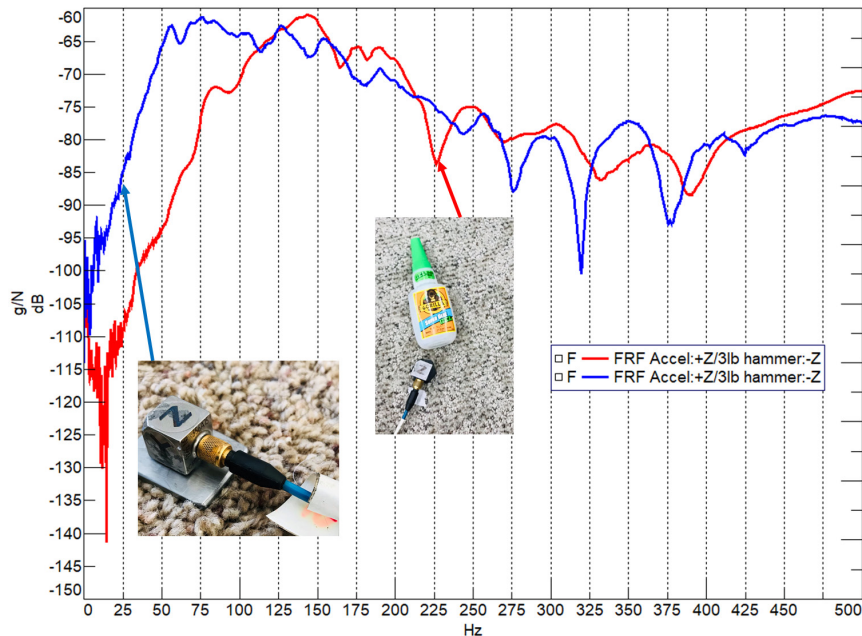


Figure A-4 The red curve was the FRF obtained by supergluing an accelerometer on carpet (destructive testing) and the blue curve was obtained using the accelerometer mounted on a $26 \times 32 \times 3$ mm steel piece with hook side of Velcro on the carpet (non-destructive

testing). A modal hammer (PCB 086D20) was used for the input force. Below 125 Hz, the FRF values are slightly higher but the comparison improved for 125 – 250 Hz, after which the metal piece shows a modal response. This non-destructive testing method can be used to mount accelerometers or force transducers on carpet with a force input

A.4 Floor impedance instrumentation details

Three PCB 356A15 accelerometers were set up in a 4 ft (1.22 m) equilateral triangle and the impact location was at the center. Figure A-5 shows the setup where the green squares represent accelerometer locations and the red circle is the input force location. This was repeated for all three input sources (the modified tapping machine, the modal hammer, and the impact ball). The measured FRFs between all accelerometer locations and the input locations (H_{FA_n} , where n represents the three accelerometer locations) was spatially averaged ($H_{F\bar{s}}$) by separately averaging the magnitude and phase, using

$$H_{F\bar{s}} = \frac{\sum |H_{FA_n}|}{3} e^{(j * \frac{\sum \angle H_{FA_n}}{3})}, \quad (A-1)$$

The averaged FRFs were converted to impedance by integrating the inverse of the FRF, using

$$imp = j\omega * (H_{F\bar{s}})^{-1} \quad (A-2)$$

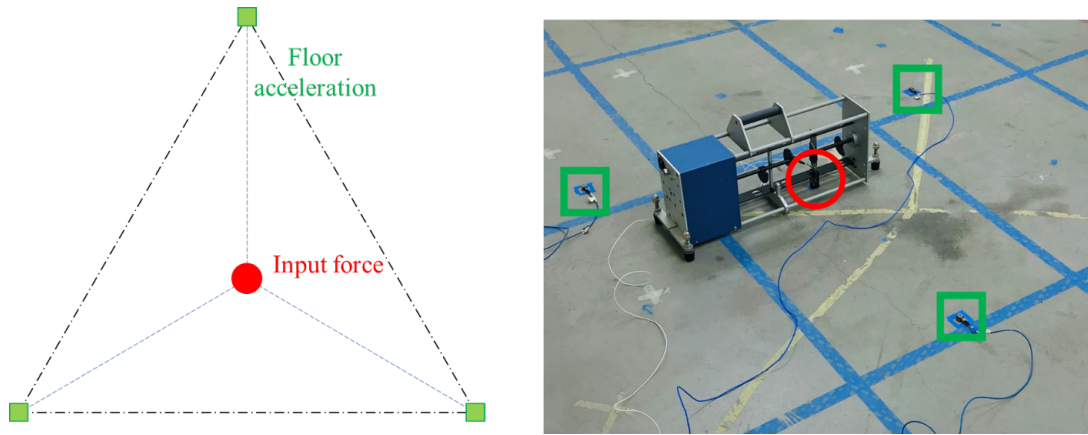


Figure A-5 Three accelerometers (green squares) were mounted equidistant from each other (1.22 m, 4 ft) and the impact location (red circle). Three individual FRFs were spatially averaged and converted to impedance

For the tapping machine, the measured FRFs were adjusted for hammer head impedance (see Section 3.1.1.1) using

$$(H_{FA_n})_{corrected} = (H_{FA_n})_{experiment} \times \left(\frac{F_{mid}}{F_{tip}} \right)_{free-free BC} \quad (A-3)$$

A.5 Validation of the simulation model

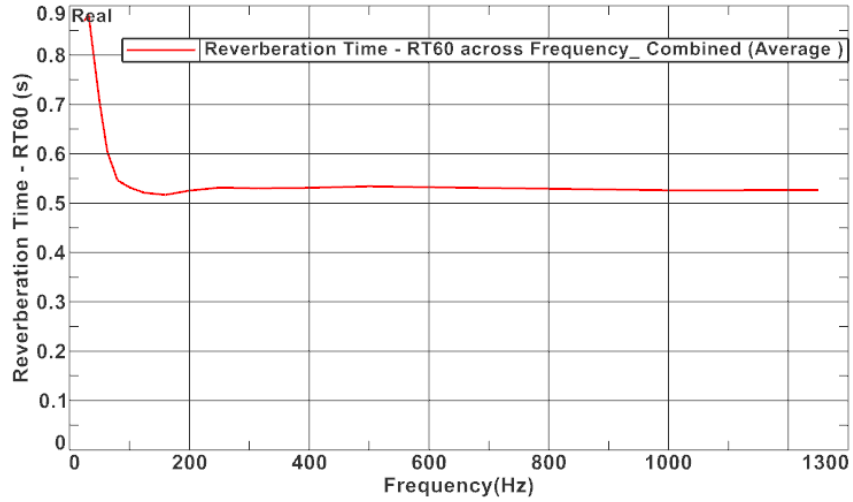


Figure A-6 The simulation room impedance boundary condition of 10414 kg/(m.s²) led to approximately 0.5 second reverberation time in the room. This was confirmed using the Simcenter Ray acoustics module.

The acoustic room modes were calculated from the literature [110] using

$$f_{lmn} = \frac{c_o}{2} \left[\left(\frac{l}{L_x} \right)^2 + \left(\frac{m}{L_y} \right)^2 + \left(\frac{n}{L_z} \right)^2 \right], \quad (\text{A-4})$$

where, l , m , and n are integers, indicating the number of nodal planes perpendicular to the three cartesian axes in the room, L_x , L_y , and L_z are the three room dimensions (in m), and the speed of sound is given by c_o (in m/s). Table A-1 shows the first ten simulated and calculated natural frequencies inside the room, and the error between the two is less than 0.1%.

Table A-1 First ten simulated and calculated acoustical natural frequencies

S. No.	Room mode number			Simulated frequency (Hz)	Calculated frequency (Hz)	Error (%)
	l	m	n			
1	1	0	0	43.31	43.28	-0.07
2	0	1	0	56.31	56.27	-0.08
3	0	0	1	62.57	62.52	-0.08
4	1	1	0	71.04	70.99	-0.07
5	1	0	1	76.10	76.04	-0.08
6	0	1	1	84.17	84.11	-0.08
7	2	0	0	86.65	86.56	-0.09
8	1	1	1	94.66	94.59	-0.08
9	2	1	0	103.34	103.24	-0.09
10	2	0	1	106.88	106.78	-0.09

The floor ceiling assembly was assumed to be a thin plate with simply supported boundary conditions and natural frequencies were calculated based on [110] using

$$\omega_{mn} = \sqrt{\frac{D}{\rho h} \left[\left(\frac{m\pi}{L_x} \right)^2 + \left(\frac{n\pi}{L_y} \right)^2 \right]}, \quad (\text{A-5})$$

where, ω_{mn} are the natural frequencies (rad/sec), D is the bending stiffness (kg/m^3), h is the thickness of the slab (m), m and n are the mode orders in the x and y directions (respectively), and L_x and L_y are the floor dimensions (m). The first ten modes calculated from the literature were compared to the simulation model (with simply supported boundary conditions) and the results are shown in Table A-2. Higher deviation is observed for higher order modes, and the maximum deviation observed is 6.5%. A part of the deviation may be due to the thin plate assumption made for the literature calculations that may not be true in the software.

Table A-2 First ten simulated and calculated structural natural frequencies

S. No.	Mode order		Simulated frequency (Hz)	Calculated frequency (Hz)	Error (%)
	m	n			
1	1	1	40.57	41.60	2.48
2	2	1	85.40	88.00	2.96
3	1	2	116.86	120.02	2.63
4	3	1	159.66	165.33	3.43
5	2	2	159.32	166.42	4.26
6	3	2	230.58	243.75	5.40
7	1	3	240.76	250.71	3.97
8	4	1	261.29	273.60	4.50
9	2	3	280.95	297.11	5.44
10	4	2	329.14	352.01	6.50

A.6 Details of additional measurement methods simulated

Some of the simulation measurement methods were not relevant for the final proposed method. Such measurement methods are discussed in this section.

A.6.1 Monte Carlo analysis

A Monte Carlo simulation [116-118] uses computer codes to generate random objects or processes such that each one of these seemingly random processes can also occur naturally. Repeating this Monte Carlo simulation several times gives a statistical understanding of the behavior of any system. For this simulation, we wanted to understand the spread of SPL measurements and single number ratings if the ASTM standard is followed for the discrete point measurement method.

Microphone nodes were placed at every 100 mm in the room and a 1N input force was applied in the middle of the floor (a tapping machine was not modeled for simplicity). Four random microphone nodes that follow the ASTM standards were selected using the Monte Carlo process and the average SPL was calculated. This process was repeated 100,000 times where the MATLAB code found a valid combination of points approximately 6% of the time. Figure A-7 (left) shows the mean and standard deviation of Monte Carlo values. Below 40 Hz (the first room mode), the standard deviation is low

but ranges from 8 – 10 dB above 40 Hz. The same test standard followed in the same room by different users may lead to a standard deviation of approximately 8 – 10 dB in low-frequencies. Figure A-7 (right) shows a histogram of the ASTM LIR [39] values calculated using the simulated data. The same assembly can lead to a variation of approximately 20 LIR points. This highlights the non-reproducibility problem with the current test standard.

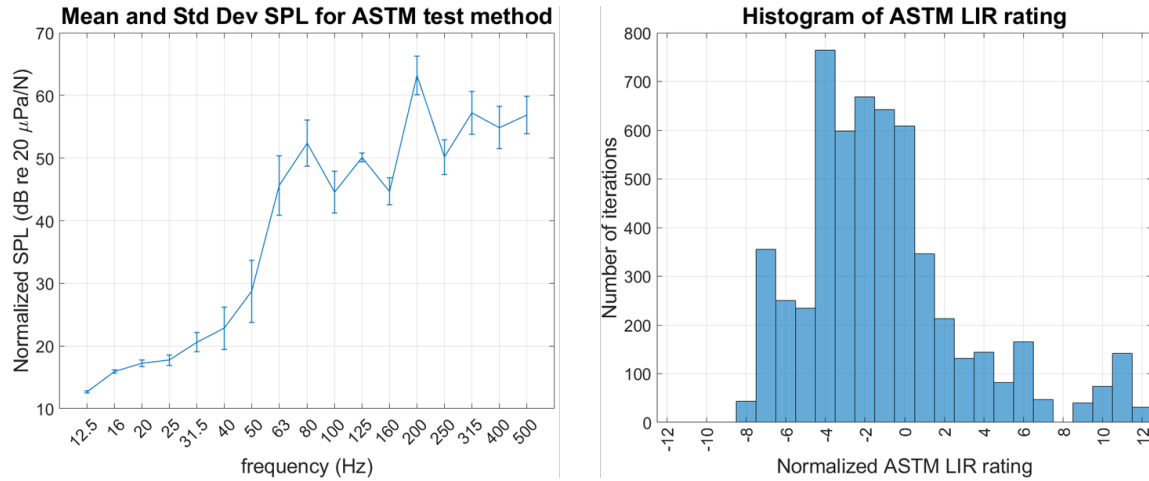


Figure A-7 The mean and standard deviation values for the ASTM Monte Carlo analysis shows that for the same assembly, the low-frequency standard deviation is 8 – 10 dB below 500 Hz (left) and the same assembly can yield a variation of 20 points for the ASTM LIR single number rating

Recall that the ASTM ISR used in the building codes is calculated using frequencies from the 100 to 3150 Hz OTO bands but the model was only simulated till the 500 Hz OTO band and the spread of the overall ASTM ISR rating was not evaluated. However, the ISR ratings for most of the assemblies are controlled by low-frequency measurements so it is expected that the standard deviation for the ISR rating would also be high.

A.6.2 ISO Corner method

A low-frequency measurement method for small rooms (volume < 25m³) was recently introduced within ISO [77]. Four corners in the room are selected – two near the floor, and two near the ceiling under test. Measurements are made between 0.2 – 0.3 m of the three room boundaries that make up the corner and the maximum SPL at any corner in any OTO band from 50 Hz – 80 Hz is recorded. These values are averaged with the room-averaged SPL with a 1:2 ratio using

$$L_{LF} = 10 \lg \sqrt{\frac{10^{0.1L_{corner}} + (2 \times 10^{0.1L_{room}})}{3}}, \quad (A-6)$$

where, L_{LF} is considered the low-frequency adjusted room SPL (only from 50 – 80 Hz OTO bands), L_{corner} is the maximum SPL measured in any of the four corners, and

L_{room} is room averaged SPL measured using normal standard methods (scanning or discrete point measurement averaging).

Twenty-seven microphone nodes were placed in the simulated room within 0.2 – 0.3 m of the room boundaries to study the reproducibility of this method. This was repeated for all eight room corners for a total of 216 microphone nodes. The mean and standard deviation of the simulated SPL is shown in Fig. A-8 (left) for all the floor corners (blue color) and all the ceiling corners (red color). The standard frequency range of 50 – 80 Hz is represented with the vertical dashed black lines. From 50 – 80 Hz, there is about a 7 – 8 dB difference in the floor and the ceiling corners, but the standard deviation is less than 1 dB (measurement uncertainty with the Class 1 sound level meters) below 100 Hz. According to this simulation model, the method is highly reproducible in low frequencies as measurements near the ceiling and floor corners are made.

Figure A-8 (right) shows the maximum corner SPL (blue line), the ASTM room averaged SPL (red line), and the adjusted spectra based on the ISO standard (dashed magenta). Due to different data processing strategies at the 80 Hz and the 100 Hz OTO bands, an additional 9 dB difference is observed in the performance spectra. This additional difference may lead to erroneous assumptions about the performance of the assembly in these OTO bands.

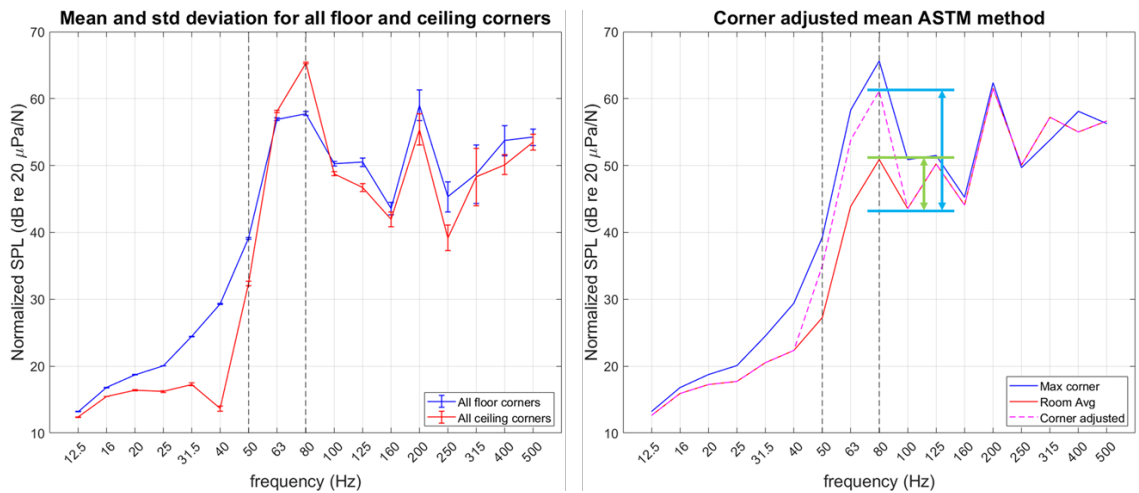


Figure A-8 (Left) The blue and red curves respectively show the mean and standard deviation for all microphone nodes near the floor and ceiling corners, respectively. Low standard deviation below 100 Hz suggests that the method is highly reproducible, at least for this simulated room, and (right) shows the adjusted corner curve (dashed magenta) which has an additional 9 dB difference between the 80 Hz and the 100 Hz OTO bands due to two different data processing methods which may lead to erroneous conclusions about the assembly performance

These conclusions are made from only one simulated room with a volume of 33 m³ (> standard volume 25 m³). The observations may change as different shapes and sizes are simulated. However, this method is restricted only for room volumes below 25 m³ and

the ISO standards do not provide any measurement guidelines for larger rooms that are often encountered in the field. In addition, the method uses the room averaged SPL for the final calculations that suffer from the non-diffuse field issues, especially for small rooms that are part of this standard. This method was not explored any further.

A.6.3 Diagonal measurement method

Schoenwald et al [37] recommended measuring SPL at six points along the room diagonal to estimate the overall room average SPL for airborne transmission tests. Such a measurement method provided results that were approximately 1 – 2 dB higher than the actual room average. This room average was calculated using a dense microphone grid in the room. The diagonal method was tested for only one room with a volume of 22 m³.

Twenty equally spaced microphone nodes were defined in the simulation model along the room diagonal. Different sets of equidistant microphones (two, four, five, seven, ten, and twenty) were considered and averaged. The average SPL values were compared to the overall room average obtained from a separate simulation model (microphones every 100 mm). Figure A-9 compares the results of different combinations of equidistant microphones (solid lines) to the room average (dashed red line) on the left. Approximately 2 – 3 dB differences are observed in the non-diffuse field (vertical dashed lines) with larger differences (7 – 10 dB) observed in higher frequencies. Figure A-9 (right) compares combinations of seven or more microphones with the room average. Overall, approximately 2 – 3 dB differences are observed with the room average. This method was not explored further.

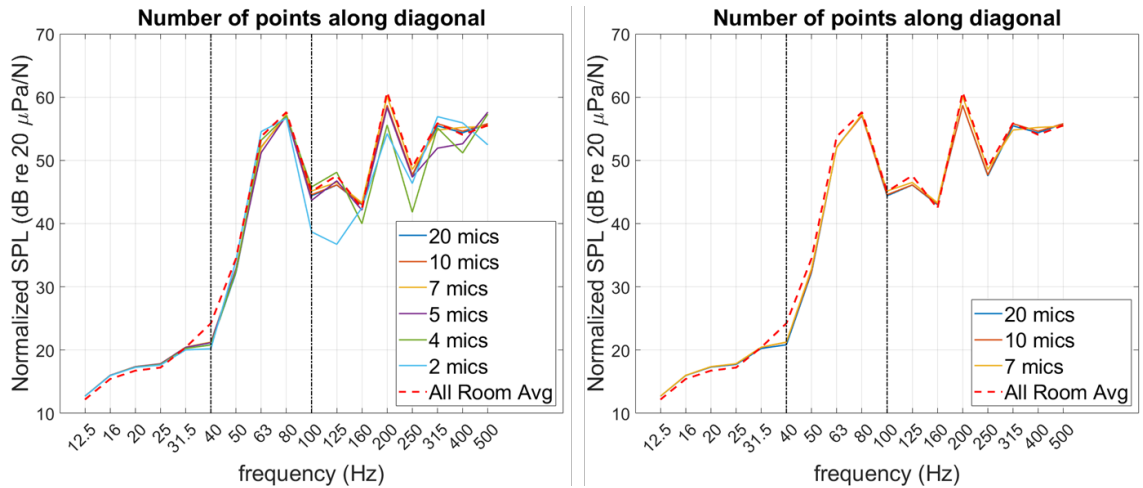


Figure A-9 Solid lines represent all different equidistant microphone combinations and the dashed red line represents the room averaged SPL. The right side of the figure only shows combinations with seven or more microphones. The high-frequency differences are lower if more microphones are used but overall, 2 – 3 dB differences are observed in the room non-diffuse (dashed vertical lines)

A.6.4 Sound Power based on room intensity

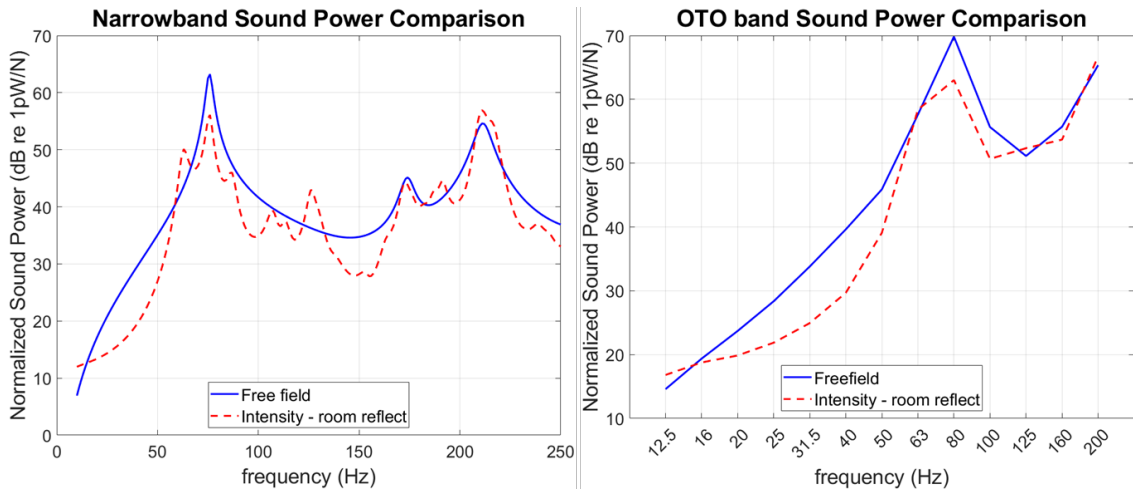


Figure A-10 The free field sound power (blue) compared with the room intensity-based sound power (red) in narrowband (left) shows approximately 7 dB difference at the 76 Hz peak and shows a strong modal behavior. In the OTO bands (right), a difference of 1 – 10 dB is observed. Intensity measured at 25mm from the ceiling still has a strong influence of the room modes

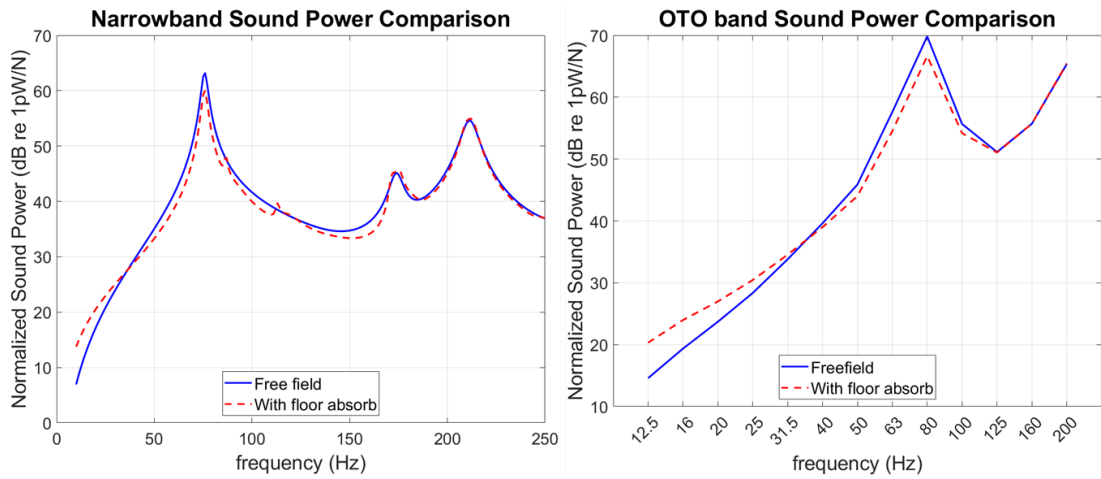


Figure A-11 Narrowband (left) and OTO band (right) comparison between the free field sound power (blue) and the intensity-based sound power with floor AML conditions (dashed red) show that with additional floor absorption, the intensity-based calculations were within 1 – 3 dB of the free field sound power calculations from the 40 – 100 Hz OTO bands. This can be achieved by adding significant absorption to the floor of the downstairs room so that the incident sound waves are absorbed. This may significantly increase the total test time and may not be acceptable to the industry

A.7 PCB Array microphone validation

The PCB 130D21 [119] microphone is rated to show a ± 1 dB deviation from 100 Hz to 4000 Hz but the focus of this work is frequencies below 100 Hz, at least down to 50 Hz. In an anechoic chamber, a speaker was set up to play a sine sweep signal from 20 Hz to 1024 Hz and the measurements are made using a PCB 378B02 (1/2" pre-polarized free field) microphone rated down to 3.15 Hz, and six different PCB 130D21 (array microphones used for the reciprocity method testing). The measured SPL autopowers are compared in Fig. A-12 where all the array microphones are plotted using solid blue lines and the free field microphone is plotted using solid red line. Above 40 Hz, less than 0.5 dB difference is observed between the two and the variation shown below 40 Hz is attributed to the speaker's repeatability in generating low-frequency signals. The array microphones are considered acceptable down to 40 Hz based on this test, and are used for all the reciprocity tests detailed in this work.

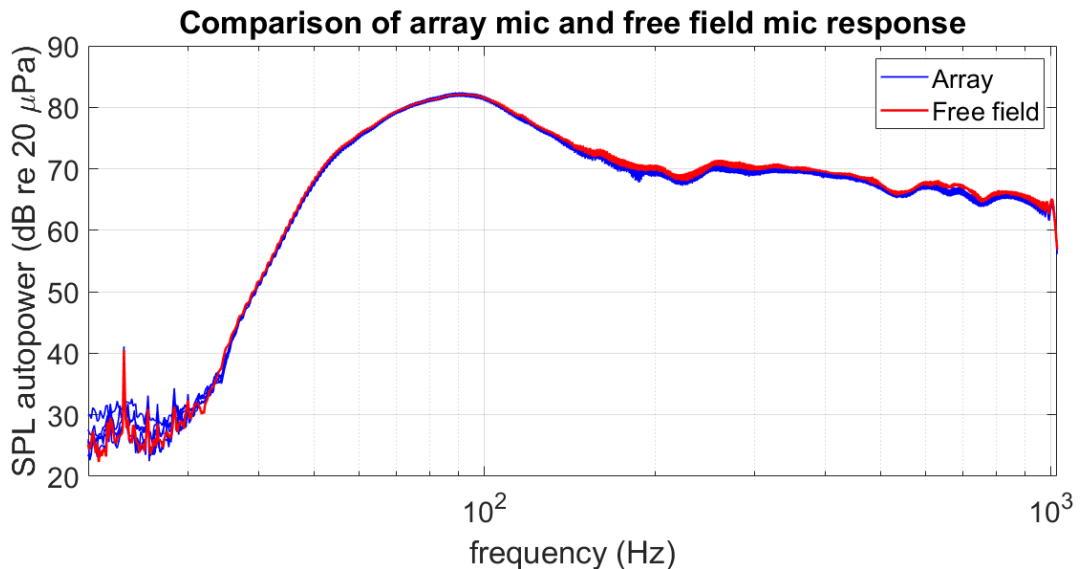


Figure A-12 The measured SPL autopower from six array microphones (solid blue) and free field mic (solid red) show less than 0.5 dB difference above 40 Hz. The array microphone is considered acceptable for this work and is used exclusively for all reciprocity testing.

A.8 Floor Impedance comparison

The floor impedance for all floors is plotted until the frequency excitation bandwidth, that is until good SNR was observed. This was defined as the highest of the following two parameters:

1. When the input force spectra drops by more than 20 dB
2. When the coherence falls below 0.5

For the plots in this section, markers have been used to signify the excitation frequency bandwidth and the impedance has not been plotted past these markers. The experimental values are also compared with infinite plate impedance from the literature [110]. The material properties of concrete and hardwood are assumed from the literature [106, 107] and the infinite plate impedance is calculated using

$$imp_{inf} = 8\sqrt{D\rho h}, \quad (A-7)$$

where, D is the flexural rigidity ($N.m^2$), ρ is the material density (kg/m^3), and h is the thickness of the plate, which is assumed to be 0.2 m (8 in) for concrete and 0.045 m (1-3/4") for hardwood.

For the tapping machine, Fig. A-13 shows the OTO based floor impedance where the asterisk markers are used to signal the frequency excitation bandwidth. The heavyweight floor impedance was approximately 30 – 40 dB higher than the lightweight floors and all the lightweight floors show an impedance value within 4 – 7 dB of each other for frequencies below 100 Hz. The black and red arrows on the right axis represent the infinite plate impedance for the concrete and hardwood structures, respectively. Overall, the measured data shows a good comparison with the infinite plate impedance. Note that the impedance for floor LC2 is not plotted beyond 50 Hz. This is because of poor measurement coherence (see Fig. 4-5).

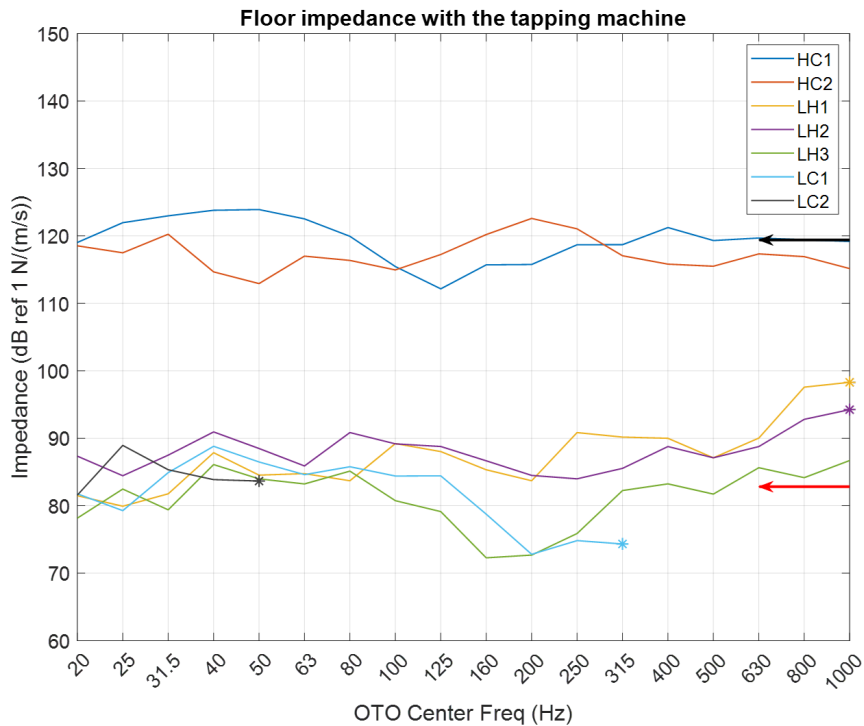


Figure A-13 Heavy floors showed approximately 30 – 40 dB higher impedance than the lightweight structures and both types of floor compare well with calculated infinite plate

impedance – black arrow for concrete and red arrow for hardwood. Asterisk markers denote the frequency excitation bandwidth for the floors

The impedance calculated with the impact ball is compared with the tapping machine in Fig. A-14 using the dotted and solid lines, respectively. The measured values compare well with the infinite plate impedance shown using the black and red arrows on the right axis for concrete and hardwood floors. Note that the impact ball data are not plotted above 80 Hz to avoid poor SNR region, denoted using square markers. For lightweight floors and the floor HC2, the impact ball based impedance compares well with the tapping machine. For floor HC1, approximately 5 – 13 dB difference is observed in low frequencies.

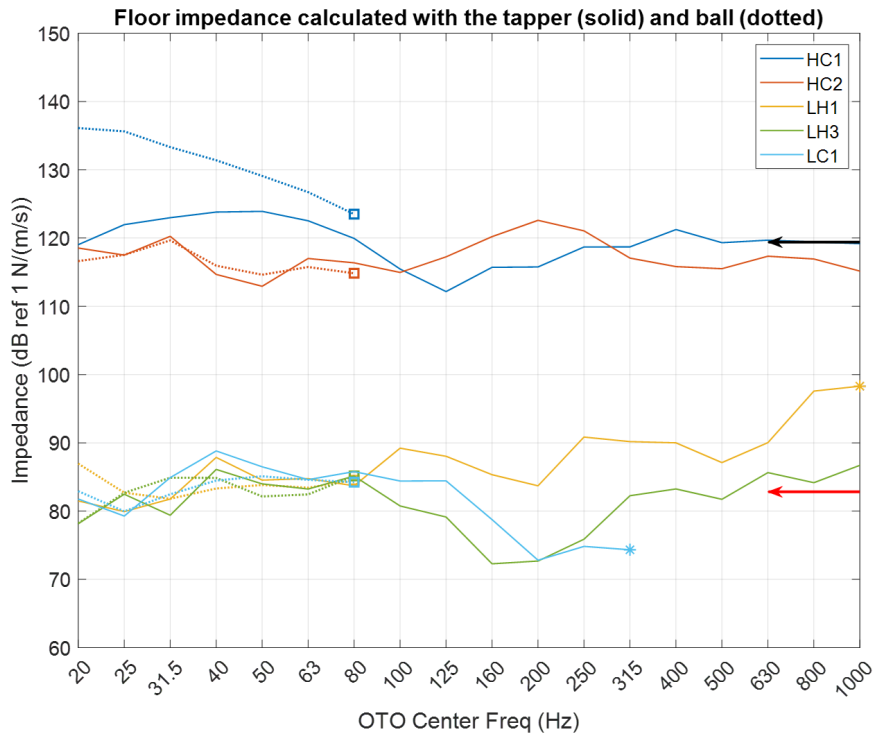


Figure A-14 Impedance calculated using the impact ball (dotted lines with square markers) compares well with the tapping machine (solid lines with asterisk markers) for all the floors except HC1, where a difference of 5 – 13 dB is observed. The impact ball has poor SNR above 80 Hz and the impedance cannot be compared, but generally, measured data compares well with the infinite plate impedance for the concrete and hardwood floors (black and red arrows)

The impedance calculated using the ‘control’ or ‘reference’ input source (the modal hammer) is compared with the tapping machine in Fig. A-15. The modal hammer data are represented with dashed lines and circle markers, while the tapping machine data are represented with solid lines and asterisk markers. The tapping machine underpredicts the floor impedance of the HC1 floor below 50 – 63 Hz by approximately 5 – 10 dB. A

heavy vibration shaker equipment sits on this floor near the test area. This shaker may be affecting the low-frequency impedance of this floor and the effect may be more pronounced for the modal hammer (or the impact ball, see Fig. A-14) because they both inject higher low-frequency force levels into the floor as compared to the tapping machine. For all other floors, the tapping machine impedance is within 3 – 5 dB of that calculated using the modal hammer. The infinite plate impedance calculated from the literature is shown on the right axis using a black arrow for concrete and red arrow for hardwood. The average measurement data compares well with the literature values.

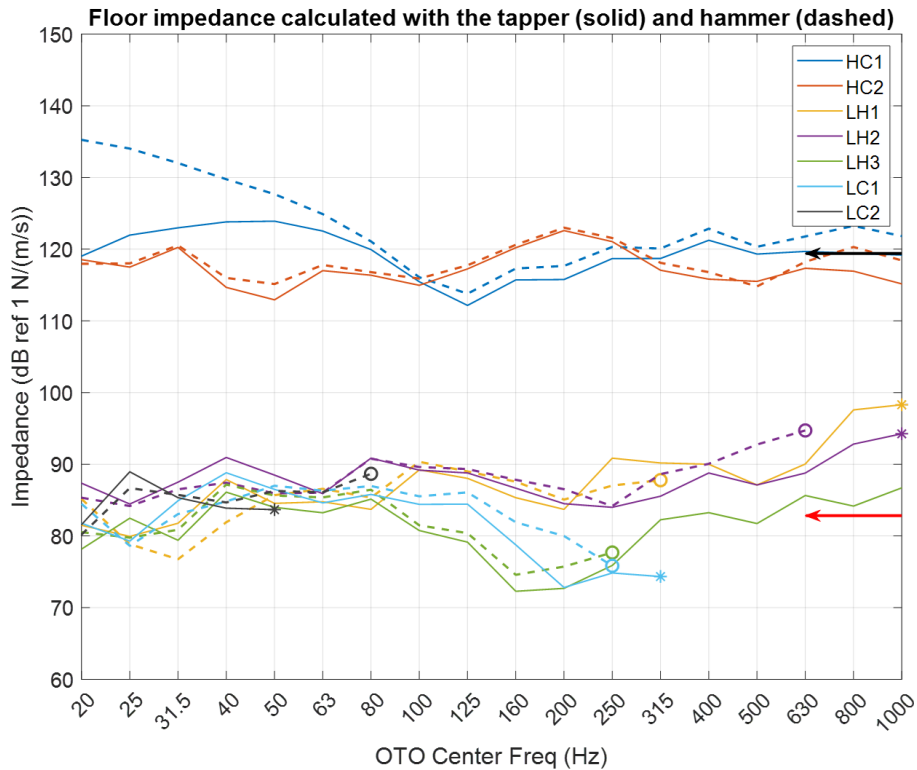


Figure A-15 The impedance calculated using the modal hammer (considered as a ‘control’ source for this study) is compared with the tapping machine. The impedance is within 3 – 5 dB for all the floors except HC1, where the tapping machine has approximately 5 – 10 dB lower levels than the modal hammer. The measured curves compare well with the infinite impedance calculated from the literature – black arrow for concrete, and red arrow for hardwood structure

The impedance calculated using the modal hammer (solid lines with circle markers) and the ISO ball (dotted lines with square markers) is compared in Fig. A-16. For all the floors, the impedance calculated using these two input sources is within 1 – 2 dB of each other, however, we are limited in comparison for frequencies below 80 Hz OTO because of the poor SNR for the impact ball above that frequency. Infinite plate impedance calculated using the literature for a concrete floor (black arrow) and hardwood (red arrow) compare well with average measured floor impedance.

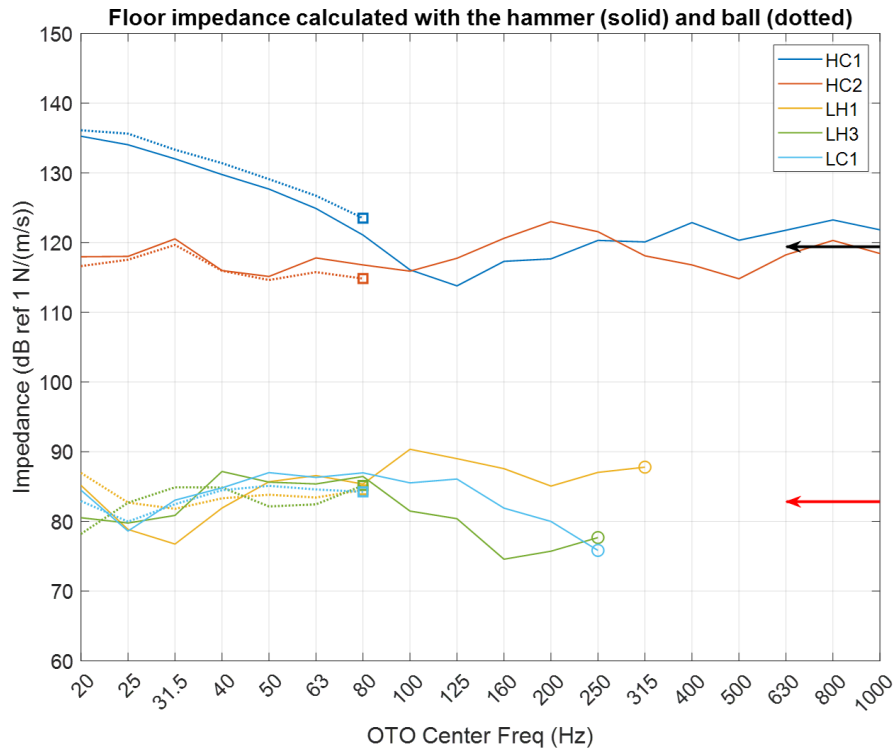


Figure A-16 Floor impedance with the impact ball (dotted lines with square markers) is limited to 80 Hz OTO due to poor SNR above that frequency, but compares well with the modal hammer data (solid lines with circle markers). The measured values compare well with the infinite plate impedance – black arrow for concrete and red arrow for hardwood structure

A.9 Additional plots for reciprocity testing

This Appendix section contains all the additional plots to aid the results for reciprocity testing. Refer the associated text in Section 4.2.2 for more details.

A.9.1 Supporting plots for Test R2

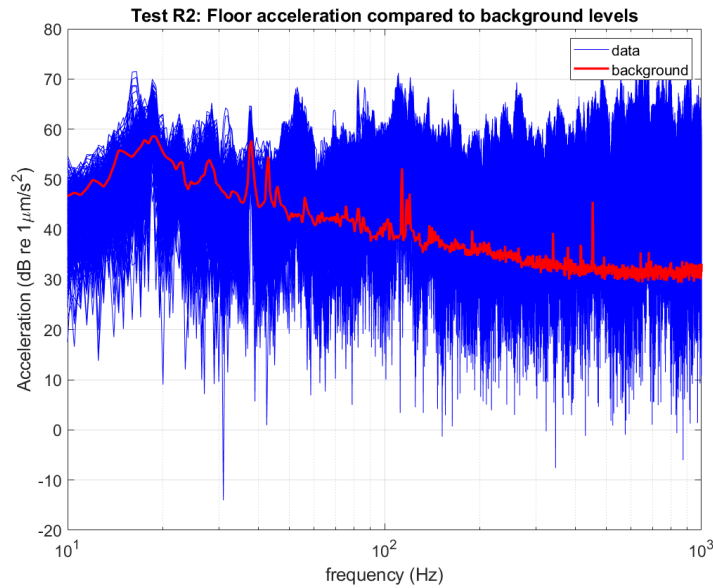


Figure A-17 The floor vibration due to the Q source (blue lines) compared to the background floor vibration levels (red line) shows that the SNR was less than 10 dB at least below 100 Hz and the background noise may affect the measurement data.

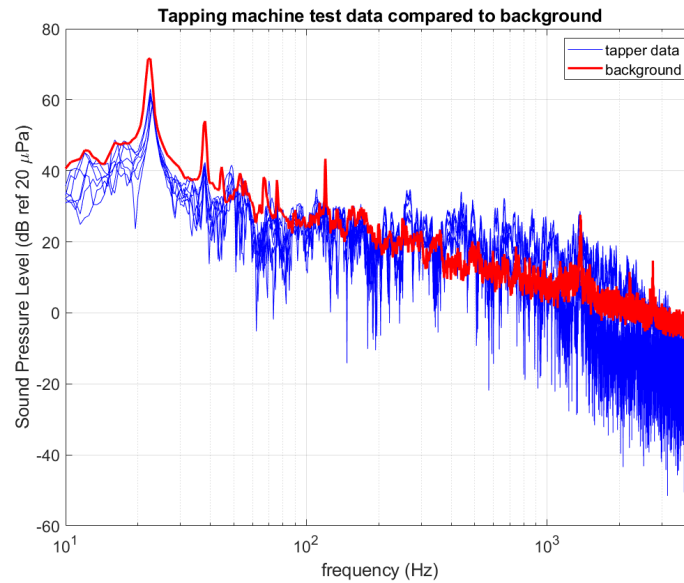


Figure A-18 The radiated SPL due to the tapping machine impacts (blue curve) compared with the background SPL data (red curve) shows that the microphone signal had poor SNR for the entire frequency range and the background noise (possibly due to nearby busy interstate) may affect the measured data. As a thumb rule, a 10 dB SNR is preferred. In some cases, for example at 22 Hz and 38 Hz, the background level was higher than the measurement, but that may be because the measurements were made a few minutes apart and the traffic patterns on the interstate may have changed.

A.9.2 Additional SoRe and ReSo combinations for Test R3

For this test, six SoRe and ReSo combinations were tested. The direct and reciprocal FRFs from one of the six combinations is compared in Section 4.3.3 and three are shown in this section. The other two combinations show a similar comparison and are not shown here.

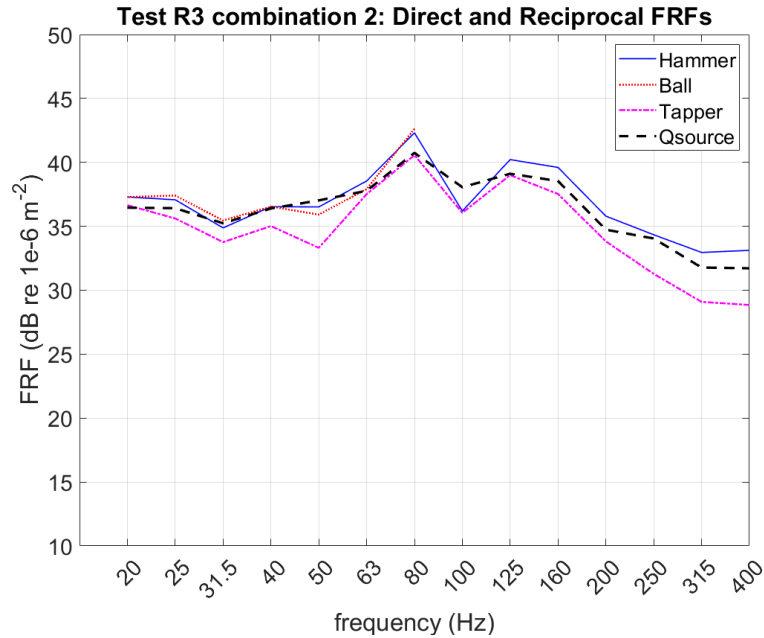


Figure A-19 The modal hammer and the impact ball FRF compare within 2 dB with the reciprocal measurements for the entire frequency bandwidth for combination 2 (test R3) but the tapping machine shows an approximate 3.5 dB difference in the 50 Hz OTO band, possibly because of low input force levels with the tapping machine. Overall, a good comparison is observed between the direct and the reciprocal measurements.

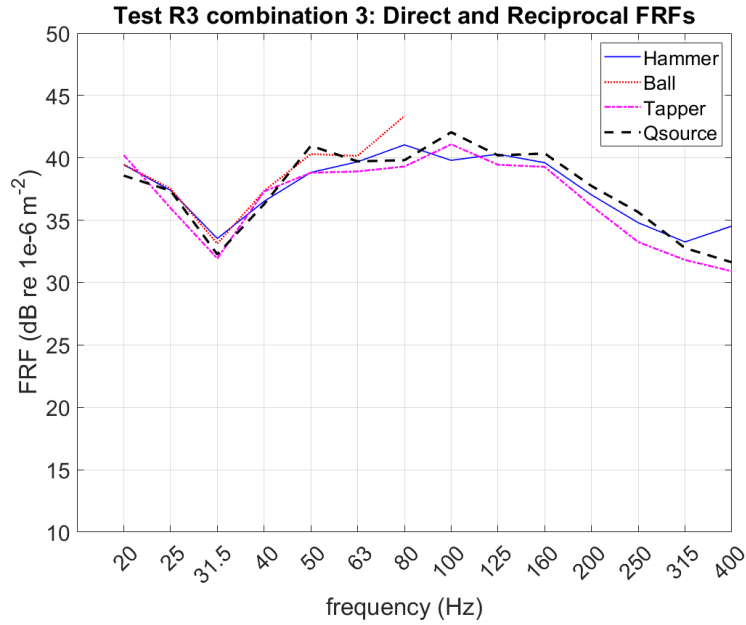


Figure A-20 The direct FRFs with the modal hammer, impact ball, and the tapping machine for combination 3 (test R3) compare within 2 dB of the reciprocal FRF measured with the Q source except for the impact ball at 80 Hz OTO band which may be because of poor SNR with the impact ball near the 80 Hz OTO band

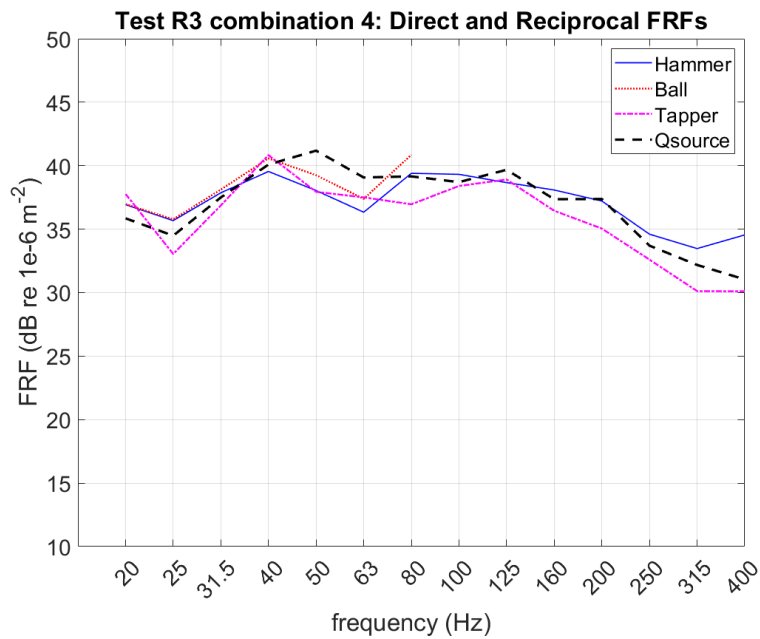


Figure A-21 The direct FRFs with the modal hammer, impact ball, and the tapping machine compare within 3 dB of the reciprocal FRF measured with the Q source for combination 4 (test R3) for the entire frequency bandwidth

A.9.3 Supporting plots for Test R3

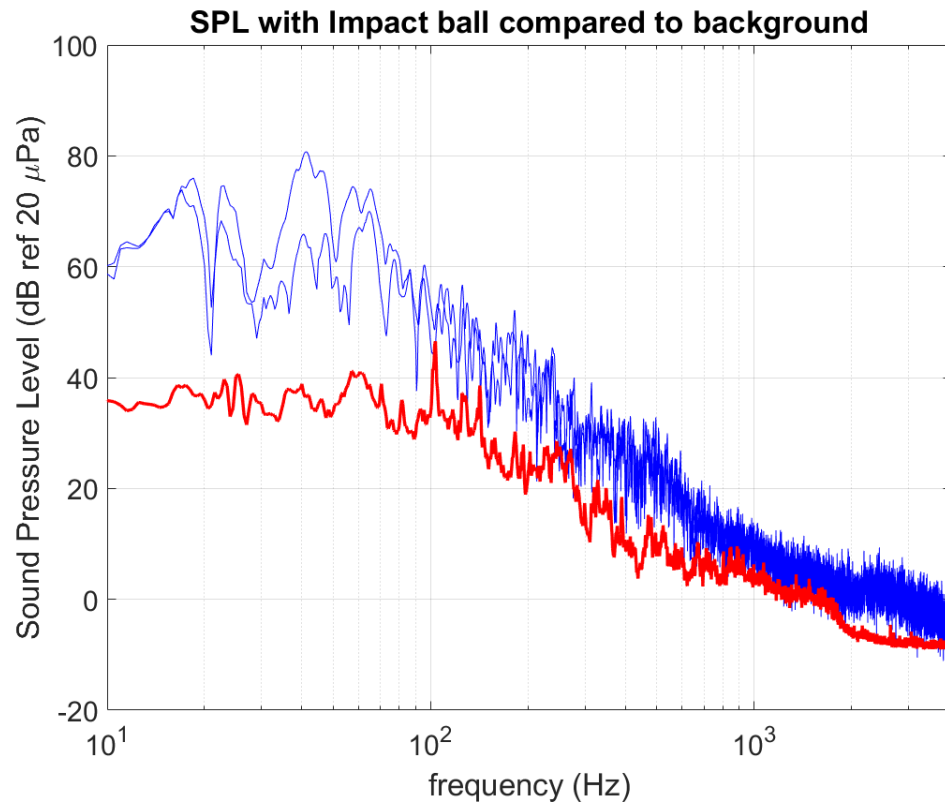


Figure A-22 The radiated SPL due to impact ball drops (blue lines) are compared with the background levels (red line) to show that the SNR was poor above 100 Hz and the measurement may be affected by background noise. Other impact locations showed a similar behavior. As a thumb rule, at least 10 dB SNR is considered acceptable. The direct FRF from the impact ball are not plotted above 100 Hz

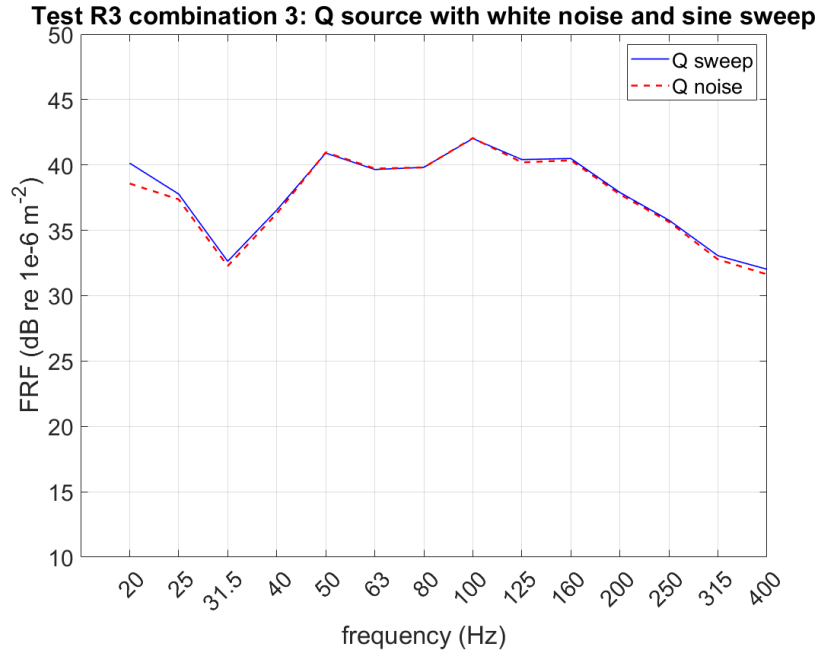


Figure A-23 The A/Q FRFs obtained using a white noise and a sine sweep signal played through the Q source for SoRe/ ReSo combination 3 shown with solid blue and dashed red line, respectively. Less than 0.5 dB variation is observed above 25 Hz and only the white noise data was used for comparison with the direct FRFs

A.9.4 Supporting plots for Test R4

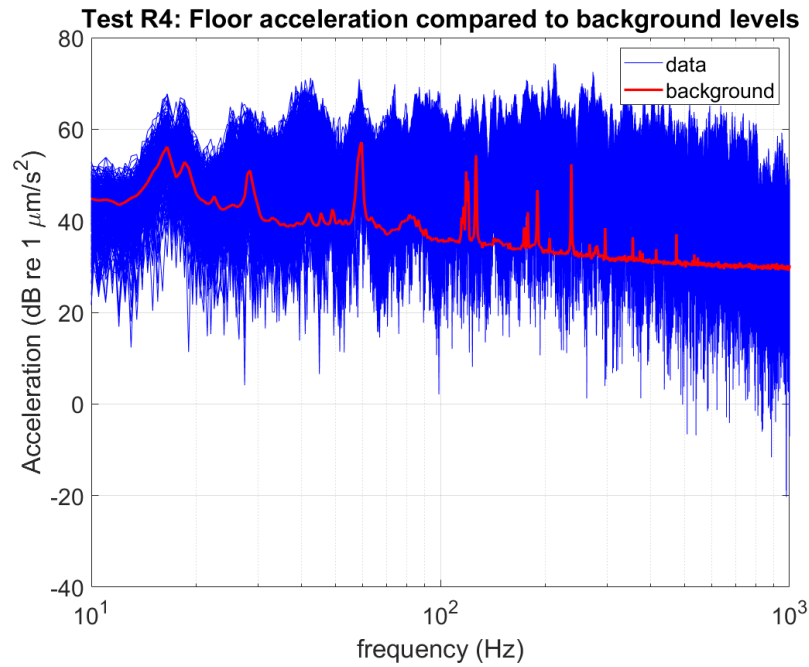


Figure A-24 The measured floor acceleration due to the Q source input (blue lines) compared with the background floor acceleration (red line) shows that the SNR for the

measurement is poor for some of the averages and this may affect the comparison of direct and reciprocal FRFs for this assembly. As a thumb rule, SNR of 10 dB or higher is considered acceptable.

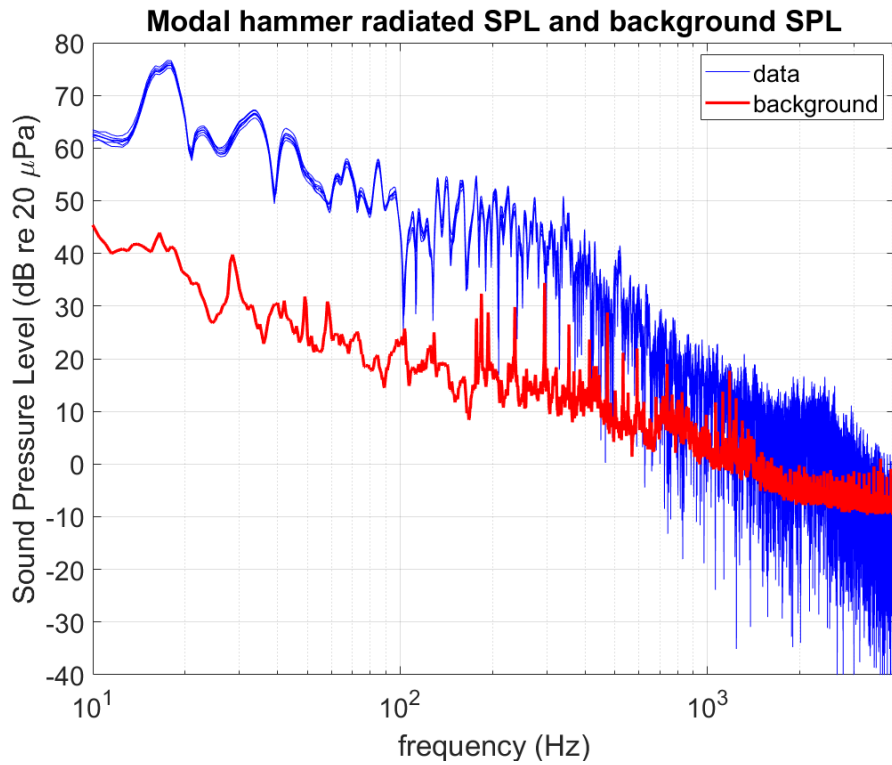


Figure A-25 The radiated SPL due to modal hammer impacts (blue lines) compared to the background noise (red curve) show more than 10 dB SNR below 100 Hz. The SNR falls at approximately 100 Hz and the radiated SPL is almost the same level as the noise signal. Background noise may affect measurement data at approximately 100 Hz. This may partly explain the 4.5 dB difference observed between the hammer FRF and reciprocal FRF.

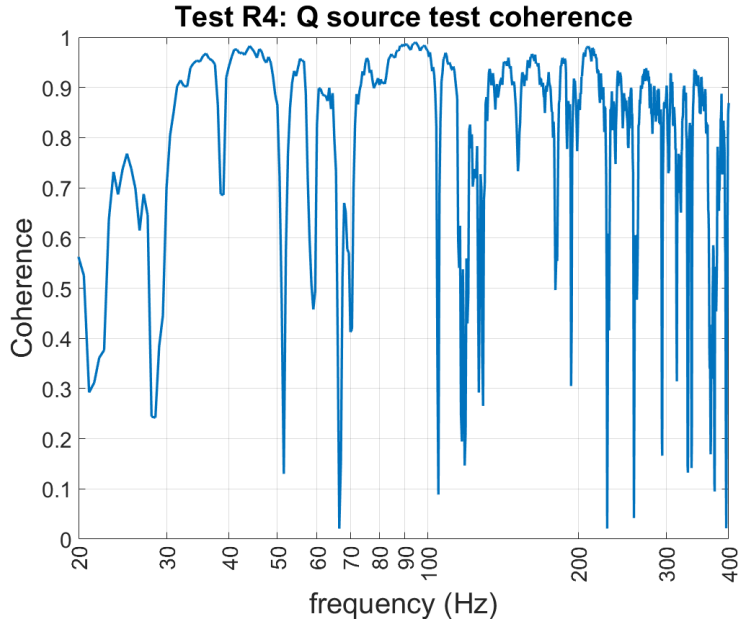


Figure A-26 The measurement coherence for the Q source for test R4 is poor in low-frequencies, especially at approximately 105 Hz which may cause the higher differences observed between the direct and the reciprocal FRFs in the 100 Hz OTO band

A.10 Additional plots for reciprocity simulation models

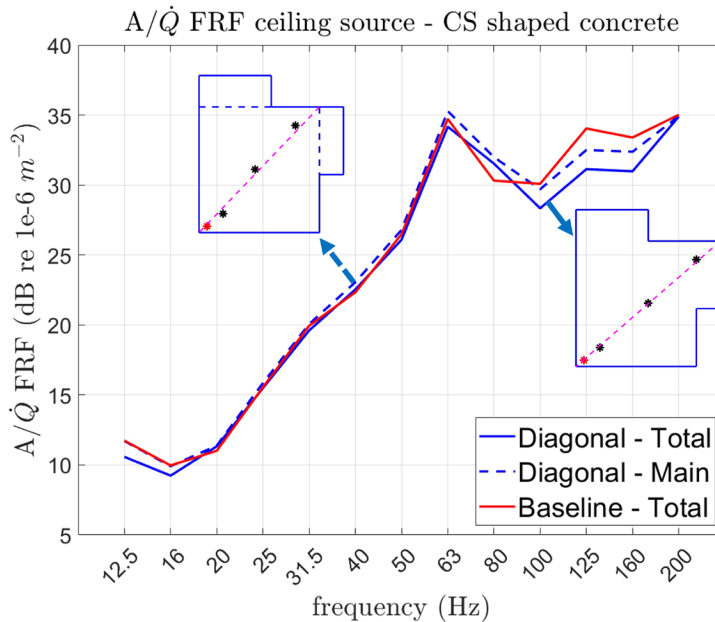


Figure A-27 The baseline A/\dot{Q} FRF (solid red) compared with the diagonal FRF of the main floor (dashed blue) and the entire floor (solid blue) showed less than 1.5 dB difference except at the 100 Hz OTO band where the entire floor FRF differs by approximately 1.8 dB for the CS concrete structure when the Q source is placed near the ceiling. Only the main floor diagonal can predict the performance of the floor

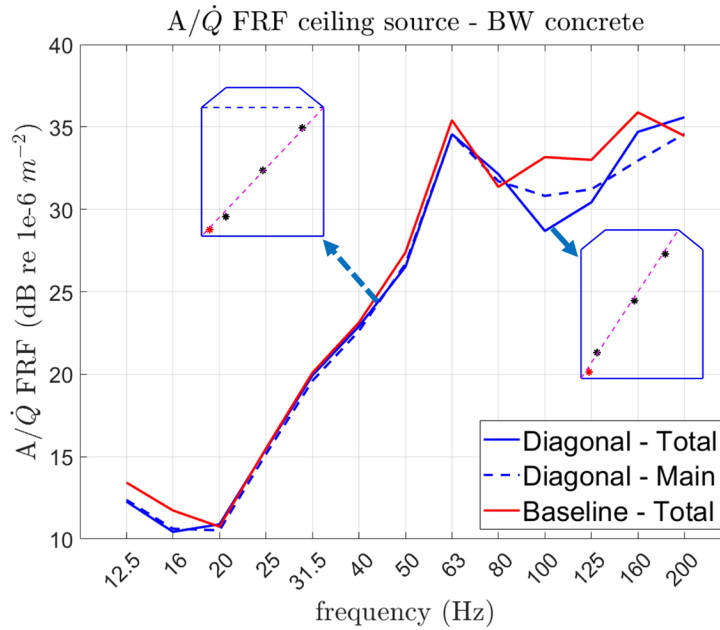


Figure A-28 The baseline A/\dot{Q} FRF (solid red) compared with the diagonal FRF of the main floor (dashed blue) and the entire floor (solid blue) showed less than 0.5 dB difference from the 40 – 80 Hz OTO bands for the BW concrete floor when the Q source is placed near the ceiling. The main floor and the entire floor FRF showed a difference of approximately 2.3 dB and 4.5 dB at 100 Hz OTO band when compared with the baseline FRF

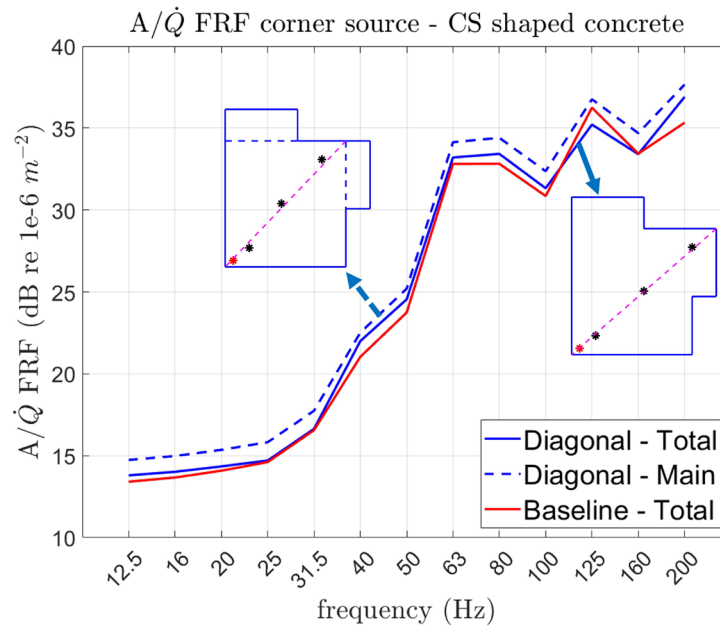


Figure A-29 The baseline A/\dot{Q} FRF (solid red) compared with the diagonal FRF of the main floor (dashed blue) and the entire floor (solid blue) showed less than 1.5 dB difference

for the CS concrete structure when the Q source is placed near a corner. Only the main floor diagonal can be used to predict the performance of the floor

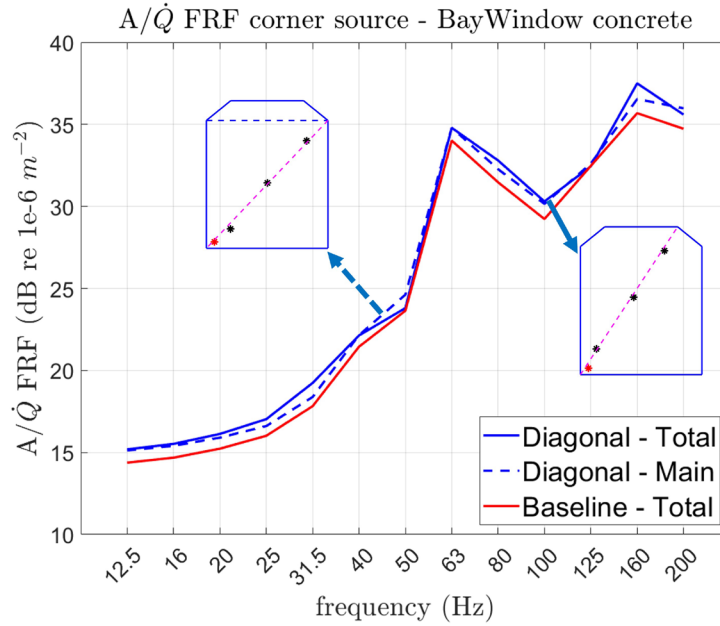


Figure A-30 The baseline A/\dot{Q} FRF (solid red) compared with the diagonal FRF of the main floor (dashed blue) and the entire floor (solid blue) showed approximately 1 – 1.5 dB difference for the BW concrete floor when the Q source is placed near a room corner. Only the main floor space can be used to study the performance of the entire floor

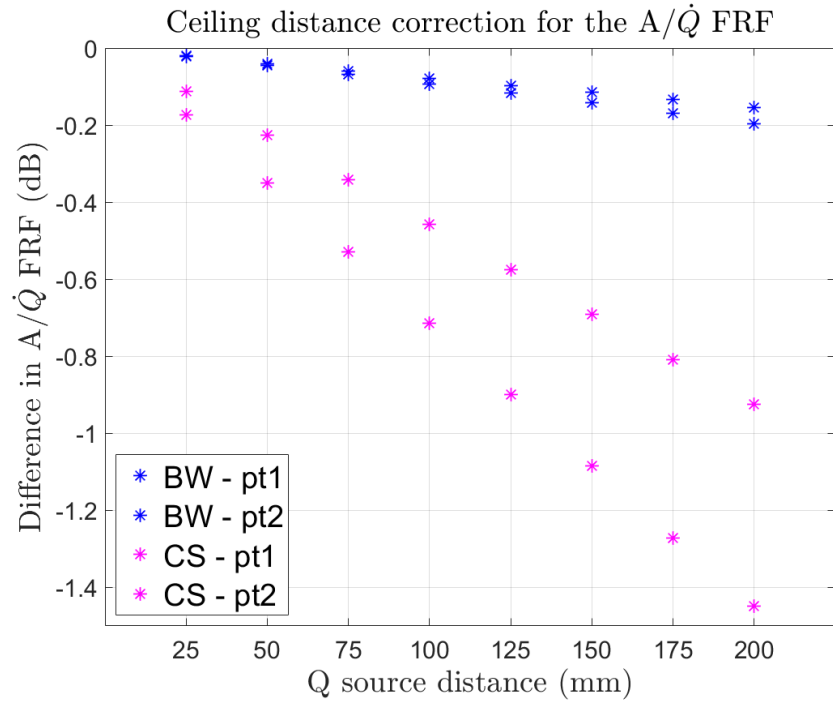


Figure A-31 The ceiling Q source correction needed based on the distance from the ceiling for two randomly selected measurement points on the CS wood-joint and BW concrete floor shows that the correction needed is different for different structures. Two points on the same structure can also provide different correction factors based on the distance of the Q source from the ceiling. If the speaker is placed far away from the ceiling for field testing, the FRFs can not be corrected from the simulation model

A.11 Additional plots for the Proposed method tests

A.11.1 Supporting plots for Test O1

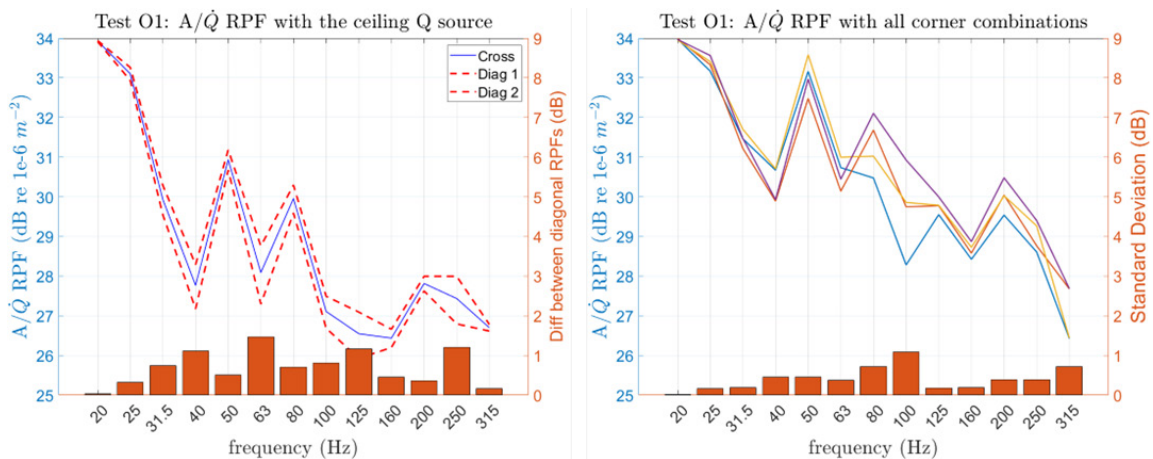


Figure A-32 Test O1: Q source placed near the ceiling (left) and near the corners (right). The two diagonal RPFs (dashed red) with the ceiling Q source locations show a comparison

of less than 1.5 dB for the entire frequency bandwidth shown and compare well with the overall cross RPF (solid blue) measurements. This shows that only one diagonal can be used for the measurements with the ceiling location (left). All possible combinations of RPFs obtained by placing the Q source at two room corners are shown on the right. Maximum 1 dB standard deviation is observed between all combinations showing that using two randomly chosen corners is acceptable

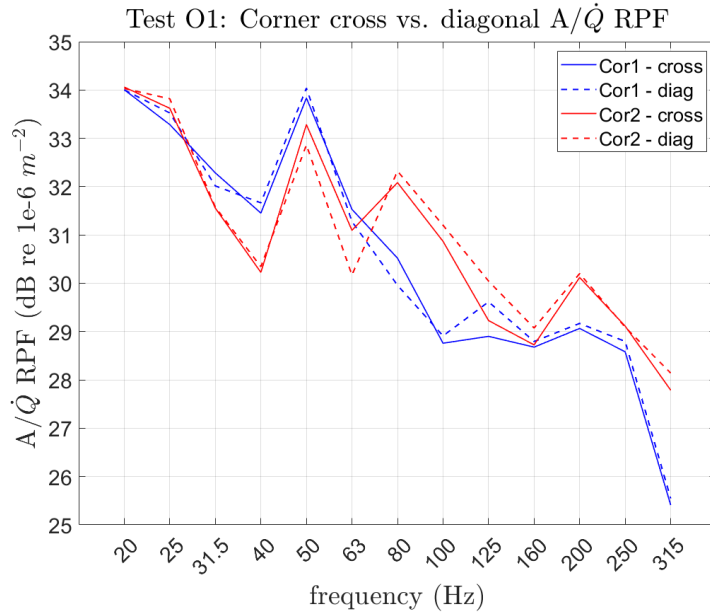


Figure A-33 Test O1: The cross (solid) and diagonal (dashed) averaged RPFs for two corners (blue and red lines) compared within 1 dB of each other so only three diagonal locations can be used to get the corner Q source RPF. Other two corners showed a similar performance and are not shown here

A.11.2 Supporting plots for Test O2

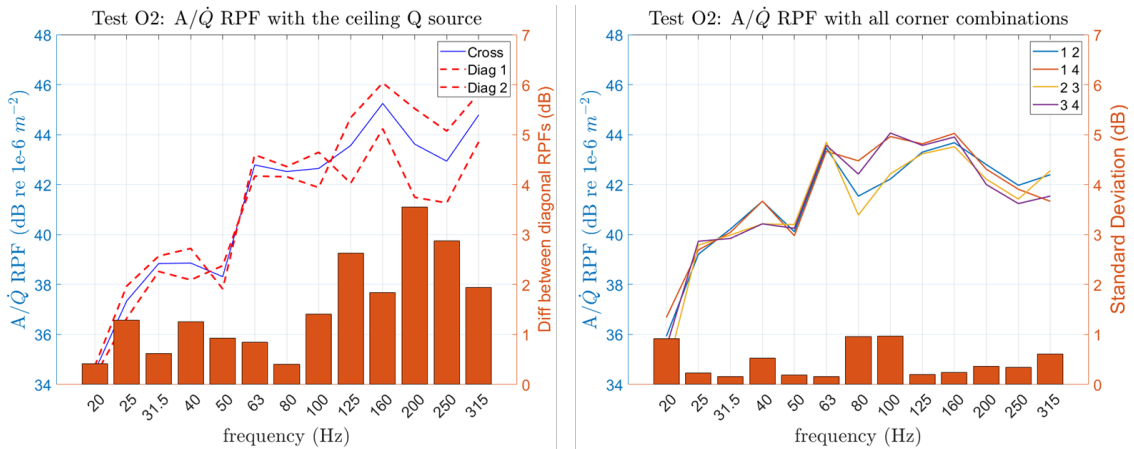


Figure A-34 Test O2: Q source placed near the ceiling (left) and near the corners (right). The two diagonal RPFs with the ceiling Q source locations show a comparison of less than

1.5 dB below 100 Hz and the differences increase for higher frequencies. Only one diagonal can be used for measurements with the ceiling location (left). All possible combinations of RPFs obtained by placing the Q source at two room corners are shown on the right. Maximum 1 dB standard deviation is observed below 315 Hz. Two randomly selected room corners for the test would show acceptable reproducibility

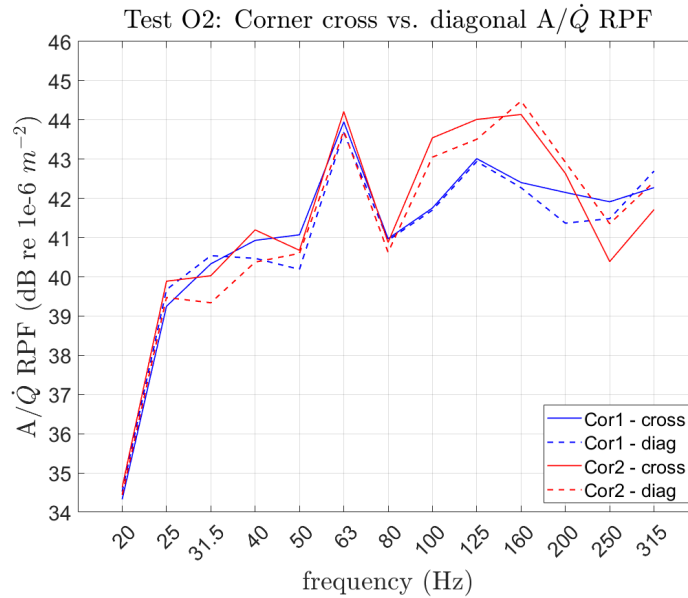


Figure A-35 Test O2: The cross (solid) and diagonal (dashed) averaged RPFs for two corners (blue and red lines) compare within 1 dB of each other so only three diagonal locations can be used to get the corner Q source RPF. Other two corners showed a similar performance and are not shown here

A.11.3 Supporting plots for Test O3

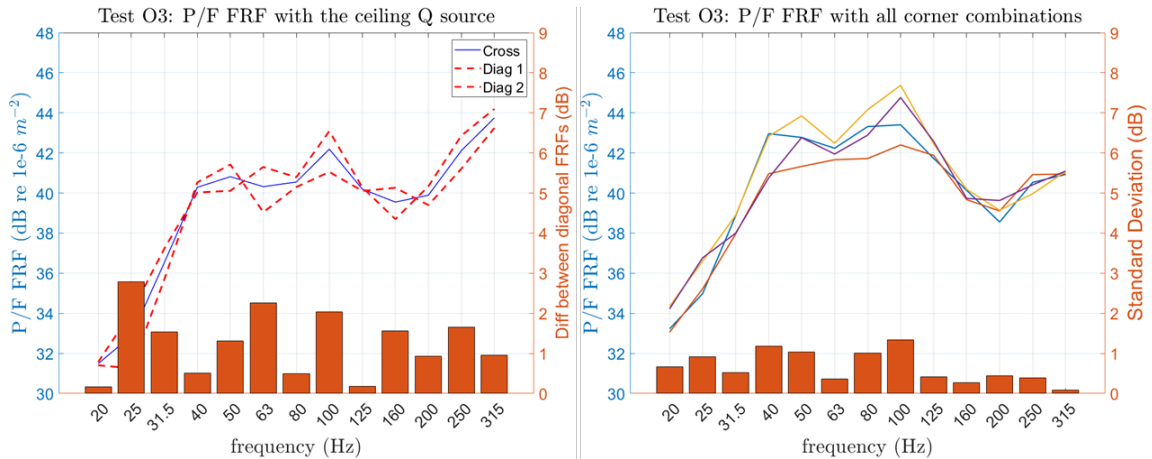


Figure A-36 Test O3: Microphone placed near the ceiling (left) and near the corners (right) for hammer impacts on the floor. The two diagonal FRFs with the ceiling mic locations showed a comparison of approximately 1 – 2 dB above 25 Hz. Only one diagonal was used

for measurements with the ceiling location (left). All possible combinations of FRFs obtained by placing the microphones at two room corners are shown on the right. Maximum 1.3 dB standard deviation was observed. Two randomly selected room corners for the test would show acceptable reproducibility

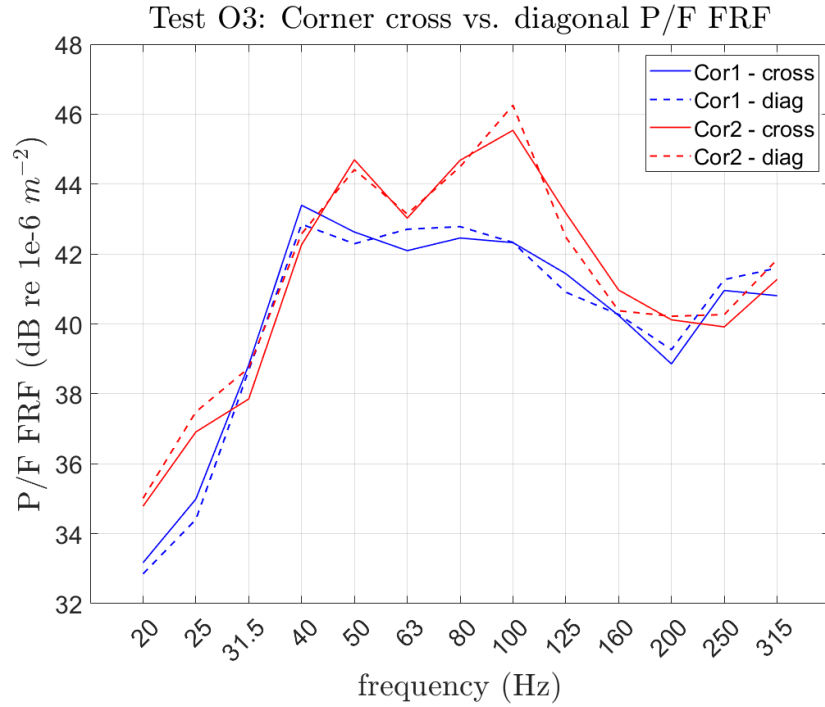


Figure A-37 Test O3: The cross (solid) and the diagonal (dashed) averaged FRFs for the two corners (blue and red lines) compared within 0.5 dB so only three diagonal locations can be used to get the corner FRF. Other two corners showed a similar performance and are not shown here

A.11.4 Ceiling RPF comparison for all assemblies

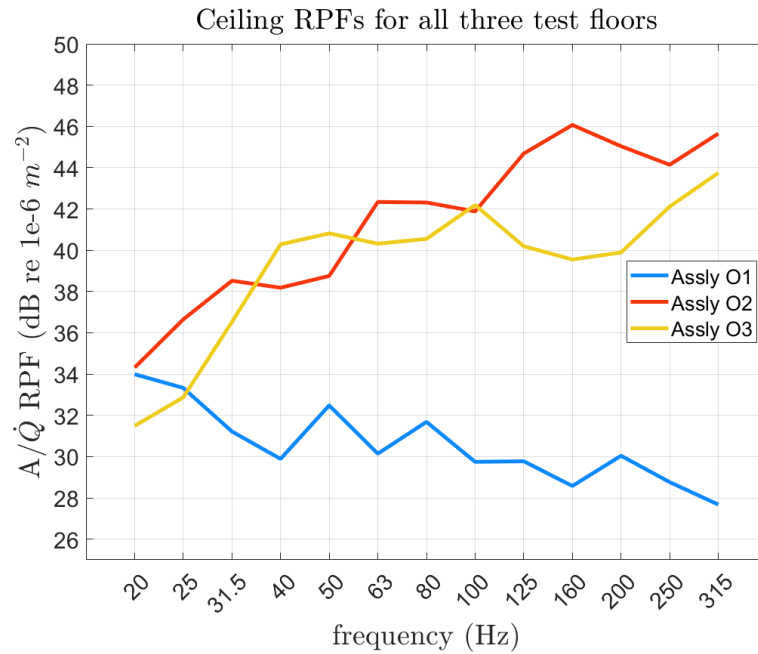


Figure A-38 Ceiling RPFs compared for all three floors based on the proposed measurement method showed that assembly O1 significantly outperforms the other two and assembly O2 slightly outperformed assembly O3 in low and high frequencies. This is in line with the conclusions from the corner RPFs and the adjusted tapping machine based *P/F* RPFs

B Copyright documentation

B.1 Copyright permission for Figure 2-4



Impact Sound Insulation: The Standard Tapping Machine Shall Learn to Walk!

Author: W. Scholl
Publication: Building Acoustics
Publisher: SAGE Publications
Date: 2001-12-01

Copyright © 2001, © SAGE Publications

Gratis Reuse

Permission is granted at no cost for use of content in a Master's Thesis and/or Doctoral Dissertation, subject to the following limitations. You may use a single excerpt or up to 3 figures tables. If you use more than those limits, or intend to distribute or sell your Master's Thesis/Doctoral Dissertation to the general public through print or website publication, please return to the previous page and select 'Republish in a Book/Journal' or 'Post on intranet/password-protected website' to complete your request.

[BACK](#)

[CLOSE WINDOW](#)

B.2 Copyright permission for Figure 2-5



Impact Sound Insulation of Timber Floors: Interaction between Source, Floor Coverings and Load Bearing Floor

Author: W. Scholl, W. Maysenhölder
Publication: Building Acoustics
Publisher: SAGE Publications
Date: 1999-03-01

Copyright © 1999, © SAGE Publications

Gratis Reuse

Permission is granted at no cost for use of content in a Master's Thesis and/or Doctoral Dissertation, subject to the following limitations. You may use a single excerpt or up to 3 figures tables. If you use more than those limits, or intend to distribute or sell your Master's Thesis/Doctoral Dissertation to the general public through print or website publication, please return to the previous page and select 'Republish in a Book/Journal' or 'Post on intranet/password-protected website' to complete your request.

[BACK](#)

[CLOSE WINDOW](#)